

Development of a Photo-Fenton Catalyst Supported on Modified Polymer Films. Preparation, Characterization and Implication for Water Decontamination by Solar Photocatalysis

THÈSE N° 4701 (2010)

PRÉSENTÉE LE 28 MAI 2010

À LA FACULTÉ SCIENCES DE BASE

GROUPE DE GÉNIE ÉLECTROCHIMIQUE

PROGRAMME DOCTORAL EN CHIMIE ET GÉNIE CHIMIQUE

ÉCOLE POLYTECHNIQUE FÉDÉRALE DE LAUSANNE

POUR L'OBTENTION DU GRADE DE DOCTEUR ÈS SCIENCES

PAR

Félicien MAZILLE

acceptée sur proposition du jury:

Dr C. Wandrey, présidente du jury

Dr C. Pulgarin, directeur de thèse

Dr S. Hug, rapporteur

Prof. T. Kohn, rapporteur

Dr S. Malato, rapporteur



ÉCOLE POLYTECHNIQUE
FÉDÉRALE DE LAUSANNE

Suisse
2010

L'imagination est plus importante que le savoir.

Albert Einstein

ACKNOWLEDGEMENTS

Je souhaiterais remercier chaleureusement tous ceux qui m'ont soutenu, directement ou indirectement, pendant ce travail de thèse. Je ne pourrais peut être pas les mentionner tous mais j'espère n'oublier personne ayant contribué activement à l'accomplissement de ce travail. Je tiens particulièrement à exprimer ma gratitude aux personnes suivantes :

A César pour m'avoir fait confiance et m'avoir soutenu et encouragé au cours de ces années enrichissantes.

Aux rapporteurs, Prof. Tamar Kohn, Dr. Stephan Hug, Dr Sixto Malato, ainsi qu'à la présidente du jury Dr. Christine Wandrey pour avoir accepté de lire et d'évaluer cette thèse.

A mes amis et collègues Thomas Schoettl, Adrien Rollux, Dorothee Spuhler, Anna Serra qui m'ont beaucoup aidé entre autre pour la partie expérimentale de ce travail.

Aux membres du groupe, entre autres Alejandro Moncayo, Ricardo Torres, Julian Rengifo, Fabiola Mendez, et bien sur mon collègue et ami de longue date, Nikola Castillo, pour leur collaboration scientifique ou technique et pour les moments partagés.

A Joël Kocher et John Kiwi, pour avoir relu et corrigé ce manuscrit, à Nicolas Xanthopoulos, Pierre-Yves Pfirter et Robin Humphry-Baker pour leur aide lors de la caractérisation des surfaces.

Aux participants du projet Européen comme Wolfgang Gernac, Sixto Malato, Anna Zapata, Carla Sitori, Antonio Lopez et Giuseppe Mascolo pour leur collaboration.

A mes amis Jeroun, Momo, Samos, Ouiloum, Jojo, les filles des Olières et du pays de la Filière et mes amis latinos et autres amis de Lausanne et d'ailleurs pour les bons moments de détente passés ensemble et pour tout ce qu'ils m'ont apporté.

Finalement à mes parents Claire et Richard, toute ma famille, et bien sur ma femme Monica pour leur soutien dans les moments difficiles, leur guidance, leur amour continu.

SUMMARY

The work presented in this thesis is a part of the European project INNOWATECH. The global objective of this project was to provide effective technological solutions for the treatment of industrial wastewater, to propose new concepts in wastewater treatment with potential benefits for the protection of the environment. In particular photo-assisted Fenton oxidation was investigated. It is a promising technology to decontaminate industrial wastewater as it makes use of the natural energy that provides the sun, abundant chemicals (iron ions and hydrogen peroxide) and does not produce toxic waste. Apart from short detour about homogenous photo-Fenton reaction (chapter 2) where the influence of pollutant physico-chemical properties on reactivity is studied, this thesis focuses on photo-Fenton treatment using a new solid catalysis. The immobilization of iron oxide on a suitable support is a strategy proposed to overcome the practical limitation related to homogeneous photo-Fenton treatment (i.e. the limited operational pH range and the problems caused by the separation of catalyst from the effluent). The preparation and the surface characterization of new photo-Fenton catalysts based on iron oxide supported on modified polymer films is described in chapters 3 and 4. The photocatalytic activities of prepared materials were evaluated mainly toward organic pollutant degradation both at laboratory (chapter 3-5) and at pilot (chapter 6) scales.

In detail, chapter 2 focuses on the effect of contaminant physico-chemical properties on the reactivity via photo-assisted Fenton catalysis. Several *para*-substituted phenols were used in order to cover a wide range of electronics effects. Many physico-chemical descriptors were correlated with the initial Fenton and photo-Fenton degradation rates (r_0). Electronic descriptors such as calculated zero point energy (E_{zero}) and energy of the highest occupied orbital were found to be the most adequate to predict Fenton and photo-assisted Fenton reactivity.

The preparation of iron oxide-coated polymer films is described in chapter 3. Polyvinyl fluoride (PVF) film surface was functionalized by different methods, either by Vacuum-UV radiation, radio-frequency plasma, photo-Fenton oxidation or TiO_2 photocatalysis. These pre-treatments were performed to increase iron oxide adhesion to polymer surface. Afterward the functionalized polymers films were immersed in an aqueous solution for the deposition of iron oxide layer by hydrolysis of $FeCl_3$. The catalytic activities of resulting materials were compared during

hydroquinone degradation in presence of H₂O₂ and under simulated solar light illumination. The most efficient and stable catalyst obtained was prepared by means of TiO₂ photocatalytic functionalization of polymers followed by iron oxide coating (leading to so called P^f-TiO₂-Fe oxide), therefore this preparation procedure was selected in chapters 4-6.

Chapter 4 focuses on the study of the mechanisms involved during the preparation and use of P^f-TiO₂-Fe oxide. In particular, the modifications induced by TiO₂ photocatalysis on polymer surface such as oxygen group formation and deposition of TiO₂ particles were characterized by x-ray photoelectron spectroscopy (XPS), scanning electron microscopy (SEM), and UV-visible spectrophotometry. The photocatalytic activity of P^f-TiO₂-Fe oxide in presence of H₂O₂ and under simulated solar light radiation was evaluated toward HQ degradation. The occurrence of important synergistic effects between TiO₂ and iron oxide was discussed. Finally, the effect of preparation parameters on photocatalytic activity of P^f-TiO₂-Fe oxide/H₂O₂/light system was determined allowing the optimization of preparation procedure. Hence highly efficient photocatalysts for hydroquinone degradation and *E. Coli* inactivation were obtained.

The degradation of hydroquinone and nalidixic acid (NA) mediated the system P^f-TiO₂-Fe oxide/H₂O₂/light was examined (chapter 5). The contribution of homogeneous photo-Fenton oxidation in the degradation process was determined and the mechanisms involved in iron leaching are discussed. Besides, the effect of operational parameters on degradation rates was assessed. The rates are independent on initial pH and NaCl presence but were enhanced by increasing temperature. Long-term stability of P^f-TiO₂-Fe oxide was evaluated by repetitive nalidixic acid degradation runs.

The adaptation of P^f-TiO₂-Fe oxide to pilot scale in a compound parabolic collector (CPC) solar photoreactor is described in chapter 6: solar photocatalytic degradation of phenol, nalidixic acid, mixture of pesticides, and another of emerging contaminants, in water was investigated. The influences of operational pH and pollutant structure on the degradation rates were evaluated. It was found that compounds with chelating moieties (or carboxylic acids) were the most quickly removed by P^f-TiO₂-Fe oxide/H₂O₂/light and allowed the photo-Fenton catalyst to be efficient at higher pH values.

Keywords: Structure reactivity relationship, heterogeneous photo-Fenton, polymer surface modifications, solar water decontamination, solar material preparation, TiO₂ photocatalysis, TiO₂/iron oxide synergy.

RESUME

Le travail présenté dans cette thèse fait partie du projet Européen INNOWATECH. L'objectif global de ce projet a été de fournir des solutions technologiques efficaces pour le traitement des eaux usées industrielles, de proposer de nouveaux concepts dans le domaine du traitement des eaux usées avec des bénéfices potentiels pour la protection de l'environnement. L'oxydation par la réaction Fenton photo-assistée (photo-Fenton) a été étudiée en particulier. Il s'agit d'une technologie prometteuse pour décontaminer les eaux usées industrielles car elle utilise l'énergie naturelle offerte par le soleil, des produits chimiques abondants (des ions fer et de l'eau oxygénée) et ne produit pas de déchets toxiques. Mis à part un court détour au sujet de la réaction photo-Fenton homogène (chapitre 2), où l'influence des propriétés physico-chimiques des polluants sur la réactivité a été étudiée, cette thèse se concentre sur le traitement photo-Fenton utilisant un nouveau catalyseur solide. L'immobilisation d'oxyde de fer sur un support est une stratégie proposée pour surmonter les limitations pratiques liées au traitement photo-Fenton homogène (i.e. le domaine de pH limité où la réaction est efficace et les problèmes induits par la séparation du catalyseur de l'effluent). La préparation et la caractérisation d'un nouveau catalyseur constitué d'oxyde de fer déposé sur des films polymériques modifiés est décrit aux Chapitres 3 et 4. L'activité photocatalytique des matériaux préparés a été évaluée principalement en dégradant des polluants organiques à l'échelle du laboratoire (chapitres 3-5) mais aussi à plus grande échelle (chapitre 6).

Plus précisément le chapitre 2 traite de l'influence des propriétés physico-chimiques des polluants sur leur réactivité lors du traitement photo-Fenton. Plusieurs phénols *para*-substitués ont été utilisés pour couvrir une large gamme d'effets électroniques. De nombreux paramètres physico-chimiques ont été corrélés avec les vitesses de dégradation initiales lors des traitements Fenton et photo-Fenton. Les paramètres électroniques tels que l'énergie du point zéro, l'énergie de la plus haute orbitale occupée ont été les plus adéquats pour prédire la réactivité Fenton et photo-Fenton.

La préparation de polymères couverts d'oxyde de fer est décrite au chapitre 3. Des films de polyvinyle fluorure ont été fonctionnalisés par différentes méthodes : par irradiation ultraviolette du vide ; plasma ; oxydation photo-Fenton ; photocatalyse utilisant TiO₂. Ces prétraitements ont

été effectués pour favoriser l'adhésion d'oxyde de fer sur la surface des polymères. Pour la déposition d'oxyde de fer, les films polymériques fonctionnalisés ont été immergés dans une solution aqueuse où s'est déroulée l'hydrolyse du FeCl_3 . Les activités catalytiques des matériaux préparés ont été comparées pendant la dégradation de l'hydroquinone en présence d'eau oxygénée et sous illumination solaire simulée. Les matériaux les plus efficaces et les plus stables ont été obtenus en fonctionnalisant des polymères par photocatalyse au TiO_2 puis en y déposant l'oxyde de fer (conduisant au matériau appelé $\text{P}^{\text{f}}\text{-TiO}_2\text{-Fe}$ oxyde). Par conséquent cette procédure de préparation a été sélectionnée pour les chapitres 4-6.

Le chapitre 4 se concentre sur l'étude des mécanismes impliqués lors de la préparation du $\text{P}^{\text{f}}\text{-TiO}_2\text{-Fe}$ oxyde. En particulier, les modifications induites à la surface des polymères lors du traitement photocatalytique au TiO_2 , telles que la formation de groupes oxygénés et la déposition de particules de TiO_2 , ont été caractérisées par spectroscopie photoélectronique à rayonnements X (XPS), par microscopie électronique à balayage (SEM), et par spectrophotométrie UV-visible. L'activité catalytique du $\text{P}^{\text{f}}\text{-TiO}_2\text{-Fe}$ oxyde a été évaluée en dégradant de l'hydroquinone en présence d'eau oxygénée et sous illumination solaire simulée. L'occurrence d'effets synergiques importants entre le TiO_2 et l'oxyde de fer a été étudiée. Finalement l'influence des paramètres de préparation sur l'activité photocatalytique du système $\text{P}^{\text{f}}\text{-TiO}_2\text{-Fe}$ oxyde/ H_2O_2 /lumière a été déterminée ce qui a permis d'optimiser la procédure de préparation. Ainsi des catalyseurs efficaces pour dégrader l'hydroquinone et inactiver *E. Coli* ont été obtenus.

La dégradation de l'acide nalidixique et de l'hydroquinone par le système $\text{P}^{\text{f}}\text{-TiO}_2\text{-Fe}$ oxyde/ H_2O_2 /lumière a été examinée (chapitre 5). La contribution de la réaction photo-Fenton homogène dans le procédé de dégradation a été déterminée et les mécanismes impliqués lors de la dissolution des ions fer ont été discutés. Par ailleurs, l'effet des paramètres de réaction sur les vitesses de dégradation ont été évalués. Il a été observé que la vitesse de dégradation est indépendante du pH initial et de la présence de NaCl mais augmente avec la température. La stabilité du $\text{P}^{\text{f}}\text{-TiO}_2\text{-Fe}$ oxyde a été évaluée en répétant des dégradations d'acide nalidixique.

Au chapitre 6 est décrite l'utilisation du $\text{P}^{\text{f}}\text{-TiO}_2\text{-Fe}$ oxyde à plus grande échelle dans des photo-réacteurs paraboliques pour la dégradation photocatalytique solaire de phénol, d'acide nalidixique, un mélange de pesticides et un autre mélange de polluants émergents. L'influence du pH et de la structure des polluants sur les vitesses de dégradation a été étudiée. Il a été observé que les polluants contenant des groupes chélates (ou des acides carboxyliques) ont été

plus rapidement éliminés et ont permis au catalyseur d'être plus efficace a des valeurs de pH élevées.

Mots clefs: Relation structure réactivité, photo-Fenton hétérogène, modifications de la surface des polymères, décontamination de l'eau avec le soleil, préparation de matériaux avec le soleil, photocatalyse au TiO₂, synergie TiO₂/oxyde de fer.

TABLE OF CONTENTS

ACKNOWLEDGEMENTS	i
SUMMARY	iii
RESUME	v
TABLE OF CONTENTS	ix
LIST OF SYMBOLS	xv
LIST OF FIGURES	ixx
LIST OF TABLES	xxv
1. INTRODUCTION	1
1.1. Overview	1
1.2. Background	3
1.2.1. Advanced Oxidation Processes (AOP)	3
1.2.2. Semiconductor photocatalysis	4
<i>1.2.2.1. Semiconductors properties</i>	<i>4</i>
<i>1.2.2.2. TiO₂ photocatalysis</i>	<i>6</i>
1.2.3. Homogeneous photo-Fenton	9
<i>1.2.3.1. Aquatic iron chemistry</i>	<i>9</i>
<i>1.2.3.2. Fenton chemistry</i>	<i>10</i>
<i>1.2.3.3. Fenton reaction in presence of inorganic and organic substances</i>	<i>11</i>
<i>1.2.3.4. Photo-assisted Fenton reaction</i>	<i>15</i>
1.2.4. Photo-Fenton reaction using iron from solid source	17
<i>1.2.4.1. Fenton reaction with iron oxides</i>	<i>17</i>
<i>1.2.4.2. Iron oxide photocatalysis</i>	<i>18</i>
<i>1.2.4.3. Photo-Fenton reaction using iron from oxides</i>	<i>18</i>

1.2.4.4.	<i>Photo-Fenton reaction with iron from other solid sources</i>	20
1.2.4.5.	<i>Photo-Fenton reaction using designed heterogeneous catalyst.</i>	21
1.3.	Objectives	24
1.4.	Studied water contaminants	24
1.4.1.	<i>Substituted phenols</i>	24
1.4.2.	<i>Model contaminants</i>	25
1.4.3.	<i>Real pollutants</i>	25
1.5.	References	28
2.	PHYSICO-CHEMICAL PROPERTIES AND PHOTOREACTIVITY RELATIONSHIP IN PHOTOASSISTED FENTON SYSTEM	37
2.1.	Introduction	37
2.2.	Experimental	38
2.2.1.	Chemicals	38
2.2.2.	Photoreactor and irradiation procedures	39
2.2.3.	Analysis of the irradiated solutions	40
2.3.	Results and discussions	41
2.3.1.	Preliminary experiments	41
2.3.1.1.	<i>Selection of Fenton reactant concentration</i>	41
2.3.1.2.	<i>UV-visible spectrum measurements</i>	42
2.3.1.3.	<i>Photolysis experiments</i>	42
2.3.1.4.	<i>Fenton degradation of para-substituted phenols</i>	43
2.3.2.	Photo-Fenton experiments	45
2.3.3.	Quantitative structure reactivity relationship	47
2.3.3.1.	<i>QSRR for Fenton degradation</i>	48
2.3.3.2.	<i>QSRR for photo-Fenton degradation</i>	49
2.3.4.	Evaluation of biodegradability of photo-Fenton treated solution	49
2.4.	Conclusions	51
2.5.	References	51
3.	SYNTHESIS OF IRON OXIDE COATED FUNCTIONALIZED POLYMERS : EFFECT OF SURFACE TREATMENT ON PHOTOCATALYTIC ACTIVITY	55

3.1. Introduction	55
3.1.1. Radiative treatments of polymer surfaces	
3.1.1.1. <i>Plasma treatments</i>	56
3.1.1.2. <i>Vacuum UV (V-UV) treatments</i>	57
3.1.2. Photocatalytic treatments of polymer surfaces	58
3.2. Material and method	59
3.2.1. Chemicals	59
3.2.2. Photocatalyst preparation	59
3.2.2.1. <i>Functionalization with radio frequency Plasma (RF-P)</i>	60
3.2.2.2. <i>Functionalization with V-UV</i>	60
3.2.2.3. <i>Functionalization with photo-Fenton</i>	60
3.2.2.4. <i>Functionalization with TiO₂ photocatalysis</i>	61
3.2.3. Photoreactor and irradiation procedure	61
3.2.4. Analysis of the irradiated solutions	62
3.2.5. Catalyst characterization by UV-visible spectrophotometry	62
3.3. Results and discussions	63
3.3.1. Effect of functionalization on photocatalytic activity of PVF^f-Fe oxide	63
3.3.2. Effect of functionalization on long-term stability of PVF^f-Fe oxide	66
3.4. Conclusions	68
3.5. References	69
4. TiO₂ AND IRON OXIDE COATED POLYMERS: CHARACTERIZATION, OPTIMISATION, SYNERGISTIC PHOTO-ACTIVITY.	71
4.1. Introduction	71
4.2. Experimental	72
4.2.1. Chemicals	72
4.2.2. Photocatalyst preparation	72
4.2.3. Photoreactor and irradiation procedure	73
4.2.4. Analysis of the irradiated solutions	73
4.2.5. Bacterial strain and growth media	73
4.2.6. Photocatalyst characterization	75
4.2.6.1. <i>X-ray photoelectron spectroscopy (XPS)</i>	75

4.2.6.2.	<i>Scanning electron spectroscopy (SEM)</i>	76
4.2.6.3.	<i>UV-Visible Spectrophotometry</i>	77
4.3.	Results and discussions	77
4.3.1.	PVF^f-TiO₂-Fe oxide characterization	77
4.3.1.1.	<i>XPS study of the influence of pH on TiO₂ photocatalytic surface functionalization-deposition (PSFD) treatment of polyvinyl fluoride film</i>	77
4.3.1.2.	<i>XPS studies of iron species and overall atomic profile of the PVF^f-TiO₂-Fe oxide photocatalyst</i>	81
4.3.1.3.	<i>Scanning electron microscopy (SEM)</i>	83
4.3.1.4.	<i>UV-Visible absorbance study</i>	84
4.3.2.	Photocatalytic activity	85
4.3.3.	Synergistic effects	89
4.3.4.	Optimization: effect of preparation parameters on the activity of catalysts	92
4.3.4.1.	<i>Effect of polymer film nature</i>	92
4.3.4.2.	<i>Effect of the pH during TiO₂ PSFD treatment</i>	94
4.3.4.3.	<i>Effect of TiO₂ concentration used for the TiO₂ PSFD treatment</i>	95
4.3.4.4.	<i>Effect of iron oxide coating conditions</i>	96
4.3.4.5.	<i>Effect of preparation on Bacterial inactivation</i>	97
4.4.	Conclusions	99
4.5.	References	100
5.	TiO₂ AND IRON OXIDE COATED POLYMERS: INFLUENCE OF REACTION PARAMETERS ON PHOTOCATALYTIC ACTIVITY , LONG-TERM STABILITY	103
5.1.	Introduction	103
5.2.	Experimental	104
5.2.1.	Chemicals	104
5.2.2.	Photocatalyst preparation	104
5.2.3.	Photoreactor and irradiation procedure	104
5.2.4.	Analysis of the irradiated solutions	105
5.2.5.	Photocatalyst characterization.	105

5.3. Results and discussions	105
5.3.1. Photocatalytic activity toward hydroquinone and nalidixic acid degradation	105
5.3.2. Iron leaching and homogeneous photocatalytic contribution	107
5.3.3. Initial activation of PVF^f-TiO₂-Fe oxide photocatalyst	109
5.3.4. Correlations between surface modifications and activation processes	110
5.3.4.1. <i>X-ray photoelectron spectroscopy (XPS) analysis of PVF^f-TiO₂-Fe oxide</i>	<i>110</i>
5.3.4.2. <i>Secondary electron microscopy (SEM)</i>	<i>112</i>
5.3.4.3. <i>Discussion about initial activation of PVF^f-TiO₂-Fe oxide and increase of synergistic effects</i>	<i>113</i>
5.3.5. Effect of reaction conditions on photocatalytic activity	113
5.3.5.1. <i>Effect of pH</i>	<i>113</i>
5.3.5.2. <i>Effect of temperature</i>	<i>115</i>
5.3.5.3. <i>Effect of NaCl</i>	<i>117</i>
5.3.6. Long term Stability of PVF^f-TiO₂-Fe oxide	118
5.3.7. Reversible iron dissolution	119
5.4. Conclusions	120
5.5. References	121
6. SCALE UP: FIELD SOLAR DEGRADATION OF PESTICIDES AND EMERGING WATER CONTAMINANTS	123
6.1. Introduction	123
6.1.1. Solar resource	113
6.1.2. Solar collector technology	125
6.1.2.1. <i>Concentrating collectors</i>	<i>125</i>
6.1.2.2. <i>Non concentrating collectors</i>	<i>126</i>
6.1.2.3. <i>Compound parabolic collectors (CPC)</i>	<i>126</i>
6.2. Experimental	128
6.2.1. Chemicals	128
6.2.2. Photocatalyst preparation	129
6.2.3. Photo-reactor and irradiation procedure	129

6.2.4. Analysis of the irradiated solutions	130
6.2.5. Photocatalyst characterization	131
6.3. Results and discussions	131
6.3.1. Photocatalytic degradation of single compounds	131
6.3.2. Photocatalytic degradation of compound mixtures	134
6.3.2.1. Pesticide mixture	134
6.3.2.2. Emerging contaminants mixture	136
6.3.3. Long-term stability	138
6.4. Conclusions	141
6.5. References	142
7. CONCLUSIONS AND PERSPECTIVES.	145
APPENDICES	
I -Electronic descriptors (E_{HOMO} , $E_{1/2}$, σ , E_{ZERO}) as a function of initial rates of degradation (r^{F}_0) for the Fenton reaction and linear fittings (p-Cl excluded)	151
II- Electronic descriptors (E_{HOMO} , $E_{1/2}$, σ , E_{ZERO}) as a function of initial rates of degradation ($r_{\text{pf}0}$) for the photo-Fenton reaction and linear fittings (p-Cl and p-CHO excluded)	152
CURRICULUM VITAE	153

LIST OF SYMBOLS

A		Electron acceptor
AA		Aliphatic acid
AOP		Advanced oxidation processes
BE	[eV]	Binding energy
BOD	[mg/L]	Biological oxygen demand
C		Correction factor
c	[m/s]	Speed of light
CB		Conduction band
CFU		Colony forming units
CPC		Compound parabolic collectors
CPS		Counts per second
D		Electron donor
DOC	[mg/L]	Dissolved organic carbon
e^-_{cb}		Conduction band electron
E_{bg}	[eV]	Band gap energy
E_{HOMO}	[eV]	Energy of the highest occupied molecular orbital
ESCA		Electronic spectroscopy for chemical analysis
$E_{1/2}$	[V]	Experimental half wave potential
E_{zero}	[eV]	Calculated zero point corrected energy
$[Fe]_d$	[mg/L]	Dissolved iron concentration
HQ		Hydroquinone
HPLC		High performance liquid chromatography
h		Planck constant
h_t		Homogeneous percentage
h^+_{vb}		Valence band hole
k		Rate constants
K		Acidity constant

K_{ow}		1-octanol/water partition coefficient
L		Mono- and dicarboxylic acids
LB		Luria-bertani
λ	[nm]	Wavelength
λ_{max}	[nm]	Experimental maximal absorption wavelength
ν	[Hz]	Frequency
NHE	[V]	Normal hydrogen electrode
PCA		Plate count agar
P-FO		Photo-Fenton oxidation
p-H		Phenol
p-NO₂		4-nitrophenol
p-Cl		4-chlorophenol
P-CHO		4-hydroxybenzaldehyde
p-OCH₃		4-methoxyphenol
p-OH		4-hydroxyphenol
P		Polymer film
P^f		Functionalized polymer film
P-Fe oxide		Iron oxide coated polymer film
P^fTiO₂-Fe oxide		Iron oxide and titanium oxide supported on P^f
PE		Polyethylene
PET		Polyethylene terephthalate
PTC		Parabolic-trough concentrators
PSA		Plataforma solar de Almeria
PSFD		Photocatalytic surface functionalization deposition
PVF		Polyvinyl fluoride
pKa		Acidity constant
QSRR		Quantitative structure-reactivity relationships
R		Organic compound
R₀	[μmol/min]	Initial rate of degradation
R_{ads}		Adsorbed organic compound
RF-P		Radiofrequency plasma

S		Synergistic factor
σ		Hammett constants
SDT		Self degradation test
SEM		Scanning electron microscopy
t_{30w}	[min]	Normalized illumination time
Ti-PC		TiO₂ photocatalysis
TOC	[mg/L]	Total organic carbon
UV		Ultra-violet
VB		Valence band
VUV		Vacuum ultraviolet
XPS		X-ray photoelectron spectroscopy

LIST OF FIGURES

Figure 1.1 AOP recently studied implying the central role of the OH-radical.....	3
Figure 1.2 Fate of electrons and holes within a spherical particle of semiconductor in the presence of an electron acceptor (A) and donor (D), (Ollis, 1993).....	5
Figure 1.3 TiO ₂ semiconductor photocatalysis process: scheme showing some photochemical and photophysical events that might be taking place on an irradiated semiconductor particle.....	7
Figure 1.4 Ferric ion species present in aqueous solution at different pH at a concentration of 20 mg/L, calculated with equilibrium constants (Flynn, 1984), T = 20 °C.....	10
Figure 1.5 <i>Para</i> -substituted phenols (X = NO ₂ , Cl, H, CHO, H, OCH ₃ , OH).....	25
Figure 1.7 Chemical structure of nalidixic acid.....	26
Figure 1.8 Chemical structure and name of the pesticides studied.....	26
Figure 1.9 Names, structures and properties of emergent organic pollutants chosen for pilot scale study.....	27
Figure 2.1 Transversal cut and characteristics of the photo-reactor.....	39
Figure 2.2 Photocatalytic setup: (1) tanks; (2) peristaltic pump; (3) photo-reactors; (4) solar simulator.....	40
Figure 2.3 Substance (unfilled symbols) and TOC (filled symbols) removal during photo-Fenton degradation of phenol (1.8 mM) for different Fe ²⁺ concentrations (-●- : 10 mg/L; -■- : 3 mg/L; -▲- : 1 mg/L) in presence of H ₂ O ₂ (15 mM).	41
Figure 2.4 Evolution of <i>para</i> -substituted phenols concentration during photolysis in presence of Fe ²⁺ (3 mg/L) at pH = 3.....	42
Figure 2.5 Evolution of p-Cl concentration during degradation in presence of Fe ²⁺ (3 mg/L) at pH = 3 under: (a) irradiation; (b) dark conditions.	43

Figure 2.6 Evolution of <i>para</i> -substituted phenols concentration during Fenton degradation in presence of Fe ²⁺ (3 mg/L) at pH = 3 with H ₂ O ₂ (i) 1.8 mM; (ii) 7.2 mM.....	44
Figure 2.7 Evolution of <i>para</i> -substituted phenols concentration, during photo-Fenton degradation in presence of Fe ²⁺ (3 mg/L) at pH = 3 with H ₂ O ₂ 7.2 mM.....	45
Figure 2.8 TOC removal during <i>para</i> -substituted phenols photo Fenton degradation in presence of Fe ²⁺ at pH = 3 with H ₂ O ₂ 15 mM for (i) six carbon constituted compounds; (ii) seven carbon constituted compounds.....	46
Figure 3.1 Scheme of catalyst preparation strategy (not to the scale).....	59
Figure 3.2 Transversal cut and characteristics of the photo-reactor.....	61
Figure 3.3. Evolution of (i) HQ concentration, (ii) TOC and (iii) [Fe] _d during degradation of 0.18 mM of HQ at initial pH 5.7, in presence of 1.6 mM H ₂ O ₂ , 75 cm ² of catalyst under solar simulation (light): (o) photolysis; (a) PVF-Fe-oxide; (b) PVF ^{V-UV} -Fe-oxide and PVF ^{P-FO} -Fe oxide*; (c) PVF ^{RF-P} -Fe oxide; (d) PVF ^{Ti-PC} -Fe-oxide. The traces represent an average over three runs. *Due to similar result obtained for PVF ^{V-UV} -Fe-oxide and PVF ^{P-FO} -Fe oxide trace (b) represent the results relative to these two catalysts.....	63
Figure 3.4. UV-vis absorption spectrum of (a) PVF-Fe oxide, PVF ^{V-UV} -Fe oxide, PVF ^{P-FO} -Fe oxide; (b) PVF ^{RF-P} -Fe oxide; (c) PVF ^{Ti-PC} -Fe oxide.....	65
Figure 3.5 TOC removal during repetitive HQ photocatalytic degradations by (i) PVF-Fe oxide, (ii) PVF ^{V-UV} -Fe oxide, (iii) PVF ^{RF-P} -Fe oxide and (iv) PVF ^{Ti-PC} -Fe oxide (experimental conditions: 0.18 mM of HQ, solar simulation, initial pH 5.7, H ₂ O ₂ 1.6 mM).....	67
Figure 4.1 X-ray photoelectron spectra of: (i) C (1s); (ii) O (1s); (iii) F (1s) core level photoelectron spectra of (a) PVF; (b) PVF after a TiO ₂ -PSFD treatment at pH 11; (c) PVF after a TiO ₂ PSFD treatment at pH 3; (d) PVF ^f -TiO ₂ -Fe-oxide (TiO ₂ PSFD treatment at pH 3).....	78
Figure 4.2 X-ray photoelectron spectra of Ti (2p) in (a) PVF after a TiO ₂ PSFD treatment at pH 3; (b) PVF after a TiO ₂ PSFD treatment at pH 11.....	80

Figure 4.3 Mechanistic proposition for TiO ₂ photocatalytic surface functionalization-deposition as a function of pH.....	80
Figure 4.4 Fe (2p) core level photoelectron spectra of PVF ^f -TiO ₂ -Fe oxide.....	81
Figure 4.5 Depth profile of PVF ^f -TiO ₂ -Fe oxide (PSFD treatment at pH 3).....	82
Figure 4.6 Scanning electron microscopic images of: (a) PVF; (b) PVF ^f -TiO ₂ prepared at pH 5 (external side); (c) PVF ^f -TiO ₂ prepared at pH 5 (internal side); (d)-(e) PVF ^f -TiO ₂ -Fe oxide prepared at pH 5.....	84
Figure 4.7 UV-Visible absorption spectrum of: (a) PVF ^f -TiO ₂ ; (b) PVF-Fe oxide; (c) PVF ^f -TiO ₂ -Fe oxide; and (insert) photography of the three materials.....	85
Figure 4.8 Degradation of 0.18 mM of HQ, initial pH: 5.7, 75 cm ² of heterogeneous photocatalyst 1.6 mM H ₂ O ₂ under solar simulation: (a) bare light/dark adsorption; (b) PVF-TiO ₂ /light; (c) PVF ^f -TiO ₂ -Fe oxide/light; (d) PVF ^f -TiO ₂ /H ₂ O ₂ /light; (e) PVF ^f -TiO ₂ -Fe oxide/H ₂ O ₂ ; (f) PVF-Fe oxide/H ₂ O ₂ /light; (g) PVF ^f -TiO ₂ -Fe oxide/H ₂ O ₂ /light. The traces represent an average of three consecutive runs using the same photocatalysts (first run not included).....	86
Figure 4.9 TOC removal of 0.18 mM of HQ, initial pH: 5.7, 75 cm ² of heterogeneous photocatalyst 1.6 mM H ₂ O ₂ under solar simulation: (a) PVF ^f -TiO ₂ -Fe oxide/H ₂ O ₂ ; (b) Fe ²⁺ (0.3 mg/L)/H ₂ O ₂ /light; (c) PVF-Fe oxide/H ₂ O ₂ /light; (d) PVF ^f -TiO ₂ -Fe oxide/H ₂ O ₂ /light. The traces represent an average of three consecutive runs using the same photocatalysts (first run not included).....	87
Figure 4.10 Schematic representation of possible synergistic photocatalytic action in the system PVF ^f -TiO ₂ -Fe oxide/H ₂ O ₂ /light: (i) under visible light irradiation and (ii) under ultraviolet light irradiation.....	91
Figure 4.11 Structure of polymer substrate used: from left to right polyethylene terephthalate (PET), polyethylene (PE) and polyvinyl fluoride (PVF).....	92
Figure 4.12 Evolution of (i) TOC, (ii) HQ concentration and (iii) [Fe] _d during degradation of 0.18 mM of HQ at initial pH 5.7, in presence of 1.6 mM H ₂ O ₂ , 75 cm ² of catalyst (PE ^f -TiO ₂ -Fe oxide, PVF ^f -TiO ₂ -Fe oxide, PET ^f -TiO ₂ -Fe oxide) under solar simulation for different polymeric substrates. The traces represent an average over three runs.....	93

Figure 4.13 TOC removal of 0.18 mM of HQ, initial pH: 5.7, 75 cm² of heterogeneous photocatalyst 1.6 mM H₂O₂ under solar simulation: (a) PVF-Fe-oxide/H₂O₂/light; (b) PVF^f-TiO₂-Fe oxide (PSFD treatment at pH 11)/H₂O₂/light; (c) PVF^f-TiO₂ Fe oxide (PSFD treatment at pH 3)/H₂O₂/light.....95

Figure 4.14 Effect of TiO₂ concentration (used for previous PSFD treatment of PVF) on HQ mineralization (of 0.18 mM HQ, initial pH = 5.7, PVF^f-TiO₂-Fe oxide 75 cm², H₂O₂ 1.6 mM under solar simulation): (a) first; (b) second consecutive HQ degradation.....96

Figure 4.15 Photography of PET_b^f-TiO₂-Fe oxide used in this study.....97

Figure 4.16 Inactivation of *E. coli* on PET bottle reactors (experimental conditions presented in Table 4.3).....98

Figure 5.1 Degradation of 0.18 mM of HQ, initial pH 5.7, 30 °C, 1.6 mM H₂O₂, 75 cm² of heterogeneous photocatalyst under solar simulation (a) TOC removal by 0.3 mg/L Fe²⁺/H₂O₂/light; (b) TOC removal by PVF-Fe oxide/H₂O₂/light; (c) TOC removal by PVF^f-TiO₂-Fe oxide/H₂O₂/light; (d) HQ degradation by PVF^f-TiO₂-Fe oxide/H₂O₂/light. The traces represent an average over 3 runs.....106

Figure 5.2 Degradation of 0.18 mM of NA, initial pH 6.5, 30 °C, 3.2 mM H₂O₂, 75 cm² of PVF^f-TiO₂-Fe oxide under solar simulation (a) TOC removal by 0.3 mg/L Fe²⁺/H₂O₂/light; (b) TOC removal by PVF^f-TiO₂-Fe oxide/H₂O₂/light; (c) NA degradation by PVF^f-TiO₂-Fe oxide/H₂O₂/light. The traces represent average over 3 runs.....106

Figure 5.3 Evolution of dissolved iron concentration during degradation of 0.18 mM of pollutant, Initial pH 5.7, 30 °C, 75 cm² of heterogeneous photocatalyst under solar simulation (a) HQ, PVF-Fe oxide/H₂O₂(1.6 mM)/light; (b) HQ, PVF^f-TiO₂-Fe oxide/H₂O₂(1.6 mM)/light; (c) NA, PVF^f-TiO₂-Fe oxide/H₂O₂(3.2 mM)/light. The traces represent average dissolved iron over 3 runs.....107

Figure 5.4 Evolution of (i) normalized TOC concentration and (ii) Dissolved iron concentration during the two first photocatalytic mineralization of HQ: (a) first; (b) second run (experimental conditions: 0.18 mM HQ, initial pH 5.7, 30 °C, 1.6 mM H₂O₂, 75 cm² of heterogeneous photocatalyst under solar simulation).....109

Figure 5.5 F(1s) photoelectron spectra of (a) PVF ^f -TiO ₂ -Fe oxide as prepared (b) PVF ^f -TiO ₂ -Fe oxide after three runs.....	111
Figure 5.6 Scanning electron microscopic images of PVF ^f -TiO ₂ -Fe oxide (i)-(ii) before and (iii)-(iv) after three runs.....	112
Figure 5.7 Variation of (i) HQ and TOC normalized concentrations (ii) pH and (iii) [Fe] _d during degradation of 0.18 mM of HQ, 1.6 mM H ₂ O ₂ , 30 °C, 75 cm ² of PVF ^f -TiO ₂ Fe oxide under solar simulation and at different initial pHs.(a) 3.4, (b) 5.8, (c) 7.1.....	114
Figure 5.8 Variation of (i) HQ and TOC normalized concentrations and (ii) dissolved iron concentration during degradation of 0.18 mM of HQ, 1.6 mM H ₂ O ₂ , initial pH 5.7, 75 cm ² of PVF ^f -TiO ₂ -Fe-oxide under solar simulation and at different temperatures: (a) 55 °C, (b) 40 °C, (c) 30 °C.....	116
Figure 5.9 Variation of HQ and TOC normalized concentrations during degradation of 0.18 mM NA by (i) 75 cm ² of PVF ^f -TiO ₂ -Fe oxide, (ii) 2 mg/L Fe ²⁺ : TOC removal (a) in presence and (b) without NaCl; NA degradation (c) in presence and (d) without NaCl. (experimental conditions at initial pH 6.5, 30 °C, 3.2 mM H ₂ O ₂ , 0.86 M NaCl under solar simulation).....	118
Figure 5.10 Repetitive NA degradation (experimental conditions: 0.18 mM NA, 30 °C, solar simulation, initial pH = 6.5, PVF ^f -TiO ₂ -Fe oxide 75 cm ² , H ₂ O ₂ 3.2 mM).....	119
Figure 6.1 solar radiation spectrums from 0.2 to 4.5 μm.....	124
Figure 6.2 Air mass and solar components.....	125
Figure 6.3. CPCs: Collector design and radiation geometry profiles.....	127
Figure 6.4 Picture of PVF ^f -TiO ₂ -Fe oxide films in the CPC photoreactor.....	130
Figure 6.5. DOC and pH during phenol degradation (0.7 mM phenol, 6.2 mM H ₂ O ₂) (i) first and (ii) second set of experiments, (iii) DOC and pH during nalidixic acid degradation (0.13 mM nalidixic acid 3.1 mM H ₂ O ₂), and (iv) evolution of H ₂ O ₂ consumption. The degradations were mediated by PVF ^f -TiO ₂ -Fe oxide under solar light.....	133

Figure 6.6 Normalized pesticide concentrations (i), DOC (ii) during degradation mediated by PVF^f-TiO₂-Fe oxide in presence of 3.1 mM H₂O₂ (constant) under sunlight (DOC₀ = 50 mg/L).....134

Figure 6.7 Emerging contaminant concentrations during first (i)-(iii) and second (iv)-(vi) consecutive degradation tests mediated by PVF^f-TiO₂-Fe oxide under solar light and in presence of 3.1 mM (constant) H₂O₂.....137

Figure 6.8 Appearance of PVF^f-TiO₂-Fe oxide after 20 days of experiments: (i) effect of light on changes in appearance; (ii) Almost undamaged piece; (iii) severely damaged piece.....139

Figure 6.9 Fe (2p) core level photoelectron spectrum of as-prepared catalyst (PVF^f-TiO₂-Fe oxide), and pieces of catalysts (a-e) after 20 days of experiments.....139

Figure 6.10 Schematic changes occurring on PVF^f-TiO₂ Fe oxide surface after use (not to scale).....141

LIST OF TABLES

Table 2.1 Physico-chemical descriptors from literature and measured initial rate constants.....	47
Table 2.2 Correlation coefficients (R^2) obtained after linear regression in the plots of initial rates of degradation versus different descriptors (represented in appendices).....	48
Table 2.3 Homolytic dissociation energy of different bonds of the <i>para</i> -substituted phenols....	49
Table 2.4 BOD ₅ (mg/L) and ratio between (DBO ₅) and (TOC) before and after photo-Fenton treatment.....	50
Table 4.1 Atomic composition of original polymer surface (PVF), TiO ₂ PSFD treated polymer (PVF ^f -TiO ₂) at pH 3 and 11 (only principal constituents).....	79
Table 4.2 Initial HQ degradation rates relative to different photo-assisted processes.....	90
Table 4.3 Experimental conditions and observed rate constants for the bacterial inactivation tests in PET bottle reactors under simulated solar radiation.....	98
Table 5.1 Homogeneous percentage relative to different processes and times (Values calculated from Figures 1-3).....	108
Table 5.2 Composition of PVF ^f -TiO ₂ -Fe oxide surface (atomic percent) as prepared and after three runs.....	110
Table 6.1 Initial degradation rates with PVF ^f -TiO ₂ -Fe oxide /H ₂ O ₂ /light and zero order rate with Fe ³⁺ /H ₂ O ₂ /light (in µg/(L min)) for each compound in the pesticide mixture.....	135
Table 6.2 Composition of original polymer surface (PVF), as-prepared catalyst (PVF ^f -TiO ₂ -Fe oxide), and pieces of catalysts (a-e) after 20 days of experiments.....	140

1- INTRODUCTION

1.1 Overview

Water, this essential element for life, is abundant on earth (estimated volume of about $1.4 \times 10^9 \text{ km}^3$), however, 97.5% is salt water. Of the remaining 2.5% that is fresh water, 70% is frozen in the polar icecaps; the rest is mainly present as soil moisture or in inaccessible subterranean aquifers. Only less than 1% of the world's fresh water resources are readily available for human use; and this resource is very unevenly distributed (UNEP, 2003). Besides, the available fresh water is not always clean as it may contain natural toxic impurities (arsenic, fluoride, nitrate, bacteria) or be contaminated by human activities (pesticides, gasoline, solvents, and pharmaceuticals, waste from septic systems...).

Due to the lack of safe drinking water sources, every year millions of people, most of them children, die from diseases associated with inadequate water supply, sanitation, and hygiene. Every day thousands of children die because of dirty water; diseases transmitted through water or human excrement is one of the main cause of death among children worldwide (UN, 2005). Hence appropriate sanitation and water treatment systems have to be provided urgently to save lives.

The huge problem of water microbial contamination is completed by growing concerns related to the water cycle which focuses on water pollution caused by industrial, agricultural or other human activities, and the whole range of its impact on human health and ecosystems balance. Hence the actual increasing of worldwide pollution of the fresh water supply by thousands of industrial chemical compounds is also severe. Although most of these compounds are present at low concentrations, many of them are toxic, particularly when present as components of complex mixtures (Schwarzenbach, 2006). Among them, millions of tons of pesticides, which are highly toxic and bio-recalcitrant compounds, are used each year in agriculture. Other water pollutants such as pharmaceuticals, hormones, surfactants, synthetic musks etc. are more and more present in water which can lead to

bacterial resistance or sterility, among others. The degradation of bio-recalcitrant compounds before or after they are spread by adequate water treatment technologies is consequently an important issue.

The incapacity of conventional wastewater treatment methods to efficiently remove bio-recalcitrant pollutants evidences that new efficient treatment systems are needed. Advanced Oxidation Processes (AOP) are modern chemical methods for the treatment of waters containing non-biodegradable/toxic substances and to decontaminate drinking water (Legrini, 1993; Bahnemann, 1994; Herrera Melián, 2000; Rincon, 2001). With classical water treatment techniques such as flocculation, precipitation, adsorption on granular activated carbon, air stripping, reverse osmosis or combustion, pollutants are only transferred from one phase to another. AOP destroy the organic pollutants producing water, carbon dioxide and inorganic salts as end products.

For water disinfection in sunny countries, the application of solar-based AOP could constitute an alternative to conventional chlorination process, like HClO water disinfection, which leads to the generation of toxic chlorinated byproducts in the presence of natural organic matter.

The work presented in this thesis is a part of the European project INNOWATECH (innovative and integrated technologies for the treatment of industrial wastewater). The global objective of this project was to provide effective technological solutions for the treatment of industrial wastewater, to propose new concepts, processes and technologies in wastewater treatment. This should benefit for the quality of effluents, energy and operational costs saving, and protect the environment.

This thesis focuses on homogeneous and heterogeneous photo-Fenton process as well as TiO₂ photocatalysis for the treatment of water pollutants. These solar driven AOPs were used both to prepare photocatalysts absorbing the solar radiation and to degrade organic pollutants and inactivate bacteria.

1.2 Background

1.2.1 Advanced Oxidation Processes (AOP)

AOP refer to a set of chemical treatment procedures designed to remove organic compounds. AOP are also efficient to inactivate pathogenic bacteria present on water by oxidation. The AOP have in common the involvement of hydroxyl radicals ($\bullet\text{OH}$) as shown in Figure 1.1.

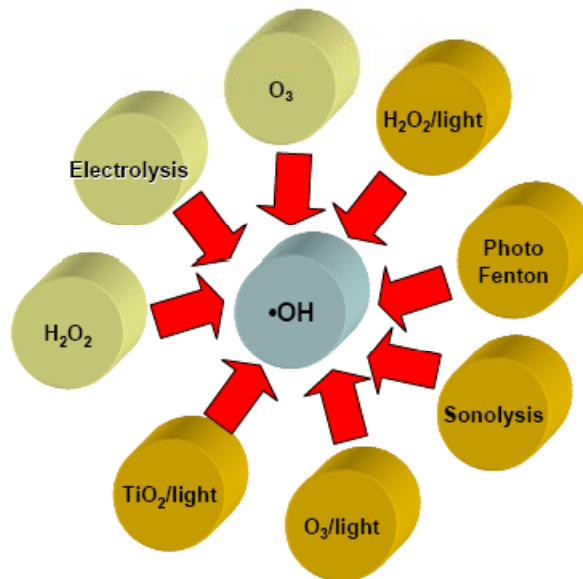
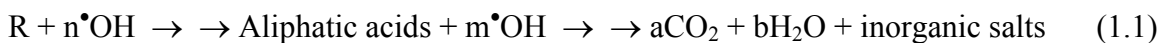


Figure 1.1 AOP recently studied implying the central role of the OH-radical

The generated oxidative radicals (such as $\bullet\text{OH}$ and $\bullet\text{O}_2^-$) are able to attack organic pollutants with an almost diffusion controlled rate constant leading to the formation of aliphatic acids (AA) and then to mineralization (Eq. 1.1). The oxidation reactions involving the hydroxyl radicals and organic substrates (R, PhX) are classified as hydrogen abstraction (Eq. 1.2), addition reactions, (Eq. 1.3) and electron transfer (Eq. 1.4, Peyton, 1990). Furthermore the radicals can induce lipid peroxidation on eukaryotic and prokaryotic cells membrane, leading to death of the microorganisms (Huang, 2000)





Recently the trend is to combine different AOP and determine the presence of synergistic effects. Among others, the combination of TiO₂ photocatalysis with photo-Fenton (Bouras et al. 2008), or sonolysis with ozonation (He, 2009) have been recently reported.

In the present work, the combination of photo-Fenton and TiO₂ photocatalysis supported on polymer substrates and the resulting synergistic effects are studied.

1.2.2 Semiconductor photocatalysis

1.2.2.1 Semiconductor properties

The electrons in semiconductors have an important feature: they do not have discrete energy levels; they present bands with continuous energy. Electronic structure of solid materials can be described in terms of electrons whose energy levels are so close that they can form a continuum of energy bands.

Semiconductors (e.g., TiO₂, ZnO, Fe₂O₃, CdS, ZnS, etc.) can act as sensitizers for light-induced redox processes due to their electronic structure, which is characterized by a filled valence band (VB) and an empty conduction band (CB). The two bands are separated by an energy gap particular to each semiconductor referred to as the band gap (E_{bg}). When the semiconductor is illuminated with light ($h\nu$) of greater energy than that of the band gap, an electron is promoted from the VB to the CB, thus leaving a positive hole in the valence band as illustrated in Figure 1-2.

After the separation, the electron (e^-) and hole (h^+) pair may recombine generating heat or can become involved in electron transfer reactions with other species in solution, like for example the oxidation or reduction of, respectively, electron-donor (D) or electron-acceptor (A) species shown in Figure 1-1. In the absence of suitable electron and hole scavengers, the stored energy is dissipated within a few nanoseconds by recombination.

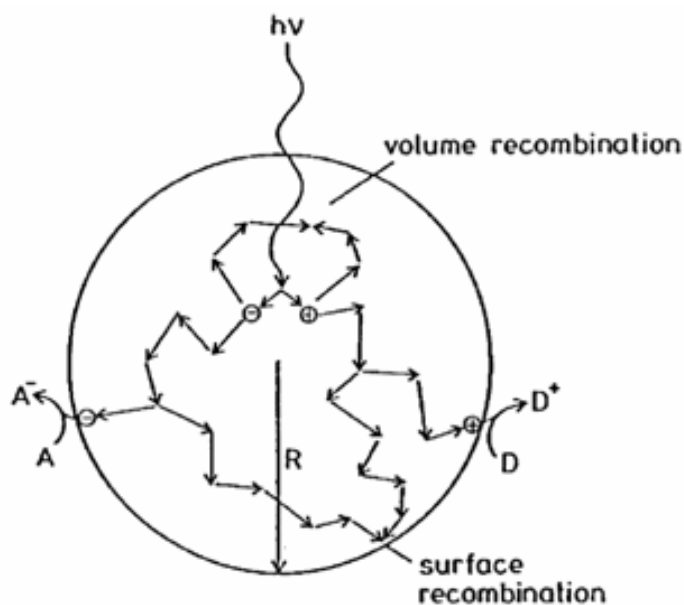


Figure 1.2 Fate of electrons and holes within a spherical particle of semiconductor in the presence of an electron acceptor (A) and donor (D), (Ollis, 1993).

For oxidation reactions to occur, the VB must have a higher oxidation potential than the reactant under consideration. The redox potential of the VB and the CB of different semiconductors varies between +4.0 and -1.5 Volts versus Normal Hydrogen Electrode (NHE). Therefore, by careful selection of the semiconductor photocatalyst, a wide range of species can be treated *via* these processes. Metal oxides and sulphides represent a large class of semiconductor materials suitable for photocatalytic purposes (Robertson 1996). However, to activate the catalyst, the radiation must have a wavelength λ equal or lower than the calculated by the Planck's equation (Eq. 1.5 where E_{bg} is the semiconductor band-gap energy, h is the Planck's constant and c is the speed of light).

$$\lambda \leq \frac{hc}{E_{bg}} \quad (1.5)$$

Another interesting feature of the semiconductor such as TiO_2 or Fe_2O_3 is the amphoteric character of their surface. Depending of the pH, a variation in the superficial charge can be observed. In aqueous media, the surface has water molecules adsorbed and alcohol groups

M-OH giving the amphoteric character to TiO_2 and Fe_2O_3 . The points charge zero (pH_{pzc}) on TiO_2 (anatase or rutile) and Fe_2O_3 are around 6-7. This means that at pH below this value, the M-OH groups will be protonated, charging positively the surface and allowing the adsorption of negatively charged molecules or surfaces. In contrast, beyond pH_{pzc} , the alcohol groups will be deprotonated, charging negatively the surface and allowing the adsorption of positively charged species.

1.2.2.2 TiO_2 photocatalysis

Among the numerous known semiconductors, titanium dioxide, TiO_2 , has proven to be the most suitable for widespread environmental applications. Titanium dioxide is abundant, chemically inert, stable to photo- and chemical corrosion; inexpensive and relatively non-toxic. The toxicity of TiO_2 under the form of nanoparticles is currently under study (IARC, 2006; Ramsden, 2009). Furthermore TiO_2 is of special interest since it can use natural (solar) UV radiation. Indeed TiO_2 has an appropriate energetic separation between its valence and conduction bands, which can be surpassed by the energy of a UV solar photon. The TiO_2 VB and CB energies are respectively +3.1 and -0.1 volts, thus its band gap energy is 3.2 eV, and therefore absorbs in the near UV light ($\lambda < 387$ nm).

TiO_2 is used for many applications. It is the most widely used white pigment because of its brightness and very high refractive index. Approximately 4 million tons of TiO_2 are consumed annually worldwide. TiO_2 pigments are employed in paints, coatings, plastics, papers, foods (E171), medicines, cosmetics, toothpastes, tattoo...

It exists in three crystalline forms: anatase, rutile, and brookite. Anatase and rutile are the most common forms, and anatase is the most effective in wastewater treatment (Mills, 1997).

The commercially available, titanium dioxide Degussa P25 has become a standard photocatalyst in environmental applications (Hoffmann, 1995; Mills, 1997; Litter 1999). It is produced through high-temperature (greater than 1200°C) flame hydrolysis of TiCl_4 , in the presence of hydrogen and oxygen. The TiO_2 is then treated with steam to remove HCl, which is also produced as by product. The end product is 99.5% pure TiO_2 (anatase:rutile ratio, 75:25), is non-porous, and in the form of rounded edges cubic particles. The P25 TiO_2

powder has a surface area of $56 \text{ m}^2 \text{ g}^{-1}$, and an average particle diameter of 25-35 nm. It is important to notice that 90% of the material does not exist as isolated particles, but rather as irreducible complex primary aggregates, of approximately $0.1 \text{ }\mu\text{m}$ in diameter. The VB and CB positions for Degussa P-25 have been calculated as +2.9 and -0.3 V, respectively, at pH=0 (Martin, 1994).

To date, the widely accepted theory is that hydroxyl radical ($\text{OH}\cdot$) is the main oxidizing specie responsible for photo-oxidation of the majority of the studied organic compounds (Legrini et al. 1993). Indeed, after absorption of near ultraviolet radiation at $\lambda < 387 \text{ nm}$, electron/hole pairs (Eq. 1.6) separated between the CB and VB are generated, as shown in Figure 1-3.

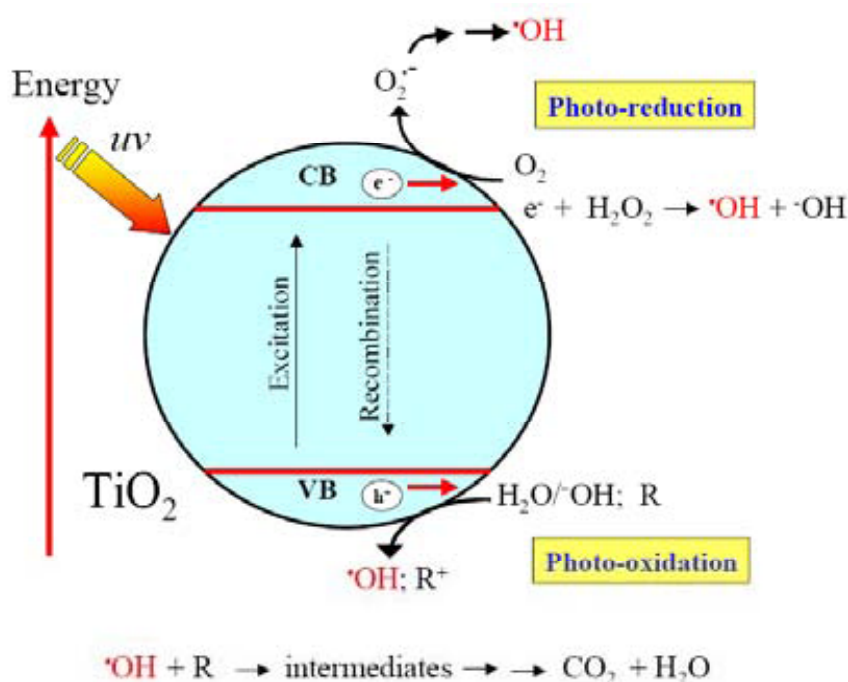
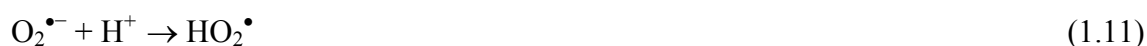
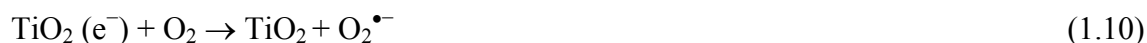


Figure 1.3 TiO_2 semiconductor photocatalysis process: scheme showing some photochemical and photophysical events that might be taking place on an irradiated semiconductor particle

The different events that take place once the UV light has been absorbed by TiO₂ particles and the subsequent electrons (e⁻_{CB}) and holes (h⁺_{VB}) have been generated and partially separated, are summarized in Equations 1.7 to 1.14 and in Figure 1-3. Three oxidation reactions have been experimentally investigated: electron transfer from adsorbed organic (Eq. 1.7), H₂O (Eq. 1.8), and OH⁻ (Eq. 1.9) adsorbed on the catalyst surface. Reactions 1.8 and 1.9 appear to be of great importance in oxidative degradation processes, most probably due to the high concentration of OH⁻ and H₂O adsorbed on the TiO₂ surface.



To avoid recombination, an electron acceptor must be present. Molecular oxygen is generally the acceptor species in an electron transfer reaction with the photocatalyst CB (Eq. 1.10). Superoxide anion or its protonated form can dismute (Eq. 1.12-1.13) to yield hydrogen peroxide or peroxide anion (Ishibashi, 1998; Nosaka, 2002).



It has also been shown that hydrogen peroxide addition considerably enhances the photodegradation rate, most probably *via* reaction 1.14, or by surface-catalysed dismutation of H₂O₂ (Wolfrum, 1994; Pichat, 1995).



1.2.3 Homogeneous photo-Fenton

1.2.3.1 Aquatic iron chemistry

Behind oxygen, silicon and aluminium, iron is the fourth most abundant element in the earth's crust. It occurs in oxidation states from $-II$ to $+VI$ with coordination numbers of 3 to 8 (Hawker, 1994). Desert sands, dust and ash make iron omnipresent in the environment and practically all natural water contains iron at least in traces. In clouds, fog, lakes and rivers the iron concentration is around $10^{-5}M$ (Faust, 1990). Iron is as well a vital element for life present in the whole biosphere.

In aqueous solution the most abundant iron species have an oxidation number of $+II$ (ferrous iron) and $+III$ (ferric iron). Other iron species are highly unstable. Dissolved ferrous and ferric iron species are present in octahedral complexes with six ligands in water. Iron is complexed by water and hydroxyl ligands provided that no other complexing substances are present. How many of these ligands are hydroxyl ions, depends on the solution's pH, which influences directly the acid/base equilibrium of the aqua-complex. Ferric iron is the more critical iron species in the photo-Fenton process, because its hydroxides precipitate at lower pH than those of ferrous iron. Consequently, only the acid/base equilibrium for the ferric iron aqua-complex is discussed here.

Figure 1.4 shows the equilibrium concentrations of the most important ferric iron aqua-complexes in the absence of further complexing substances at different pH for a ferric iron concentration of 20 mg/L. It is clear that between pH 2.5 and 3 $[Fe(H_2O)_5(OH)]^{2+}$ is the dominant species.

Because of the low solubility product of ferric iron hydroxide ($K_S (Fe(OH)_3) \approx 10^{-37}$), precipitation starts at pH 2.5-3.5 depending on the iron concentration and the temperature. The precipitation process starts with the formation of dimers and oligomers, which at continuation gradually polymerize further and lose water until forming finally insoluble iron hydroxides (e.g. goethite or hematite). This aging process is slow and can take up to a hundred days (Flynn, 1984). The resulting precipitate is of red brown colour and with no defined stoichiometry. It contains water and has a strong cationic character, thus co-precipitating anions but also organic substances. The precipitate is difficult to re-dissolve through acidification (insoluble above pH $\approx 1-1.5$), but it can be re-dissolved by

complexing substances (e.g. oxalic acid) (Mazellier, 2001) or photoleaching processes (Sulzberger, 1995). Photo-leaching refers to photo-reduction of ferric to ferrous iron and subsequent leaching of the ferrous iron from the precipitate.

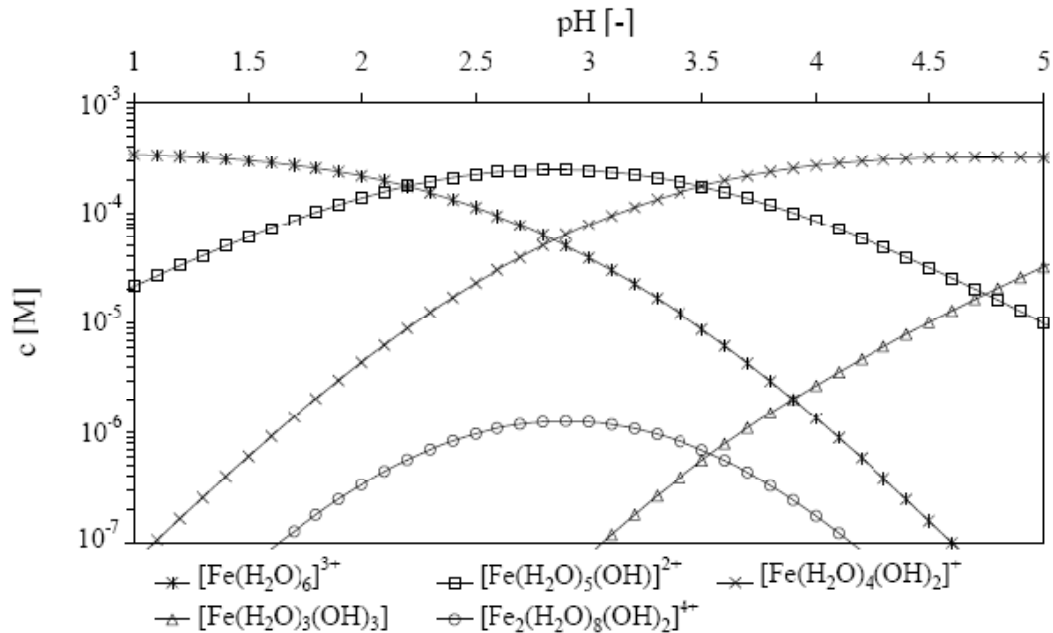
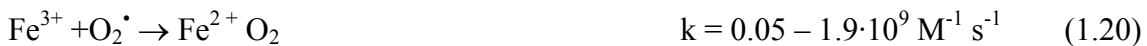
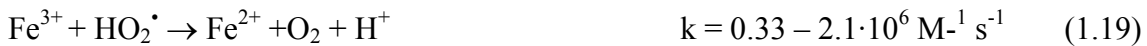


Figure 1.4 Ferric ion species present in aqueous solution at different pH at a concentration of 20 mg/L, calculated with equilibrium constants (Flynn, 1984), T = 20 °C.

1.2.3.2 Fenton chemistry

Hydrogen peroxide is decomposed to water and oxygen in the presence of iron ions in aqueous solution. A radical chain reaction (Haber-Weiss mechanism) (Haber, 1934; Walling, 1975) has been broadly accepted as mechanism for reactions in acidic milieu. It should be mentioned that the existence of ferrate and ferryl iron (+IV and +V) is still an open matter. At least intermediate complexes involving these states have been suggested (Bossmann, 1998). Mixtures of ferrous iron and hydrogen peroxide is called Fenton reagent. If ferrous is replaced by ferric iron it is called Fenton-like reagent. The Fenton reaction, Eq. 1.15, was first reported by H.J.H. Fenton in 1894 (Fenton, 1894). Eq. 1.15 - 1.21 show reactions of ferrous iron, ferric iron and hydrogen peroxide in the absence of other interfering ions and organic substances. The regeneration of ferrous iron from ferric

iron by Eq. 1.18-1.20, is the rate limiting step in the catalytic iron cycle, if iron is added in small amounts. The listed rate and equilibrium constants for Eq. 1.15-1.24 were reported by Sychev et al., (Sychev, 1995).



Furthermore, radical-radical reactions have to be taken into account.



Finally, the following acid/base equilibriums have to be regarded (Gallard, 1999):



1.2.3.3 Fenton reaction in presence of inorganic and organic substances

If organic substances (quenchers, scavengers or pollutants) are present in the system $\text{Fe}^{2+}/\text{Fe}^{3+}/\text{H}_2\text{O}_2$, they react in many ways with the generated hydroxyl radicals. Yet, in all cases

the oxidative attack is electrophilic and the rate constants are close to the diffusion-controlled limit. As discussed point 1.2.1, the reactions between OH radicals and organic substrates are:

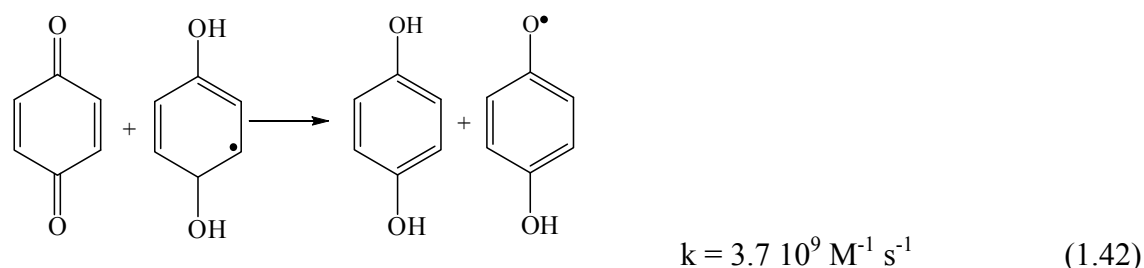
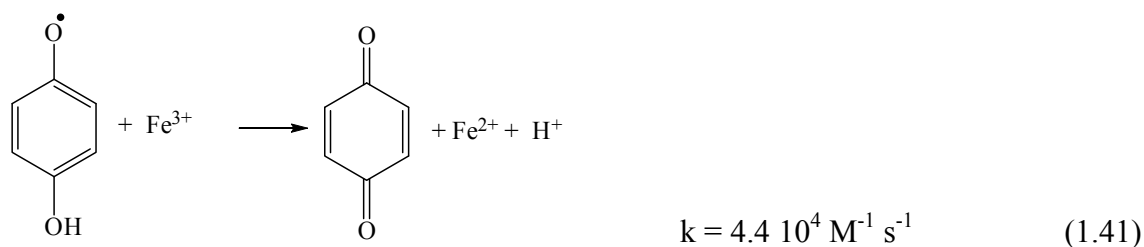
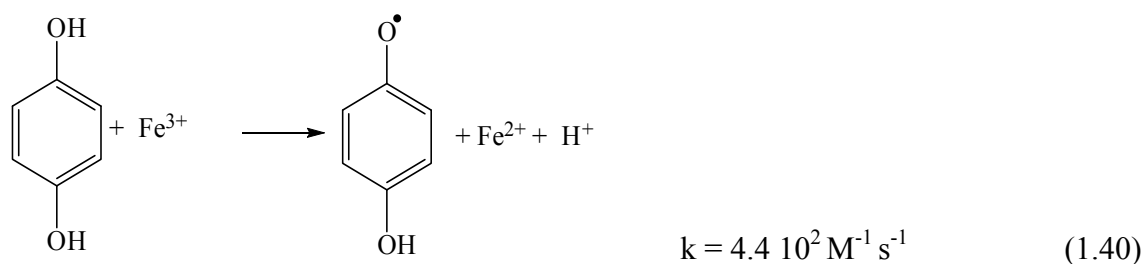
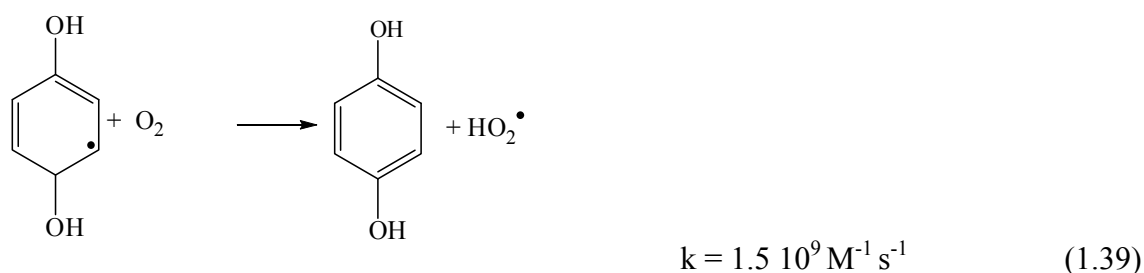
- Hydrogen abstraction from aliphatic carbon atoms, Eq. 1.2
- Electrophilic addition to double bonds or aromatic rings, Eq. 1.3.
- Electron transfer reactions, Eq. 1.4.

The generated organic radicals continue reacting prolonging the chain reaction. Depending on the oxidation-reduction potential of the organic radical generated, reactions Eq. 1.31 - 1.34 can take place. The organic peroxide generated in reaction Eq. 1.34 can further react with ferrous iron similar to the Fenton reaction, 1.35 (Huysler, 1983). Of special interest is the reaction with dissolved oxygen (Dorfman-mechanism), Eq. 1.36 and 1.37 (Von Sonntag, 1997), because the peroxy radical can regenerate hydrogen peroxide by reaction 1.23 and thereby contribute to reduce the consumption of oxidant in wastewater treatment by Fenton and photo-Fenton method.



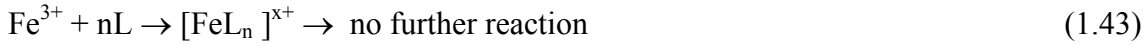
In the case of aromatic pollutants the ring system usually is hydroxylated before it is broken up during the oxidation process. Substances containing quinone and hydroquinone structures are typical intermediate degradation products, e.g. produced by reactions equivalent to Eq. 1.38 and 1.39. These are especially worth mentioning because they provide an alternative, quicker pathway for ferrous iron regeneration through Eq. 1.40 and 1.41 accelerating thereby the process. Resulting benzoquinone structures can also be reduced as in Eq. 1.42. Thereby, each molecule can reduce several ferric iron ions in a

catalytic cycle. Anyway, sooner or later this catalytic cycle is interrupted, because in competition with reactions 1.38 - 1.42 also ring opening reactions occur, which further carry on the mineralization of the molecule (Chen, 1997).



There is one great setback of the Fenton method. Especially when the treatment goal is the total mineralization of organic pollutants, carboxylic intermediates cannot be in some cases

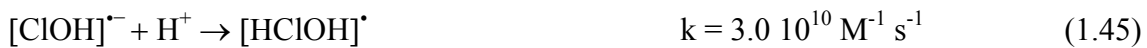
further degraded. Carboxylic and dicarboxylic acids are known to form stable iron complexes, which inhibit the reaction with peroxide (Kavitha, 2004). Hence, the catalytic iron cycle reaches a standstill before total mineralization is accomplished, in the dark, Eq. 1.43.



L: Mono- and dicarboxylic acids

Due to the high oxidation potential of the hydroxyl radical, it can also react with inorganic ions present in the solution. Several authors have described the strong negative effect of the presence of carbonate and phosphate in the Fenton reaction, while the effect of other ions such as chloride or sulfate is not so strong (Lipczynska-Kochany, 1995; Pignatello, 1992; Kiwi, 2000; De Laat, 2004; Marciel, 2004). Phosphate has a double detrimental effect; first, it precipitates iron and second, it scavenges hydroxyl radicals. Carbonate ions can scavenge hydroxyl radicals. The resulting carbonate radicals are particularly ineffective in the degradation of organic matter (Von Sonntag, 1997).

De Laat and co-workers (De Laat, 2004) recently presented a review of the additional reactions and equilibriums of importance in the presence of significant amounts of chloride and sulfate. Both anions can form complexes with ferric and ferrous iron. They can thereby hinder reactions or also open completely new reaction pathways for the decomposition of hydrogen peroxide in the presence of dissolved iron. Also, hydroxyl radicals generated can react with these ions, creating chlorine radicals and sulfate radicals as shown in Eq. 1.44-1.47.



De Laat and co-workers further calculate, that below pH = 4 practically all hydroxyl radicals end up in chlorine radicals (calculations done for 100 mM NaCl solution). In the

presence of sulfate the conversion of hydroxyl radicals is considerable at acidic pH as well. Yet, it should be mentioned that these calculations were performed for solutions without any other scavenging substances (e.g. organic pollutants). There are two negative effects; first, the chlorine and sulfate radicals are potentially weaker oxidants and the overall process efficiency becomes diminished and second, chlorine radicals can electrophilically add themselves to double bonds similar to hydroxyl radicals and generate undesired chlorinated intermediate reaction products, such as detected by Kiwi and co-workers (Kiwi, 2000).

1.2.3.4 Photo-assisted Fenton reaction

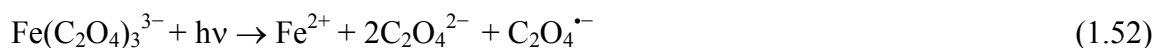
Irradiation with light up to 580 nm leads to photo-reduction of dissolved ferric iron to ferrous iron (Bauer, 1999). The primary step is a ligand-to-metal charge-transfer (LMCT) reaction. Subsequently, intermediate complexes dissociate as shown in reaction Eq. 1.48 (Zepp, 1992). The ligand can be any Lewis base able to form a complex with ferric iron (OH^- , H_2O , HO_2^- , Cl^- , R-COO^- , R-OH , R-NH_2 etc.). Depending on the reacting ligand, the product may be a hydroxyl radical such as in Eq. 1.49 and 1.50 or another radical derivated from the ligand. The direct oxidation of an organic ligand is possible as well as shown for carboxylic acids in Eq. 1.51. The omnipresence of iron makes the photo-Fenton reaction an important factor for the self-purification capacity of lakes, rivers (Sulzberger, 1995) and atmospheric water droplets (Faust, 1990).



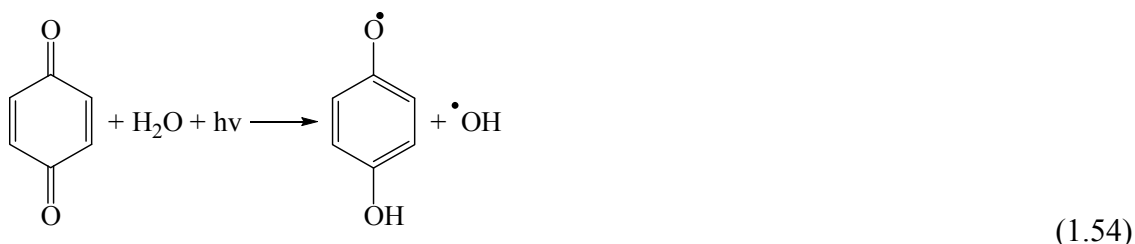
Depending on the ligand the ferric iron complex has different light absorption properties and reaction 1.48 takes place with different quantum yields and also at different wavelengths. Consequently, the pH plays a crucial role in the efficiency of the photo-Fenton reaction, because it strongly influences which complexes are formed (e.g. see

Figure 1.4). Thus, pH 2.8 was frequently postulated as an optimum pH for photo-Fenton treatment (Pignatello, 1992; Safarzadeh-Amiri, 1996a), because at this pH, precipitation does not take place yet and the dominant iron species in solution is $[\text{Fe}(\text{OH})]^{2+}$, the most photoactive ferric iron – water complex. In fact, as shown in its general form in Eq. (1.48), ferric iron can form complexes with many substances and undergo photo-reduction. Of special importance are carboxylic acids because they are frequent intermediate products in an oxidative treatment. Such ferric iron – carboxylate complexes can have much higher quantum yields than ferric iron – water complexes. It is therefore a typical observation that a reaction shows an initial lag phase, until intermediates are formed, which can regenerate more efficiently ferrous iron from ferric iron accelerating the process. This can either happen through a photochemical pathway, Eq. 1.51, a thermal pathway, e.g. Eq. 1.38-1.42, or a combination of both.

The addition of oxalate has been proposed to overcome the initial lag phase (Nogueira, 2005; Safarzadeh-Amiri, 1996b). Thereby, the wastewater throughput in a photo-Fenton plant can be raised, but these gains have to be compared to the increased reagent cost due to the addition of oxalate, because oxalate is not acting as a catalyst, as it is as well consumed during this photochemical reaction. Other chelating agents have been proposed as well with the additional aim of working at neutral pH (Sun, 1992).



Finally, another photochemical reaction should be mentioned, which is the photo-reduction of quinones to semiquinones, Eq. (1.54) (Ononye, 1986). By this reaction intermediate quinonic reaction products can be reduced and can further contribute to accelerate the reduction of ferric iron by Eq. (1.41). As a side product even a hydroxyl radical is generated.



1.2.4 photo-Fenton reaction using iron from solid sources

1.2.4.1 Fenton reaction with iron oxides

Work in the field of soils decontamination has shown the potential of iron oxides (goethite, hematite, ferrihydrite, etc.) to perform Fenton reactions for the degradation of chlorinated organic compounds (Tyre, 1991, Watts, 1993; Kong, 1998, Lu, 2000; Teel, 2001). Goethite was found to be more efficient than hematite in heterogeneous Fenton process (Watts, 1993; Huang, 2001).

To date, the role of Fe^{3+} and Fe^{2+} and their ability to promote the production of free-radical $\cdot\text{OH}$ are not totally understood. Reported data indicate that H_2O_2 initiates a chain reaction that leads to the formation of $\cdot\text{O}_2\text{H}$, by contact with Fe^{3+} sites available on the surface of goethite particles dispersed in aqueous solution (Al-Hayek, 1990; Guimaraes, 2008) Fe^{3+} is converted to Fe^{2+} on the solid surface. New reaction sites are then formed and allow H_2O_2 to generate $\cdot\text{OH}$ radicals. The Fe^{3+} sites are recovered via oxidation of Fe^{2+} in the cyclic mechanism (Eq 1.55-1.56 where $=\text{Fe(II/III)}$ represent the Fe(II/III) species at solid surface).



It was shown that the presence of Fe^{2+} sites (intrinsically on oxides such as magnetite (Kong, 1998); or generated on goethite by thermal treatment under H_2 atmosphere (Guimaraes, 2008)) on iron oxide surface enhanced the Fenton degradation of organic compounds with support the latter mechanistic proposition.

1.2.4.2 Iron oxide photocatalysis

For thirty years, hematite (Fe_2O_3) colloids are known to photocatalyse the electrolysis of water (Khung, 1977) or the oxidation of cyanide and sulfide (Franck, 1977). The photocatalytic oxidation of organic compounds such as carboxylic acids acid (Hermann, 1983, Litter, 1994), dioxin (Pellizzetti, 1988) or phenols (Chatterjee, 1994; Pulgarin, 1995; Pal, 1998; Mazellier, 2000; Bandara, 2001; Valenzuela, 2002; Bakardjieva, 2007, Karunakaran, 2008, Dindar, 2009) mediated by iron oxides (such as hematite or goethite) in aqueous solution and under visible light irradiation was reported more recently. Possible mechanisms involved in iron oxide photocatalysis (Graetzel, 1985; Mazellier, 2000 Karunakaran, 2008; Du, 2008) are presented in Eq. 1.57-1.61:



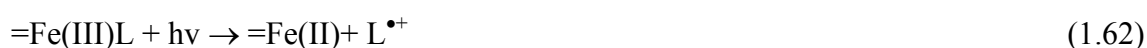
Hematite was found to present a lower efficiency than TiO_2 in photocatalytic degradation of organic compound (Kormann, 1989; Litter, 1994, Bandara, 2001, Valenzuela, 2002, Dindar, 2009). Besides iron oxides were found to dissolve under irradiation via photo-reductive dissolution (Walte, 1984), particularly at acidic pH in the presence of chlorine (Graetzel, 1985) or organic ligands (Litter, 1988) (More detail about the mechanisms involved in photo-reductive dissolution will be discussed latter). Due to these reasons, iron oxides were considered less suitable than TiO_2 as semiconductor photocatalyst.

1.2.4.3 Photo-Fenton reaction using iron from oxides.

A promising alternative was proposed: Iron oxides could be used as a heterogeneous catalyst in the presence of hydrogen peroxide and under light irradiation leading to heterogeneous photo-Fenton reactions. Such system combines semiconductors photocatalytic character to the Fenton and photo-assisted Fenton oxidation in a single

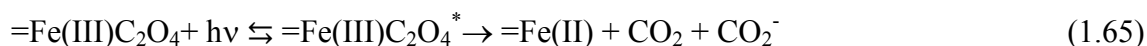
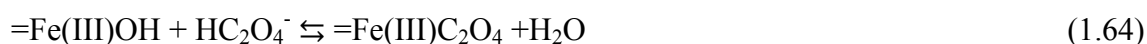
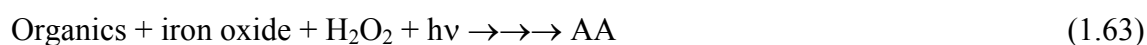
material. Different iron oxides were compared and iron oxyhydroxides (Ferrhydrite, goethite) were found to be more efficient than hematite in organics degradation (He, 2002; Du 2008). The application of goethite as solid photo-Fenton catalyst has shown to be efficient in the degradation and mineralization of organic compounds under solar irradiation (Mazellier, 2001; Ortiz de la Plata, 2008, Xu, 2009).

The mechanism occurring in photo-Fenton reaction with oxides seems quite complex involving semiconductor photocatalysis (Eq. 1.57-1.61) in the presence of H₂O₂ and Fenton reaction using iron from oxides (Eq. 1.55-1.56). In addition, heterogeneous photo-Fenton reactions (Eq. 1.62, 1.65, 1.68) on oxide are linked with iron photodissolution (Mazellier, 2001; Lu, 2002).

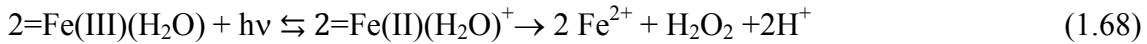


(L: complexing agent or polycarboxylic acid)

Iron leaching from oxides to solution is well documented (Sulzberger, 1995, Voelker, 1997). The leaching process can be described as follow (Eq. 1.63-1.68): (i) carboxylate ligands (like aliphatic acids (AA) produced by organic pollutant degradation (Eq. 1.63) can form surface Fe(III)-carboxylate complexes (Eq. 1.64); (ii) These complexes are thought to participate in ligand to metal charge transfer reactions (Eq. 1.65). For dissolution to take place, the Fe(II) sites formed at the surface of the Fe(III) oxide must detach (Eq. 1.66). In presence of oxidant, the surface Fe(II) sites may be re-oxidized before they leave the catalyst surface (Eq. 1.67).



Recently Sherman (Sherman, 2005) reported that leaching of iron species from the iron oxide surface to the aqueous solution is also possible via photo-reduction of bounded aqua-complexes (Eq. 1.68).



Thus the surface photo-Fenton reaction can lead to intermediates mineralization (or H_2O_2 generation) and concomitant Fe^{2+} dissolution. When dissolved iron concentration is high enough (i.e. $> 0.1 \text{ mg/L}$), homogeneous Fenton and photo-Fenton reactions described points 1.2.3.2 and 1.2.3.4 shall also play a role in the degradation processes mediated by iron oxides. This homogeneous contribution can be seen as beneficial or detrimental depending on the final values of dissolved iron concentrations allowed by sanitary authorities in water and drinking waters.

1.2.4.4 Photo-Fenton reaction with iron from other solid sources.

The use of zero valent iron in Fenton heterogeneous catalyst is another interesting possibility which has shown growing concern (Liao, 2004; Kusic, 2006; Prousek, 2007; Gomathi Devi, 2009; Kusic, 2010). In this process zero valent iron is used as a source of Fe^{2+} generated in the presence of hydrogen peroxide as shown Eq. 1.69 where Ox is hydrogen peroxide or oxygen.



Once the Fenton reagent is present in solution, homogeneous photo-Fenton oxidation is responsible of organics degradation.

Mixed oxides such as Fe- TiO_2 (Tryba, 2006), $\text{Fe}^0/\text{FeOOH}/\text{Fe}_2\text{O}_3$ (Nie, 2007) Fe-Ce oxide (Zhang, 2007), CuOx-FeOOH (Nie, 2009), $\text{Fe}_2\text{V}_4\text{O}_{13}$ (Zhang, 2009) were also proposed as heterogeneous photo-Fenton catalysts. These materials were found to show high efficiencies in organic pollutant degradation, under visible light irradiation and presence of

H₂O₂. The occurrence of synergistic effects between iron oxide and the other oxides was found to be responsible of the high degradation rates measured. A proposition of mechanism for the synergistic effect in the Fe oxide-TiO₂/H₂O₂ system is detailed in chapter 4.

1.2.4.5 photo-Fenton reaction using designed heterogeneous catalyst.

Investigators have explored the use of iron species (ions, (mixed) oxides or complexes) immobilized on a solid support as a strategy to avoid sludge formation and to expand the effective pH range of the Fenton reaction. Some success in this regard has been achieved, notably with iron-exchanged Nafion membranes (Maletzky, 1999), iron-modified clays (Feng, 2003, De Leon, 2008) and with different iron modified supports such as silica fabric (Bozzi, 2004), Al₂O₃ (Muthuvel, 2007), zeolites (Rios-Enriquez, 2004), resins (Lv, 2005), cotton (Tryba, 2008) among others. The advantage of a suitable heterogeneous catalyst is its separability from the waste stream. Unless the catalyst provides a steady-state source of iron in solution (which was found to always occur to different extent with dissolved iron concentration between 0.1 and 10 mg/L) for the homogeneous reaction, a fundamental disadvantage is that dissolved target molecules must diffuse to the catalyst surface to reach active oxidant sites before they are degraded.

Nafion is a perfluorinated oxyalkyl polymer with sulfonate groups capable of binding cations. Ferric-exchanged Nafion membrane is claimed to be an effective photo-Fenton catalyst (Maletzky 1999; Dhananjeyan, 2001). Activity under simulated solar irradiation correlates with the presence of Fe(III) species such as iron aqua ions or dimers electrostatically associated with sulfonate groups. Fe-Nafion membranes appear to be effective up to at least operational pH 5. Although it was possible to achieve mineralization of 2,4-dichlorophenol at higher initial pH (up to 11), the pH (unbuffered) always drifted quickly to a value below 5 (Sabhi, 2001). The detailed mechanism concerning the role of surface reactions and of adsorption/desorption of iron ions and reactants in Fe–Nafion systems is unclear at this time. Fernandez et al (Fernandez, 1999) showed that Nafion-bound Fe(III) is photo-reduced to Fe(II), which subsequently undergoes the Fenton reaction (as in Eq 1.55-1.56). Whether H₂O₂ reacts with surface-bound or desorbed Fe(II) species is uncertain. Dissolved methanol inhibited orange II discoloration, which suggests that HO• is

generated in solution, or at least desorbs before it reacts. If H_2O_2 reacts in solution then the Fe(III) product must re-adsorb faster than it precipitates, since membranes retain activity over several cycles without sludge production (Sabhi and Kiwi, 2001; Dhananjeyan et al., 2001). The question of the involvement of dissolved Fe(III) species in these systems is still unanswered. Some disadvantages of Nafion membrane for practical application is their high cost and that these membranes are not totally inert. Fluorinated radicals were founded in Nafion solutions exposed to ROS produced by photo-Fenton reaction (Bosnjakovic, 2007).

Feng et al. obtained encouraging results in the degradation of dyes mediated by composites in the presence H_2O_2 and light. The nanocomposite materials composed of crystallites of Fe_2O_3 and clays (laponite (Feng, 2003) or bentonite (Feng 2004) were more efficient than bare FeOOH or Fe_2O_3 suspensions in photo-Fenton dye degradation. The catalysts leach iron into solution, up to 3 mg/L during the runs, however, the catalyst efficiency did not decline much in repeated runs. The catalyst efficiency was maximal at initial pH 3 (Feng, 2006). The amount of leached iron was diminished (0.5 mg/L) by immobilizing an iron modified bentonite film on the inner surface of a photo-reactor (Feng, 2005) however the degradation rates were also diminished if compared with suspensions. The homogeneous photo-Fenton tests performed with the same amount of dissolve iron (3mg/L) have shown the significant contribution of dissolved iron ions in the process mediated by iron modified clays (Feng, 2003).

The performance of a Fe^{3+} -exchanged zeolite Y (Rios-Enriquez, 2004; Noorjahan, 2008) and Fe-ZM5 zeolite (Kasiri, 2008), as a heterogeneous photo-Fenton catalyst, was tested on degradation of organic compounds. Although some leaching of Fe^{3+} was observed, it amounted to only few percent of the total iron present in the zeolites, (0.3-2 mg/L in solution), and was thought not to play a major role in the reaction.

The use of novel structured inorganic silica fabrics loaded with Fe ions (Fe-EGF) by exchange-impregnation as a heterogeneous photocatalyst was an alternative approach proposed to degrade organic compounds (Bozzi, 2004) or deactivate bacteria (Moncayo 2008). Evidence was provided that the degradation of oxalates on the Fe-silica fabric was

due to Fe ions leaching into the solution that were re-adsorbed onto the silica fabric when compounds were mineralized.

Ferric species were also immobilized on different types of ionic exchange resins, and used as a heterogeneous catalyst for degradation of cationic and anionic dye pollutants under visible light ($\lambda > 450$ nm) irradiation in the presence of H_2O_2 . Whereas the cationic dyes are efficiently photodegraded on a cationic resin exchanged Fe(III) catalyst, the anionic dye is preferably photodegraded on an anionic resin supported catalyst (Lv, 2005).

A common characteristic of designed heterogeneous catalyst for photo-Fenton reaction is that the optimal pH is generally 3, coinciding with the most efficient dissolution of iron ions. These material are however efficient in a heterogeneous reaction at higher pH values and leaching is minimized under these conditions. The importance of homogeneous photo-Fenton contribution to the overall process depends on the kind of catalyst, experimental conditions and target contaminant and is difficult to determine with accuracy. In fact, the dissolved iron concentration is time dependent and the optical properties of photo-reactor change in absence of heterogeneous catalyst. An interesting phenomenon was observed for most of proposed catalysts, the leached iron ions are found to re-adsorb on catalyst surface allowing to maintain a good catalyst stability in repeated runs.

It can be assumed that an ideal supporting material for iron species as photocatalyst would have the following attributes: (a) to be transparent to UV and visible radiations; (b) to favor strong surface chemical-physical binding with the iron particles without affecting their reactivity; (c) to have a high specific surface area; (d) to have good adsorption capability for the organic compounds to be degraded; (e) to be in a physical configuration which favors the ultimate liquid-solid phase separation; (f) to allow a reactor design that facilitates the mass transfer processes; and (g) to be chemically inert.

From the coating point of view, the ideal situation is given by two basic conditions: a good adherence catalyst/support, and no degradation of the catalyst activity by the attachment process. The first condition is essential, since the support/catalyst junction should resist to the strain derived from particle to particle and particle-fluid mechanical interactions in the reactor environment, in order to avoid detachment of catalyst particles from the support (Pozzo et al. 1997). Moreover, the light penetration length in the solid-liquid medium is

another important parameter, which depends on catalyst charge and support transparency to radiation. Hence polymer films were selected as supports in this work because these materials can be transparent and chemically inert.

1.3 Objectives

This research work contributes to the study and development of new kind of heterogeneous photo-Fenton photocatalysts active under solar light, for the degradation of bio-recalcitrant organic substances and for the inactivation of bacteria present in aqueous media. Understanding of the processes involved catalyst preparation and studying the effect of some parameters influencing the reactivity of homogeneous and heterogeneous photo-Fenton processes are the objectives of this thesis. More specific objectives are:

- To assess the influence of physicochemical properties of the pollutant on photo-reactivity for homogeneous photo-Fenton system (chapter 2).
- To compare different surface modification methods for the preparation of supported photo-Fenton catalyst on polymer substrates (chapter 3).
- To characterize the most efficient materials and understand the mechanisms involved in the preparation processes (chapter 4).
- To study the ability of supported photocatalyst to degrade organic pollutant degradation and inactivate bacteria (chapter 4).
- To assess the influence of process parameters such as solution temperature or salt content (chapter 5).
- To performed a scale up and test the photocatalyst at field scale under natural solar light in compound parabolic collector (CPC) photo-reactors for the degradation of real pollutants. (chapter 6).

1.4 Studied water contaminants

1.4.1 Substituted phenols

Phenolic compounds are a significant threat to the environment and are common dilute contaminants found in ground and surface water. Figure 1.5 shows the *para*-substituted

phenols used to study the structure-photoreactivity relationship for photo-assisted Fenton reaction presented in Chapter 2. Several *para*-substituted phenols were tested in order to cover a wide variety of electronic effects ranging from strong electro-donating to strong electron withdrawing groups.

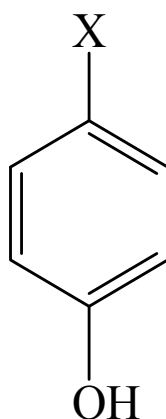


Figure 1.5 *Para*-substituted phenols (X = NO₂, Cl, H, CHO, H, OCH₃, OH)

1.4.2 Model contaminants

Hydroquinone was selected as a model of organic substances because it is representative of phenols and also of natural organic matter. The model *Escherichia-Coli* K12 was chosen since this bacterium is commonly used as a biological indicator of disinfection efficiency in water treatment. These model contaminants were used in the determination of heterogeneous photocatalysts performances and stability presented in chapter 3 to 5. For the experiments performed at field scale (chapter 6) phenol was used as model compound.

1.4.3 Real pollutants

Nalidixic acid, a quinolone antibiotic (which structure is shown in Figure 1.6) was selected as a real pollutant for laboratory and pilot scale experiments since this compound is present in the wastewater of an INNOWATECH partner.

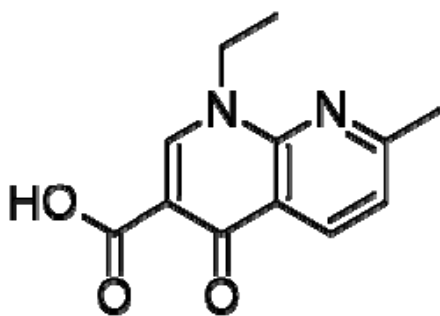


Figure 1.6 Chemical structure of nalidixic acid.

The degradation of many real pollutants was also performed at pilot scale in solar compound parabolic collector photo-reactors. Figure 1.7 shows the name and structure of the pesticides present in the mixture. Figure 1.8 shows the name and structure of emerging contaminants studied and their properties. Many of these compounds are common pharmaceutical, pesticides and personal care products.

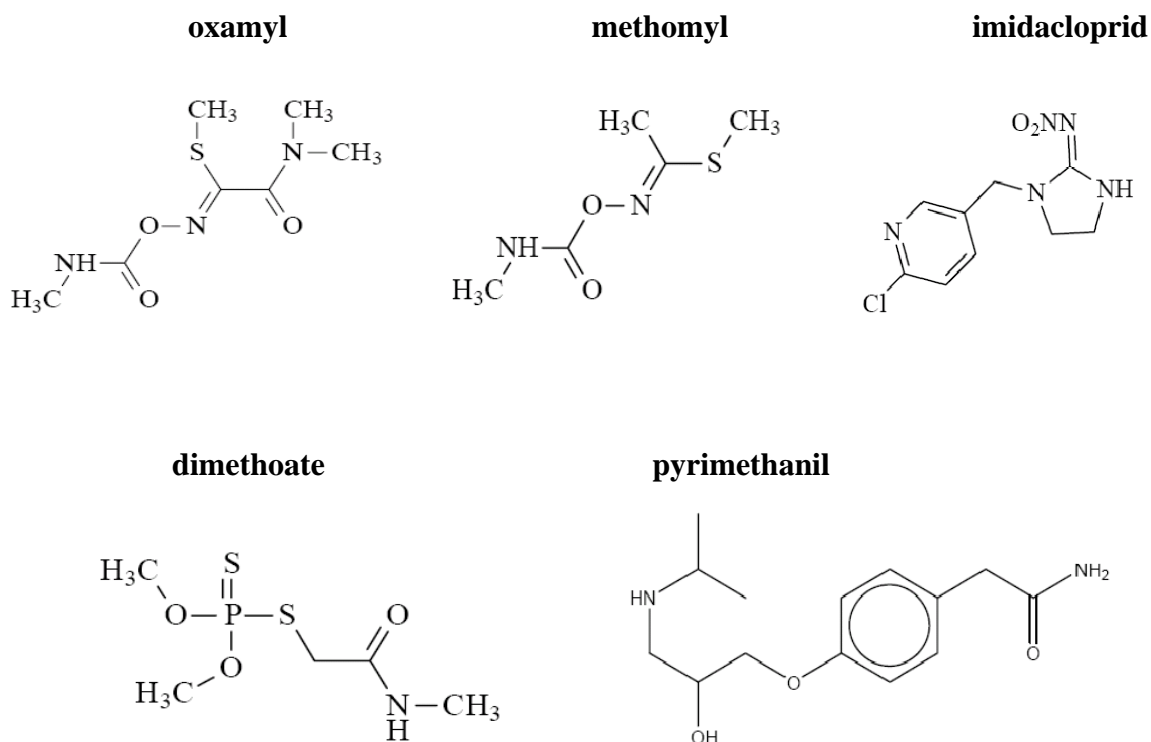
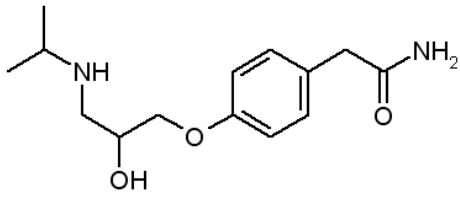
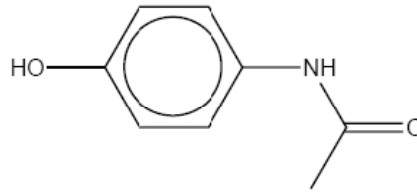


Figure 1.7 Chemical structure and name of the studied pesticides.

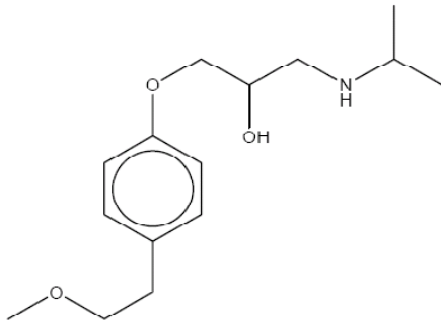
atenolol
(beta-blocker)



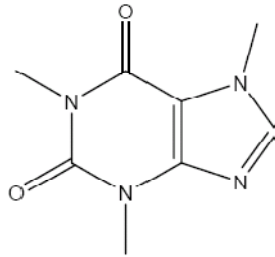
acetaminophen
(analgesic/antipyretic)



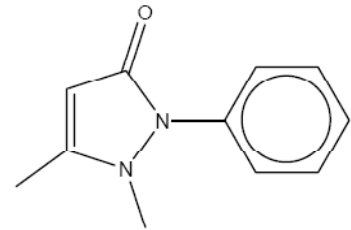
metoprolol
(beta-blocker)



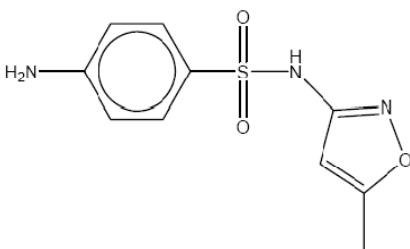
caffeine
(stimulant)



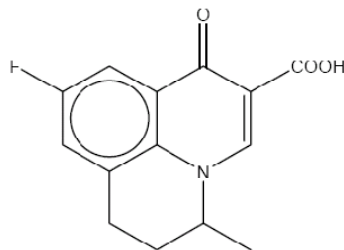
antipyrine
(analgesic)



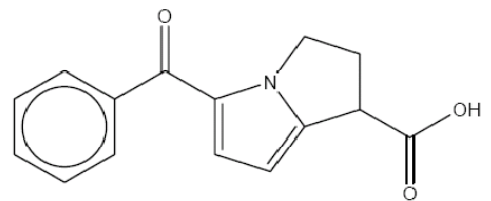
sulfamethoxazole
(Bacteriostatic antibiotic)



flumequine
(broad-spectrum antibiotic)



ketorolac
(anti-inflammatory)



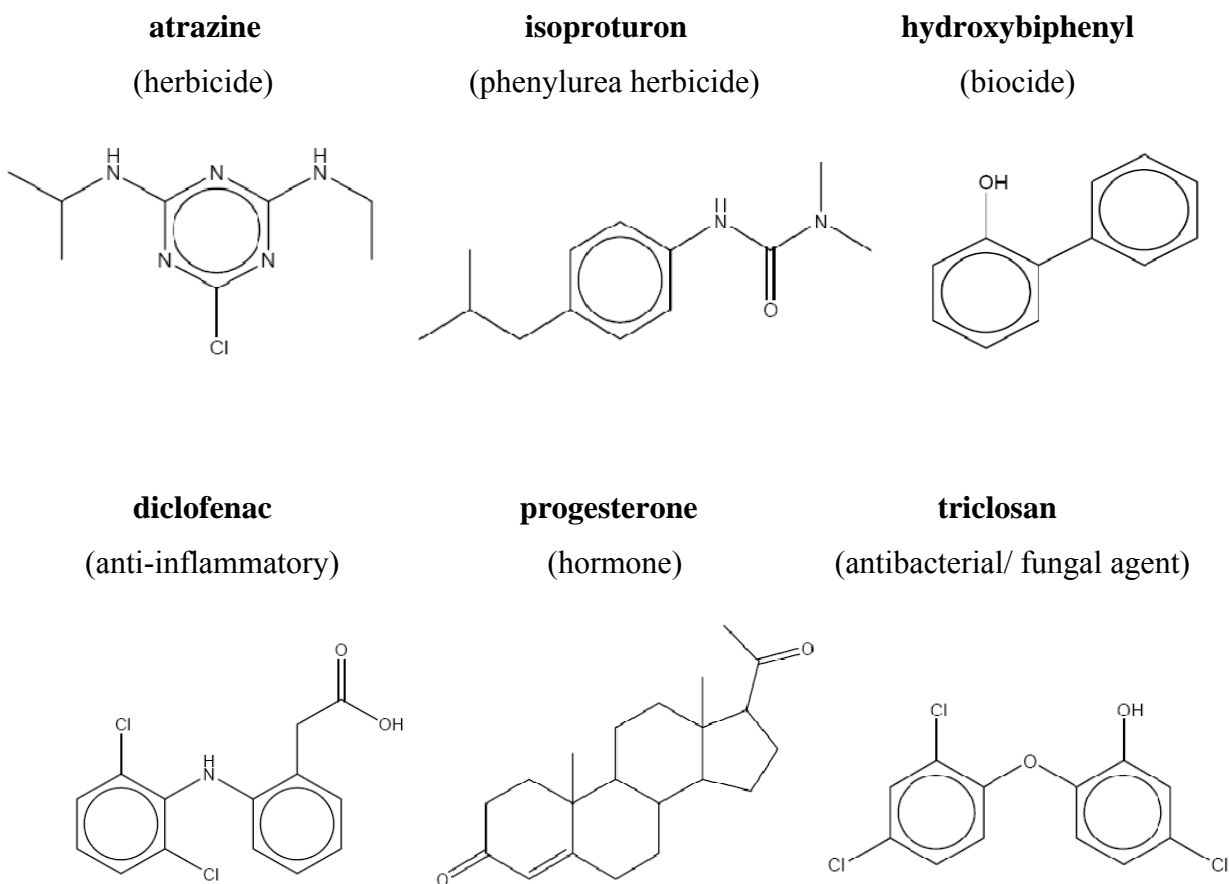


Figure 1.8 Names, structures and properties of emergent organic pollutants chosen for pilot scale study.

1.5 References

- Al-Hayek N., Dore M. (1990) Oxidation of phenols in water by hydrogen peroxide on alumine supported iron. *Water Research* 24: 973-982.
- Bahnemann D.C.J., Fox M.A., Pelizzetti E., Pichat P., Serpone N. (1994) Photocatalytic Treatment of Waters. Boca Raton, Lewis Publishers.
- Bakardjieva S., Stengl V., Subrt J., Houskova V., Kalenda P. (2007) Photocatalytic efficiency of iron oxides: Degradation of 4-chlorophenol. *Journal of Physics and Chemistry of Solids* 68: 721-724.
- Bandara J., Mielczarski J.A., Lopez A., Kiwi J. (2001) 2. Sensitized degradation of chlorophenols on iron oxides induced by visible light comparison with titanium oxide. *Applied Catalysis B: Environmental* 34: 321-333.
- Bauer R., Waldner G., Fallmann H., Hager S., Klare M., Krutzler T., Malato S., Maletzky P. (1999) The photo-Fenton reaction and the TiO₂/UV process for wastewater treatment – novel developments. *Catalysis Today*, 53: 131-144.

- Bosnjakovic A., Kadirov M.K., Schlick S. (2007) Using ESR spectroscopy to study radical intermediates in proton-exchange membranes exposed to oxygen radicals. *Research on Chemical Intermediates* 33: 677-687.
- Bossmann S H., Oliveros E., Göb S., Siegwart S., Dahlen E.P., Payawan L. Jr., Straub M., Worner M., Braun A.M. (1998) New evidence against hydroxyl radicals as reactive intermediates in the thermal and photochemically enhanced Fenton reactions. *Journal of Physical Chemistry* 102: 5542-5550.
- Bouras P., Lianos P. (2008) Synergy effect in the combined photodegradation of an azo dye by titanium dioxide photocatalysis and photo-fenton oxidation. *Catalysis Letters* 123: 220-225.
- Bozzi A., Yuranova T., Mielczarski J., Lopez A., Kiwi J. (2002) Abatement of oxalates catalyzed by Fe-silica structured surfaces via cyclic carboxylate intermediates in photo-Fenton reactions. *Chemical Communications* 19: 2202-2203.
- Chatterjee S., Sarkar S., Bhattacharyya S.N.(1994) Photodegradation of phenol by visible light in the presence of colloidal Fe₂O₃. *Journal of Photochemistry and Photobiology, A: Chemistry* 81: 199-203.
- Chen R., Pignatello J.J. (1997) Role of quinone intermediates as electron shuttles in Fenton and photoassisted Fenton oxidations of aromatic compounds. *Environmental Science and Technology* 31: 2399–2406.
- De Laat J., Truong Le G., Legube B. (2004) A comparative study of the effects of chloride, sulfate and nitrate ions on the rates of decomposition of H₂O₂ and organic compounds by Fe(II)/H₂O₂ and Fe(III)/H₂O₂. *Chemosphere* 55: 715-723.
- De León M.A., Castiglioni J., Bussi J., Sergio M. (2008) Catalytic activity of an iron-pillared montmorillonitic clay mineral in heterogeneous photo-Fenton process. *Catalysis Today* 133-135: 600-605.
- Dhananjeyan M.R., Kiwi J., Albers P., Enea O. (2001) Photo-assisted immobilized Fenton degradation up to pH 8 of azo dye orange II mediated by Fe³⁺/Nafion/glass fibers. *Helvetica Chimica Acta* 84: 3433-3445.
- Dindar B., Seven O. (2009) Photodegradation of 2,4-Dichlorophenoxy acetic acid on TiO₂ ZnO and Fe₂O₃ by sunlight. *Asian Journal of Chemistry* 21: 2270-2282.
- Du W., Xu Y., Wang Y. (2008) Photoinduced degradation of orange II on different iron (Hydr)oxides in aqueous suspension: Rate enhancement on addition of hydrogen peroxide, silver nitrate, and sodium fluoride. *Langmuir* 24: 175-181
- Faust B., Hoigné J. (1990) Photolysis of hydroxy-complexes as sources of OH• radicals in clouds, fog and rain. *Atmospheric Environment-Part A General Topics* 24A: 79-89.
- Feng J., Hu X., Yue P.L. (2003) A novel laponite clay-based Fe nanocomposite and its photo-catalytic activity in photo-assisted degradation of orange II. *Chemical Engineering Science* 58: 679-685.
- Feng J., Hu X., Po L.Y. (2004) Discoloration and mineralization of Orange II using different heterogeneous catalysts containing Fe: A comparative study. *Environmental Science and Technology* 38: 5773-5778.
- Feng J., Hu X., Yue P.L. (2005) Discoloration and mineralization of Orange II by using a bentonite clay-based Fe nanocomposite film as a heterogeneous photo-Fenton catalyst. *Water Research* 39: 89-96.

- Feng J., Hu X., Yue P.L. (2006) Effect of initial solution pH on the degradation of Orange II using clay-based Fe nanocomposites as heterogeneous photo-Fenton catalyst. *Water Research* 40: 641-646.
- Fenton H.J.H. (1894). Oxidation of tartaric acid in presence of iron. *Journal of the Chemical Society, Transactions* 65: 899-910.
- Fernandez J., Bandara J., Lopez A., Buffat P., Kiwi, J. (1999) Photoassisted Fenton degradation of nonbiodegradable azo dye (orange II) in Fe-free solutions mediated by cation transfer membranes. *Langmuir* 15: 185–192.
- Flynn C.M. Jr. (1984). Hydrolysis of inorganic iron(III) salts. *Chemical Review* 84: 31-41.
- Frank S.N., Bard A.J. (1977) Heterogeneous photocatalytic oxidation of cyanide and sulfite in aqueous solutions at semiconductor powders. *Journal of Physical Chemistry* 81: 1484-1488.
- Gallard H., De Laat J., Legube B. (1999) Spectrophotometric study of the formation of iron(III)–hydroperoxy complexes in homogeneous aqueous solution. *Water Research* 33: 2929-2936.
- Gomathi Devi, L., Girish Kumar, S., Mohan Reddy, K., Munikrishnappa, C. (2009) Photo degradation of Methyl Orange an azo dye by Advanced Fenton Process using zero valent metallic iron: Influence of various reaction parameters and its degradation mechanism. *Journal of Hazardous Materials* 164: 459-467.
- Grätzel M., Kiwi J., Morrison C.L., Davidson R.S., Tseung A.C.C. (1985) Visible-light-induced photodissolution of α -Fe₂O₃ powder in the presence of chloride anions. *Journal of the Chemical Society, Faraday Transactions 1: Physical Chemistry in Condensed Phases* 81: 1883-1890.
- Guimarães I.R., Oliveira L.C.A., Queiroz P.F., Ramalho T.C., Pereira M., Fabris J.D., Ardisson J.D. (2008) Modified goethites as catalyst for oxidation of quinoline: Evidence of heterogeneous Fenton process. *Applied Catalysis A: General* 347: 89-93.
- Haber F., Weiss J. (1934) The catalytic decomposition of hydrogen peroxide by iron salts. *Proceedings of the Royal Society A, London* 147: 332-351.
- Hawker P.N., Twigg M.V. (1994). Iron: inorganic & coordination chemistry. In: King, P.B. (Ed.). *Encyclopedia of Inorganic Chemistry*. Wiley, Chichester, 1698-1725.
- He J., Tao X., Ma W., Zhao J. (2002) Heterogeneous photo-Fenton degradation of an azo dye in aqueous H₂O₂/iron oxide dispersions at neutral pHs. *Chemical Letters* 1: 86-87.
- He, Z., Zhu, R., Xu, X., Song, S., Chen, J., Xia, M. (2009) Ozonation combined with sonolysis for degradation and detoxification of m-nitrotoluene in aqueous solution. *Industrial and Engineering Chemistry Research* 48: 5578-5583.
- Herrera Melián J.A., Doña Rodríguez J.M., Viera Suárez A., Tello Rendón E., Valdés Do Campo C., Arana J., Pérez Peña J. (2000) The photocatalytic disinfection of urban waste waters. *Chemosphere* 41: 323-327.
- Herrmann J. M. (1999) Heterogeneous photo-catalysis: fundamentals and applications to the removal of various types of aqueous pollutants. *Catalysis Today* 53: 115-129.
- Hoffmann M.R., Martin S.T., Choi W., Bahnemann D.W. (1995) Environmental applications of semiconductor photocatalysis. *Chemical Reviews* 95: 69-96.
- Huang H.-H., Lu M.-C., Chen J.-N. (2001) Catalytic decomposition of hydrogen peroxide and 2-chlorophenol with iron oxides. *Water Research* 35: 2291-2299.

- Huang Z., Maness P.C., Blake D.M., Wolfrum E.J., Smolinski S.L., Jacoby W.A. (2000) Bactericidal mode of titanium dioxide photocatalysis. *Journal of Photochemistry and Photobiology A: Chemistry* 130: 163-170.
- Huysen S., Hawkins G.W. (1983) Ferrous ion catalyzed oxidations of 2-propanol with peroxyacetic acid. *Journal of Organic Chemistry* 48: 1705-1708.
- IARC. (2006) Titanium dioxide Group 2B, Monographs on the evaluation of carcinogenic risks to humans, International Agency for Research on Cancer, World Health Organization, Lyon, vol. 9.
- Ishibashi K-I., Nosaka Y., Hashimoto K., Fujishima A. (1998) Time-dependent behavior of active oxygen species formed on photoirradiated TiO₂ films in air. *Journal of Physical Chemistry B* 102: 2117-2120.
- Karunakaran C., Dhanalakshmi R. (2008) Semiconductor-catalyzed degradation of phenols with sunlight. *Solar Energy Materials and Solar Cells* 92: 1315-1321.
- Kasiri M.B., Aleboyeh H., Aleboyeh A. (2008) Degradation of Acid Blue 74 using Fe-ZSM5 zeolite as a heterogeneous photo-Fenton catalyst. *Applied Catalysis B: Environmental* 84: 9-15.
- Kavitha V., Palanivelu K. (2004) The role of ferrous ion in Fenton and photo-Fenton processes for the degradation of phenol. *Chemosphere* 55: 1235-1243.
- Kiwi J., Lopez A. and Nadtochenko V. (2000) Mechanism and kinetics of the OH radical intervention during Fenton oxidation in the presence of a significant amount of radical scavenger (Cl⁻). *Environmental Science and Technology* 34: 2162-2168.
- Kong S.-H., Watts R.J., Choi J.-H. (1998) Treatment of petroleum-contaminated soils using iron mineral catalyzed hydrogen peroxide. *Chemosphere* 37: 1473-1482.
- Kormann C., Bahnemann D.W., Hoffmann M.R. (1989) Environmental photochemistry: Is iron oxide (hematite) an active photocatalyst? A comparative study: α -Fe₂O₃, ZnO, TiO₂. *Journal of Photochemistry and Photobiology, A: Chemistry* 48: 161-169.
- Kung H.H., Jarrett H.S., Sleight A.W., Ferretti A. (1977) Semiconducting oxide anodes in photoassisted electrolysis of water. *Journal of Applied Physics* 48: 2463-2469.
- Kušić H., Koprivanac N., Božić A.L., Selanec I. (2006) Photo-assisted Fenton type processes for the degradation of phenol: A kinetic study. *Journal of Hazardous Materials* 36: 632-644.
- Kusic H., Koprivanac N., Horvat S., Bakija S., Bozic A.L. (2010) Modeling dye degradation kinetic using dark- and photo-Fenton type processes. *Chemical Engineering Journal* 155: 144-154.
- Legrini O.O.E., Braun E.M. (1993) Photochemical processes for water-treatment. *Chemical Reviews* 93: 671-698.
- Liao C.-H., Wantawin C., Lu M.-C., Huang C.-I. (2004) Fe⁰-based system as innovative technology for degrading trichloromethane: Redox removal characteristics. *Environmental Science and Pollution Research* 11: 254-259.
- Lipczynska-Kochany E., Sprah G., Harms S. (1995) Influence of some groundwater and surface waters constituents on the degradation of 4-chlorophenol by the Fenton reaction. *Chemosphere* 30: 9-20.
- Litter M.I., Blesa M.A. (1988) Photodissolution of iron oxides. I. Maghemite in EDTA solutions. *Journal of Colloid And Interface Science* 125: 679-687.

- Litter M.I., Navío J.A. (1994) Comparison of the photocatalytic efficiency of TiO₂, iron oxides and mixed Ti(IV)Fe(III) oxides: photodegradation of oligocarboxylic acids. *Journal of Photochemistry and Photobiology, A: Chemistry* 84: 183-193.
- Litter M. I. (1999). Heterogeneous photocatalysis: Transition metal ions in photocatalytic systems. *Applied Catalysis B: Environmental* 23: 89-114.
- Lu M.-C. (2000) Oxidation of chlorophenols with hydrogen peroxide in the presence of goethite. *Chemosphere* 40:125-130.
- Lv X., Xu Y., Lv K., Zhang G. (2005) Photo-assisted degradation of anionic and cationic dyes over iron(III)-loaded resin in the presence of hydrogen peroxide. *Journal of Photochemistry and Photobiology A: Chemistry* 173: 121-127.
- Maciel R., Sant'Anna G.L. and Dezotti M. (2004). Phenol removal from high salinity effluents using Fenton's reagent and photo-Fenton reactions. *Chemosphere* 57: 711-719.
- Maletzky P., Bauer R., Lahnsteiner J., Pouresmael B. (1999) Immobilisation of iron ions on Nafion® and its applicability to the Photo-Fenton method. *Chemosphere* 38: 2315-2325.
- Martin S., Herrmann H., Hoffmann M. (1994). Time-resolved microwave conductivity, Part 2. Quantum sized TiO₂ and the effect of adsorbates and light intensity on charge-carrier dynamics. *Journal of Chemical Society Faraday Transactions* 90: 3323-3330.
- Mazellier P., Bolte M. (2000) Heterogeneous light-induced transformation of 2,6-dimethylphenol in aqueous suspensions containing goethite. *Journal of Photochemistry and Photobiology A: Chemistry* 132: 129-135.
- Mazellier P., Sulzberger B. (2001) Diuron degradation in irradiated, heterogeneous iron/oxalate systems: The rate-determining step. *Environmental Science and Technology* 35: 3314-3320.
- Mills A., Le Hunte S. (1997) An overview of semiconductor photocatalysis. *Journal of Photochemistry and Photobiology A: Chemistry* 108: 1-35.
- Muthuvel I., Swaminathan M. (2007) Photoassisted Fenton mineralisation of Acid Violet 7 by heterogeneous Fe(III)-Al₂O₃ catalyst. *Catalysis Communications* 8: 981-986.
- Nie Y., Hu C., Qu J., Zhou L., Hu X. (2007) Photoassisted degradation of azodyes over FeO_xH_{2x-3}/Fe₀ in the presence of H₂O₂ at neutral pH values. *Environmental Science and Technology* 41: 4715-4719.
- Nie Y., Hu C., Qu J., Zhao X. (2009) Photoassisted degradation of endocrine disruptors over CuO_x-FeOOH with H₂O₂ at neutral pH. *Applied Catalysis B: Environmental* 87: 30-36.
- Noorjahan M., Durga Kumari V., Subrahmanyam M., Panda L.(2005) Immobilized Fe(III)-HY: An efficient and stable photo-Fenton catalyst. *Applied Catalysis B: Environmental* 57: 291-298.
- Nosaka Y., Nakamura M., Hirakawa T. (2002) Behavior of superoxide radicals formed on TiO₂ powder photocatalysts studied by a chemiluminescent probe method. *Physical Chemistry Chemical Physics* 4: 1088-1092.
- Ollis D.F., Al-Ekabi H. (1993). Photocatalytic Purification and Treatment of Water and Air. D. F. (Eds). Amsterdam, Elsevier.

- Ononye A.I., McIntosh A.R, Bolton J.R. (1986) Mechanism of the photochemistry of p-benzoquinone in aqueous solutions. 1. Spin trapping and flash photolysis electron paramagnetic resonance studies. *Journal of Physical Chemistry*, 90: 6266-6270.
- Ortiz de la Plata G.B., Alfano O.M., Cassano A.E. (2008), Optical properties of goethite catalyst for heterogeneous photo-Fenton reactions. Comparison with a titanium dioxide catalyst. *Chemical Engineering Journal* 137: 396-410.
- Pal B., Sharon M.(1998) Photocatalytic degradation of salicylic acid by colloidal Fe₂O₃ particles. *Journal of Chemical Technology and Biotechnology* 73: 269-273.
- Pelizzetti E., Borgarello M., Minero C., Pramauro E., Borgarello E., Serpone N. (1988) Photocatalytic degradation of polychlorinated dioxins and polychlorinated biphenyls in aqueous suspensions of semiconductors irradiated with simulated solar light. *Chemosphere* 17: 499-510.
- Peyton G. R. (1990) Oxidative treatment methods for removal of organic compounds from drinking water supplies. Chelsea MI, Lewis Publishers.
- Pichat P., Guillard C., Amalric L., Renard A.-C., Plaidy O. (1995). Assessment of the importance of the role of H₂O₂ and O₂⁻ in the photocatalytic degradation of 1,2-dimethoxybenzene. *Solar Energy Materials and Solar Cells* 38: 391-399.
- Pignatello J.J. (1992). Dark and Photoassisted Fe³⁺-Catalyzed Degradation of Chlorophenoxy Herbicides by Hydrogen Peroxide. *Environmental Science and Technology* 26: 944-951.
- Pignatello J.J., Oliveros E., MacKay A. (2006) Advanced oxidation processes for organic contaminant destruction based on the fenton reaction and related chemistry. *Critical Reviews in Environmental Science and Technology* 36:1-84.
- Pozzo R.L., Baltanas M.A., Cassano A.E. (1997) Supported titanium oxide as photocatalyst in water decontamination: State of the art. *Catalysis Today* 39: 219-231.
- Pulgarin C., Kiwi J. (1995) Iron oxide-mediated degradation, photodegradation, and biodegradation of aminophenols. *Langmuir* 11: 519-526.
- Prousek J., Palacková E., Priesolová S., Marková L., Alevová A. (2007), Fenton- and Fenton-like AOPs for wastewater treatment: From laboratory-to-plant-scale application. *Separation Science and Technology* 42:1505-1520.
- Ramsden C.S., Smith T.J., Shaw B.J., Handy R.D. (2009) Dietary exposure to titanium dioxide nanoparticles in rainbow trout, (*Oncorhynchus mykiss*): No effect on growth, but subtle biochemical disturbances in the brain. *Ecotoxicology* 18: 939-951.
- Rincón A.G., Pulgarin C., Adler N., Peringer, P. (2001) Interaction between E. coli inactivation and DBP-precursors - dihydroxybenzene isomers - in the photocatalytic process of drinking-water disinfection with TiO₂. *Journal of Photochemistry and Photobiology A: Chemistry* 139: 233-241.
- Rios-Enriquez M., Shahin N., Durán-De-Bazúa C., Lang J., Oliveros E., Bossmann S.H., Braun A.M. (2004) Optimization of the heterogeneous Fenton-oxidation of the model pollutant 2,4-xylydine using the optimal experimental design methodology. *Solar Energy* 77: 491-501.
- Robertson P.K.J. (1996). Semiconductor photocatalysis: An environmentally acceptable alternative production technique and effluent treatment process. *Journal of Cleaner Production* 4: 203-212.
- Sabhi S., Kiwi J. (2001) Degradation of 2,4-dichlorophenol by immobilized iron catalysts, *Water Research*. 35: 1994–2002.

- Safarzadeh-Amiri A., Bolton J.R., Carter S.R. (1996a). The use of iron in Advanced Oxidation Processes. *Journal of Advanced Oxidation Technology* 1: 18-26.
- Safarzadeh-Amiri A., Bolton J.R. and Carter S.R. (1996b). Ferrioxalate-mediated solar degradation of organic contaminants in water. *Solar Energy* 56: 439-444.
- Schwarzenbach R. P., Escher B. I., Fenner K., Hofstetter T. B., Johnson C. A., Von Gunten U., Wehrli B. (2006) The challenge of micropollutants in aquatic systems. *Science* 313: 1072-1077.
- Sherman D.M. (2005) Electronic structures of iron(III) and manganese(IV) (hydr)oxide minerals: Thermodynamics of photochemical reductive dissolution in aquatic environments. *Geochimica et Cosmochimica Acta* 69: 3249-3255.
- Sulzberger B., Laubscher H. (1995) Photoredox reactions at the surface of iron(III)(hydr)oxides. *Marine chemistry* 50: 103-115.
- Sun Y., Pignatello J.J. (1992). Chemical treatment of pesticide wastes. Evaluation of Fe(III) chelates for catalytic hydrogen peroxide oxidation of 2,4-D at circumneutral pH. *Journal of Agricultural and Food Chemistry* 40: 322-327.
- Sychev A.Y., Isaak V.G. (1995). Iron compounds and the mechanisms of the homogeneous catalysis of the activation of O₂ and H₂O₂ and of the oxidation of organic substrates. *Russian Chemical Review* 64: 1105-1129.
- Teel A.L., Warberg C.R., Atkinson D.A., Watts R.J. (2001) Comparison of mineral and soluble iron Fenton's catalysts for the treatment of trichloroethylene. *Water Research* 35: 977-984.
- Tryba B., Morawski A.W., Inagaki M., Toyoda M. (2006) The kinetics of phenol decomposition under UV irradiation with and without H₂O₂ on TiO₂, Fe-TiO₂ and Fe-C-TiO₂ photocatalysts. *Applied Catalysis B: Environmental* 63: 215-221.
- Tryba B. (2008) Immobilization of TiO₂ and Fe-C-TiO₂ photocatalysts on the cotton material for application in a flow photocatalytic reactor for decomposition of phenol in water. *Journal of Hazardous Materials* 151: 623-627.
- Tyre B.W., Watts R.J., Miller G.C., Tyre B.W., Watts R.J., Miller G.C. (1991) Treatment of four biorefractory contaminants in soils using catalyzed hydrogen peroxide. *Journal of Environmental Quality* 20: 832-838.
- UN (2005) <http://www.un.org/waterforlifedecade/background.html>
- UNEP (2002) Global environment outlook 3. Nairobi, Kenya.
- Valenzuela M.A., Bosch P., Jiménez-Becerrill J., Quiroz O., Páez A.I. (2002) Preparation, characterization and photocatalytic activity of ZnO, Fe₂O₃ and ZnFe₂O₄. *Journal of Photochemistry and Photobiology A: Chemistry* 148:177-182
- Voelker B.M., Morel F.M.M., Sulzberger B. (1997) Iron redox cycling in surface waters: Effects of humic substances and light. *Environmental Science and Technology* 31: 1004-1011
- von Sonntag C., Dowideit P., Fang X., Mertens R., Pan X., Schuchmann M. N. and Schuchmann H.-P. (1997). The fate of peroxy radicals in aqueous solution. *Water Science and Technology* 35: 9-15.
- Walling C. (1975). Fenton's reagent revisited. *Accounts of Chemical Research* 8: 125-131.
- Walte T.D., Morel F.M.M. (1984) Photoreductive dissolution of colloidal iron oxides in natural waters. *Environmental Science and Technology* 18: 860-868.

- Watts R.J., Udell M.D., Monsen R.M. (1993) Use of iron minerals in optimizing the peroxide treatment of contaminated soils *Water. Environment Research* 65: 839-844.
- Wolfrum E. J., Ollis D.F. (1994). Hydrogen peroxide in heterogeneous photocatalysis., in *Aquatic and Surface Photochemistry*. G. R. Helz, R. G. Zepp and D. G. Crosby, (Eds). Boca Raton, Lewis Publishers. 451-463.
- Xu M.-J., Wang Q.-S., Hu C.-X. (2009) Treatment of wastepaper pulp wastewater by heterogeneous photo-Fenton process. *Harbin Gongye Daxue Xuebao/Journal of Harbin Institute of Technology* 41:142-148.
- Yaping Z., Jiangyong H. (2008) Photo-Fenton degradation of 17 β -estradiol in presence of α -FeOOHR and H₂O₂. *Applied Catalysis B: Environmental* 78: 250-258.
- Zepp R.G., Faust B.C., Hoigné J. (1992). Hydroxyl radical formation in aqueous reactions (pH 3-8) of iron(II) with hydrogen peroxide: The photo-Fenton reaction. *Environmental Science And Technology* 26: 313-319.
- Zhang Y., Dou X., Liu J., Yang M., Zhang L., Kamagata Y. (2007) Decolorization of reactive brilliant red X-3B by heterogeneous photo-Fenton reaction using an Fe-Ce bimetal catalyst. *Catalysis Today* 126: 387-393.
- Zhang Y.-Y., He C., Deng J.-H., Tu Y.-T., Liu J.-K., Xiong Y. (2009) Photo-Fenton-like catalytic activity of nano-lamellar Fe₂V₄O₁₃ in the degradation of organic pollutants. *Research on Chemical Intermediates* 1-11.
- Zhang Q., Jiang W.-F., Wang H.-L., Chen M.-D. (2010) Oxidative degradation of dinitro butyl phenol (DNBP) utilizing hydrogen peroxide and solar light over a Al₂O₃-supported Fe(III)-5-sulfosalicylic acid (ssal) catalyst. *Journal of Hazardous Materials* 176: 1058-1064.

2- PHYSICO-CHEMICAL PROPERTIES AND PHOTOREACTIVITY RELATIONSHIP IN HOMOGENEOUS PHOTO-FENTON SYSTEM

2.1 Introduction

The photocatalytic degradation rate of different compounds depends on various parameters, such as temperature, pH, initial concentration of the pollutant, Fe^{2+} and H_2O_2 concentrations, light intensity, and chemical nature (structure) of the reactants. The photochemical degradation of phenol and its derivatives using TiO_2 photocatalysis (Serpone, 1997; Chun, 2000; Arana, 2001; Villasenor, 2002; Colon, 2003; Sobczynski, 2004; Vione, 2005; Colon, 2006) or photo-Fenton oxidation (Herrera, 1998; Arana, 2001; Goi, 2002; Gernac, 2003; Kavitha, 2004; Kusic, 2006) has been reported during the last decade. The catalytic degradation is affected by the number of substituents, their electronic nature and their position in the aromatic ring (Tseng, 1991; D'Oliviera, 1993; O'Shea, 1994; Amalric 1996; Assabane, 2000; Torres, 2002; Parra, 2003; Lapertot, 2006; Karunakaran, 2006; Palmisano, 2007). In particular, quantitative structure-reactivity relationships (QSRR) during the degradation of *para*-substituted phenols for TiO_2 photocatalysis (Parra, 2003) and electrocatalytic oxidation (Torres, 2002) have been reported. The results have shown correlation between molecular structure and the kinetic parameters showing that *p*-halogen-phenols react in a different way than their non-halogenated analogues. A recent study predicted the oxidation positions in the benzene ring using frontier electron density theory to describe the reactivity (Byung-Dae, 2001). In photo-Fenton processes, only few reports are available on nitrophenol degradation (Kiwi, 1994; Kavitha, 2005), cyclic organic water contaminant (Ruppert, 1993) and for polychlorinated dibenzo-*p*-dioxins (Sun, 2008). However, no systematic correlation of molecular structure and degradation kinetics was performed.

In this chapter, the Hammett constants (σ), 1-octanol/water partition coefficient (K_{ow}), calculated energy of the highest occupied molecular orbital (E_{HOMO}), zero point energy (E_{ZERO}) and experimental half-wave potential ($E_{1/2}$) were correlated with the experimental initial rates of degradation calculated with Eq. 2.1.

$$r_0 = \frac{[\text{Substance}]_0 - [\text{Substance}]_t}{t} \quad (2.1)$$

Hammett constants (σ) describe the effect different substituent induced on the electronic density of the aromatic ring. σ directly relates the ionization potential and the susceptibility of a molecule to undergo electrophilic attack. The energy of the highest occupied molecular orbital (E_{HOMO}) is a useful parameter to model radical reactions and was calculated by Aptula et al (Aptula, 2002). K_{ow} represents the molecular hydrophobicity of a given compound. A high value of K_{ow} (>1000) means that the molecule has a great affinity for organic solvents but not for water. Some studies have correlated K_{ow} with the molecular biological properties. The half wave potential ($E_{1/2}$) corresponds to the oxidation of phenols to phenoxyl radicals via Eq. 2.2. The zero point energies were calculated by Gross et al (Gross, 2001). The absorption peaks were measured by UV-visible spectrophotometry.



The biodegradability of substituted phenols solutions depends on electronic effects, on their transport ability through the bacteria membranes and on the toxic effect of a given substituent. In this chapter, the biodegradability of *para*-substituted phenol solutions degraded by a photo-Fenton process was determined to see how the nature of the substituent affects the biodegradability of the generated degradation intermediate.

2.2 Experimental

2.2.1 Chemicals

The used organic compounds: phenol (p-H), 4-nitrophenol (p-NO₂), 4-chlorophenol (p-Cl), 4-hydroxybenzaldehyde (p-CHO), 4-hydroxyphenol (p-OH) and iron sulfate (II)

heptahydrated, were supplied by Flucka, 4-methoxyphenol (p-OCH₃) by Acros Organics. Ferrous iron sulphate (FeSO₄·7H₂O) as well as the solutions of sodium bisulfite (38-40%) and hydrogen peroxide (35%) stabilized, were supplied by Sigma Aldrich, the nitric acid (65%) by VWR BDA Prolabo.

2.2.2 Photo-reactor and irradiation procedures

All degradation experiments were carried out under simulated solar light, using thin film Pyrex glass reactors with an illuminated volume of 25 mL (Figure 2.1). A peristaltic pump allows circulation of the water from a glass bottle, acting as recirculation tank, to the reactors with a flow rate of 100 ml/min. The total volume of the system (110 mL) can be distinguished in two parts: 25 mL irradiated volume and the dead volume. The reactor was illuminated in the cavity of a solar simulator CPS Suntest system (Atlas GmbH). This solar box has a spectral distribution of about 0.5% of the emitted photons at wavelengths shorter than 300 nm, and about 7% within 300 and 400 nm. The emission spectrum between 400 and 800 nm follows the solar spectrum. The temperature of the solution increased up to approximately 30 °C during the course of the reaction. Control experiments in the dark were performed under similar conditions.

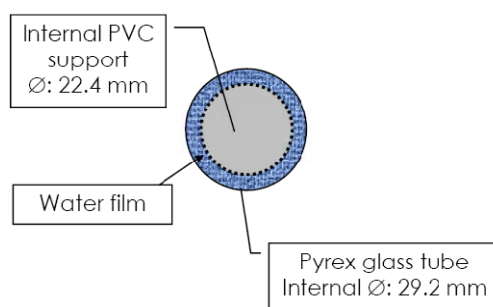


Figure 2.1. Transversal cut and characteristics of the photo-reactor.

Three reactors have been placed in parallel inside the solar box (Figure 2.2). The degradation experiments were performed using *para*-substituted phenols solutions (1.8 mM), each compound in separated solutions. All the experiments were performed in triplicate and the presented results correspond to the average.

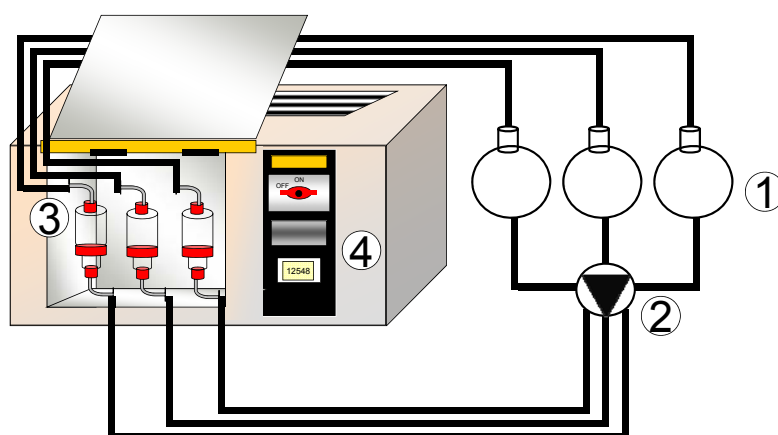


Figure 2.2 Photocatalytic setup: (1) tanks; (2) peristaltic pump; (3) photo-reactors; (4) solar simulator.

2.2.4 Analysis of the irradiated solutions.

The quantitative determination of organic compounds was carried out by HPLC chromatography using a LC system HPLC-UV: Shimadzu LC-2010A equipped with a UV detector. Samples, injected via autosampler, were eluted at a flow rate of 1 ml/min through a column (Nucleosil C18, Marcherey-Nagel) using as mobile phase acetonitrile – acetic acid solution (10%) in a 40/60 ratio. The total organic carbon (TOC) was monitored via a instrument (Shimadzu 500) equipped with an ASI automatic sample injector. The peroxide concentrations were determined by Merckoquant[®] paper at levels between 0.5 and 25 mg/l. The UV-visible spectra were recorded using a Varian Cary 1E UV-visible spectrophotometer. The BOD₅ was determined measuring the oxygen consumption during the biochemical degradation of the organic compounds. This analysis was made by means of a WTW 2000 Oxitop unit thermostated at 20 °C. The pH was adjusted between 6.8 and 7.5 by addition of 1 mL of decanted sludge (inoculums from the biological plant of Morges) Vaud, Switzerland.

2.3 Results and Discussion

2.3.1 Preliminary experiments

2.3.1.1 Selection of Fenton reagent concentration

The concentration of the Fenton reagents ($\text{Fe}^{2+}/\text{H}_2\text{O}_2$) during pollutant degradation has to be chosen carefully, to be able to observe the slight differences caused by the different substituents. In the case of photo-Fenton degradation of 2 mM phenol, optimal concentrations are $[\text{Fe}^{2+}] = 45 \text{ mg/L}$ and $[\text{H}_2\text{O}_2] = 30 \text{ mM}$ (Kavitha, 2004).

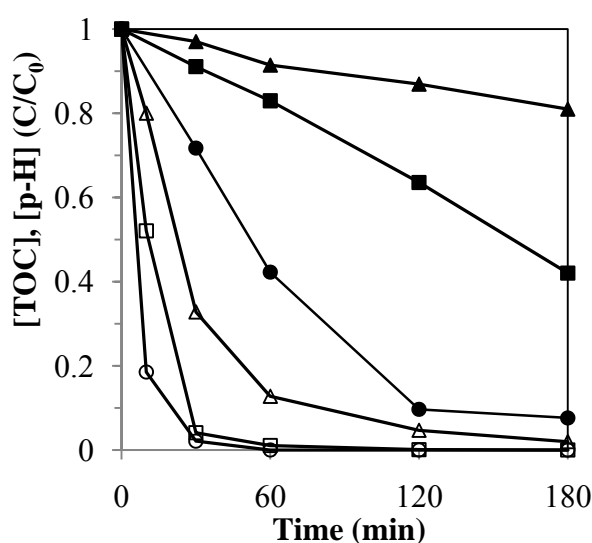


Figure 2.3 Substance (unfilled symbols) and TOC (filled symbols) removal during photo-Fenton degradation of phenol (1.8 mM) for different Fe^{2+} concentrations (-●- : 10 mg/L; -■- : 3 mg/L; -▲- : 1 mg/L) in presence of H_2O_2 (15 mM).

Figure 2.3 presents the evolution of phenol and TOC concentrations during photo-Fenton oxidation for different Fe^{2+} concentrations (1, 3 and 10 mg/L) in the presence of H_2O_2 (15 mM). Figure 2.3 shows that total phenol degradation is achieved in three hours and that the initial degradation rate depends on iron concentration leading to 10, 50 and 80% abatement within 15 min. for 1, 3 and 10 mg/L, respectively. Figure 2.3 shows as well that the mineralization process is dependent on $[\text{Fe}^{2+}]$, with 20, 60, 95% TOC removal for $[\text{Fe}^{2+}] = 1, 3$ and 10 mg/L, respectively. For the intermediate concentration of 3 mg/L, the

degradation is not too fast and TOC removal is sufficient to allow the reaction to be compared with other substituted phenols. This concentration was chosen to assess the effect of the substituent group nature on the Fenton and photo-Fenton degradation rates.

2.3.1.2 UV-visible spectrum measurements

The UV-visible spectrum (between 200 and 800 nm) of solution of *para*-substituted phenols (0.05 mM) at pH = 3 in presence and in absence of 0.18 mM FeSO₄ was measured (results not shown here). It was observed that all the *para*-substituted phenols absorb between 250 and 350 nm (Table 2.1). In presence of Fe²⁺ in *para*-substituted phenols solutions, the iron complex formation proceeded only with p-OH and p-OCH₃.

2.3.1.3 Photolysis experiments

Under irradiation at pH 3, no significant degradation (<5%) of *para*-substituted phenols was observed (results not shown here). The addition of Fe²⁺ considerably affected the compounds reactivity.

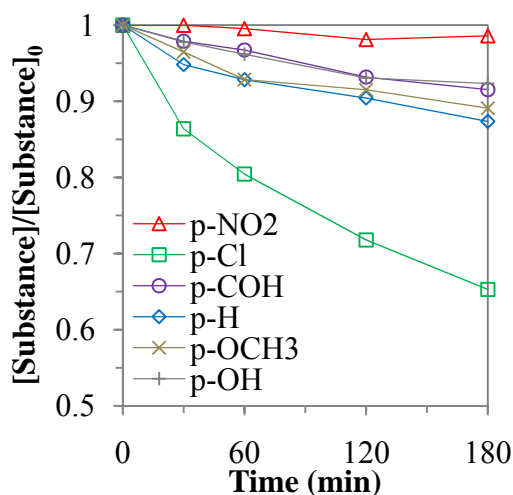


Figure 2.4. Evolution of *para*-substituted phenols concentration during photolysis in presence of Fe²⁺ (3 mg/L) at pH 3.

For p-OCH₃, p-OH, p-H and p-COH a degradation of about 10% was attained within 3 hours (see Figure 2.4). Although p-OH and p-OCH₃ form complexes with Fe²⁺, these compounds showed similar degradation rates as the other *para*-substituted phenols, in presence of Fe²⁺ and light. p-NO₂ degradation remained unchanged when Fe²⁺ was present or not.

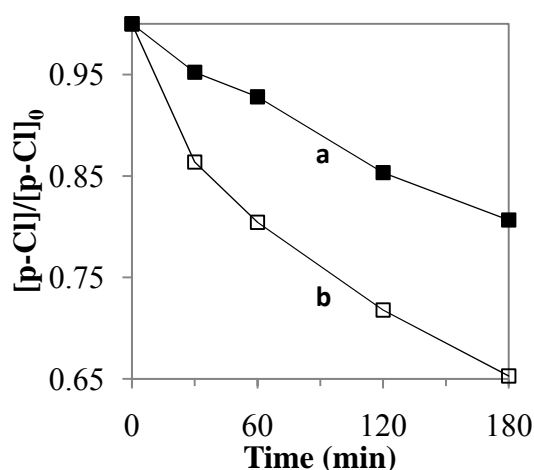


Figure 2.5. Evolution of p-Cl concentration during degradation in presence of Fe²⁺ (3 mg/L) at pH = 3 under: (a) dark conditions; (b) irradiation.

In the case of p-Cl, the presence of Fe²⁺ accelerated the degradation leading to 35% p-Cl degradation after 3 hours irradiation. In order to determine if the p-Cl photo-degradation in the presence of Fe²⁺ was due to the effect of light, we run the degradation of p-Cl solution in the dark. Figure 2.5 shows that the presence of Fe²⁺ ions in the dark (trace a) was sufficient to degrade 20% of p-Cl within 3 hours. Light irradiation was seen to accelerate the degradation (trace b).

2.3.1.4 Fenton degradation of *para*-substituted phenols.

The degradation of *para*-substituted phenols by the Fenton reagent (Fe²⁺/H₂O₂) was carried out using different H₂O₂ concentrations (1.8 and 7.2 mM). In order to discriminate between the different substituents, slow degradation kinetics is desired. When the reaction starts, the

solution becomes orange-brown within few minutes. Figure 2.6 (i) shows the *para*-substituted phenols degradation versus time for an initial H₂O₂ concentration of 1.8 mM.

From this result, it was found that for the electron-donating substituents (i.e. -H, -OCH₃ and -OH), the Fenton degradation process stops after 30 min treatment (with about 40, 50 and 30% degradation respectively) even if H₂O₂ was not totally consumed. The p-OH, p-OCH₃, p-H and/or their degradation intermediates form stable complexes with iron. This complex formation induces an inhibition of initial compounds degradation since the iron ions were not available for a subsequent degradation. However, the degradation of intermediates continues and the production of polymers (tannins Arana, 2001) might occur as well, since no residual H₂O₂ was detected at the end of the treatment.

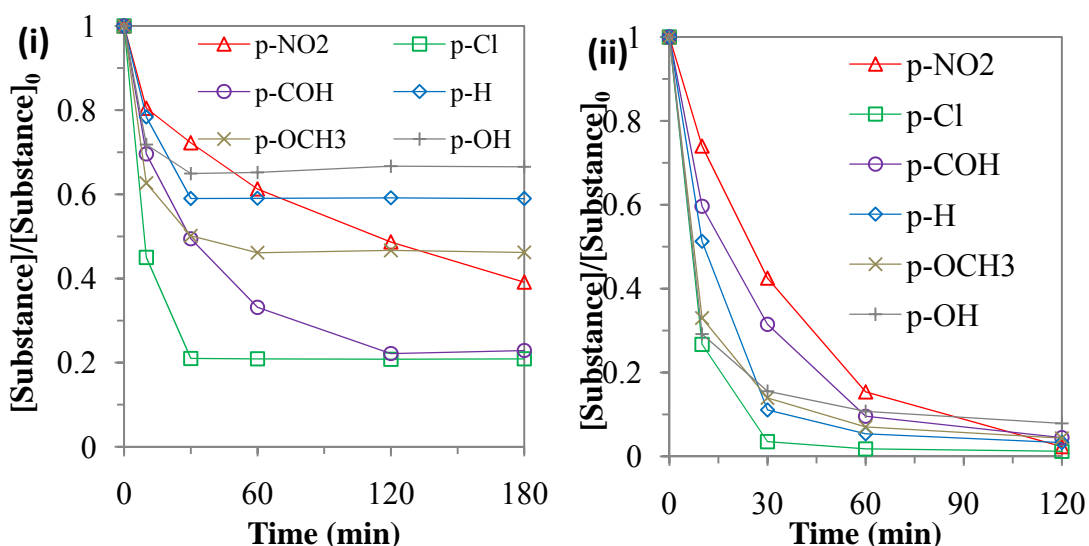


Figure 2.6. Evolution of *para*-substituted phenols concentration during Fenton degradation in presence of Fe²⁺ (3 mg/L) at pH = 3 with H₂O₂ (i) 1.8 mM; (ii) 7.2 mM.

For the electron-withdrawing substituents, (i.e. -COH and -NO₂), the inhibition was not observed since the degradation continues until the H₂O₂ was totally consumed. The remaining H₂O₂ concentration was zero and 0.03 mM for p-CHO and p-NO₂ respectively. In the case of p-Cl, H₂O₂ final concentration was observed to be still high (>0.8 mM) despite the fast p-Cl degradation. Consequently these results suggest that p-Cl reacts via a different pathway than other *para*-substituted phenols.

Figure 2.6 (ii) shows the *para*-substituted phenols degradation versus time for an initial H_2O_2 concentration of 7.2 mM. Under these conditions (closer to the optimal Fenton concentration), almost total degradation was achieved after 2 hours for all the compounds and the reaction inhibition was not observed.

2.3.2 Photo-Fenton experiments

Figure 2.7 depicts the evolution of the *para*-substituted phenol concentrations versus time for homogeneous photo-Fenton reaction with H_2O_2 7.2 mM. The results show that, except for p-NO₂, the degradation was fast reaching 80-90% in 15 min treatment. p-NO₂ was slowly degraded by TiO₂ (Parra, 2003) and is highly bio-recalcitrant. The degradation of p-Cl was the fastest among the tested *para*-substituted phenols in analogy with Fenton oxidation (point 2.3.1.4). The compounds p-OCH₃, p-COH, p-OH have similar degradation rates confirming the low selectivity of photo-Fenton reaction. The substances degradation is faster as shown in Figure 2.7 than in Figure 2.6, confirming the light enhancement of the Fenton rates.

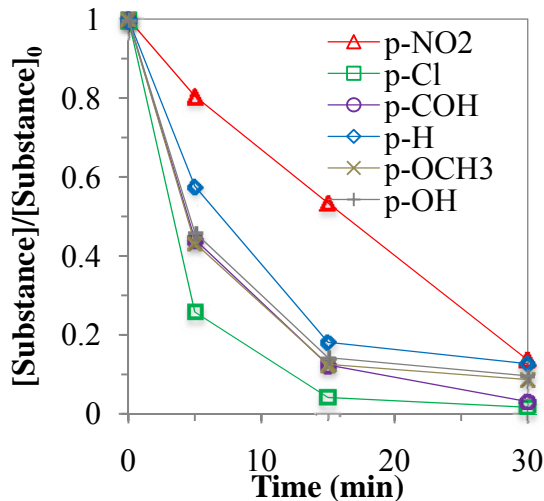


Figure 2.7 Evolution of *para*-substituted phenols concentration, during photo-Fenton degradation in presence of Fe^{2+} (3 mg/L) at pH = 3 with H_2O_2 7.2 mM.

The TOC evolution during the treatment was followed next. From Figure 2.8(i), for the 6-C compounds differences were observed in the initial degradation stages but the overall mineralization was similar, independently of the substituent nature. The differences between these compounds were within experimental error (2-3%). These observations confirm a low selectivity of photo-Fenton oxidation during mineralization. The fact that p-Cl degrades fast (point 2.3.1) did not distinguish p-Cl from the other *para*-substituted phenols in the mineralization process. For the compounds containing seven carbons, significant differences were observed between p-CHO and p-OCH₃ (Figure 2.8(ii)). The mineralization process was faster for p-CHO than for p-OCH₃ because the aliphatic carbon had an oxidation state of + I against zero for p-OCH₃.

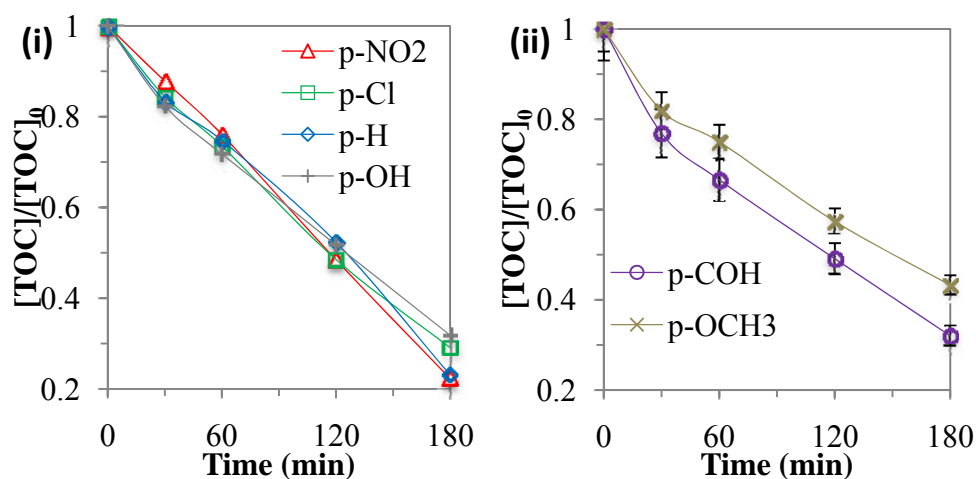
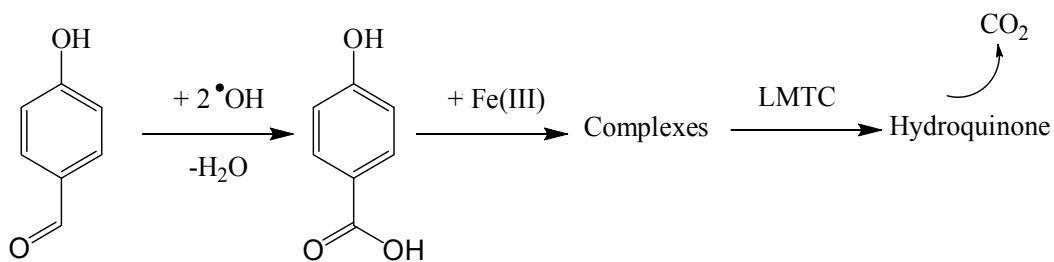


Figure 2.8. TOC removal during *para*-substituted phenols photo-Fenton degradation in presence of Fe²⁺ at pH = 3 with H₂O₂ 15 mM for (i) six carbon constituted compounds; (ii) seven carbon constituted compounds.

The Eq. 2.3 suggests how the initial mineralization is accelerated in the case of p-CHO. After a first radical attack on the carbon positioned out of the ring, a complex formation may follow and a LMCT liberates a CO₂ molecule. For the p-OCH₃ more steps are needed to attain the same result.



2.3.3 Quantitative structure reactivity relationship

Table 2.1 Physico-chemical descriptors from literature and measured initial rate constants.

X	σ^a	K_{ow}^b	E_{HOMO}^c	$E_{1/2}^d$	E_{zero}^e	λ_{max}^f	pK_a^g	$r^{F_0}{}^h$	$r^{PF_0}{}^h$
NO ₂	0.81	70.8	-10.07	1.17	4.28	316	7.65	0.046	0.070
Cl	0.28	309	-9.12	0.90	3.1	280	9.43	0.131	0.266
CHO	0.22	27.5	-9.49	n.d.	n.d.	284	7.62	0.073	0.201
H	0	30.2	-9.11	0.88	3.25	268	9.99	0.088	0.152
OCH ₃	-0.28	37.2	-8.65	0.65	2.35	275	10.20	0.122	0.204
OH	-0.38	3.9	-8.72	0.42	2.36	288	9.91	0.127	0.195

^a Hammett constants (σ) Parra, 2003

^b 1-octanol/water partition coefficient (K_{ow}) Aptula, 2002

^c Calculated energy of the highest occupied molecular orbital in eV Aptula, 2002

^d Experimental half wave potential ($E_{1/2}$) in V, Hauser, 1998

^e Calculated zero point corrected energies (E_{zero}) in eV, Gross, 2001

^f Experimental maximal absorption wavelength (λ_{max}) in nm

^g Acidity constants (pK_a), Aptula, 2002

^h Experimental initial degradation rate constants for Fenton (r^{F_0}) and photo-Fenton (r^{PF_0}) reactions in mM/min

2.3.3.1 QSRR for Fenton degradation

The relative initial rate of degradation (r_0^F) for *para*-substituted phenols and their corresponding descriptors are shown in Table 2.1. Linear regressions were performed plotting the initial Fenton rates (r_0^F) as a function of descriptors (results not shown). The correlation coefficients (R^2) are stated in Table 2.2. The p-Cl was excluded in this correlation due to its atypical reactivity (points 2.3.1 and 2.3.2).

Table 2.2 Correlation coefficients (R^2) obtained after linear regression in the plots of initial rates of degradation versus different descriptors (presented in appendices).

	σ	K_{ow}	E_{HOMO}	$E_{1/2}$	E_{zero}	pK_a
Fenton degradation ^a	0.949	0.711	0.961	0.977	0.995	0.723
Photo-Fenton degradation ^b	0.975	0.679	0.996	0.847	0.986	0.662

^a p-Cl excluded

^b p-Cl, p-CHO excluded

The plots of the electronic descriptors (E_{HOMO} , $E_{1/2}$, σ , E_{ZERO}) as a function of r_0^F show correlations with $R^2 = 0.961, 0.977, 0.949, 0.995$, respectively. E_{HOMO} and E_{ZERO} are calculated descriptors corresponding to the molecule electronic energy. The degradations were initially faster for molecules having low E_{HOMO} and E_{ZERO} . σ describes the effect induced by a given substituent on the electronic character of the aromatic ring. It was observed that the lower the Hammett constant, the faster the degradation process due to the electrophilic nature of hydroxyl radical. $E_{1/2}$ describes the oxidation of phenols to phenoxyl radicals via Eq. 2.2. The fact that the degradation kinetics was related to $E_{1/2}$ suggests that electrophilic attack on the ring and on the alcohol group occurs. The plots for $\log K_{ow}$, pK_a , as a function of r_0 show a poor correlation.

The behavior of p-Cl is different from its analogues reacting faster than predicted by the model. This p-Cl deviation was reported by Parra, 2003, for TiO_2 photocatalytic treatment and by Torres, 2002, for electrochemical oxidation, possibly due to the low C-Cl dissociation energy (Table 2.3) and the high electronegativity of Cl.

2.3.3.2 QSRR for photo-Fenton degradation

The initial rate of photo-Fenton degradation (r_0^{PF}) for the different studied *para*-substituted phenols and their corresponding descriptors are represented in Table 2.1. These descriptors were used to establish a correlation with the initial degradation rates. Linear regressions were performed plotting initial Fenton rates (r_0^{PF}) as a function of descriptors (results not shown) and the correlation coefficients (R^2) are represented in Table 2.2. Although the plots of E_{HOMO} , $E_{1/2}$, σ , E_{ZERO} versus r_0 showed a poor correlation (results not shown), when p-Cl is evaluated separately and p-COH is not taken in account, a good correlation ($R^2 = 0.996, 0.846, 0.975, 0.985$, respectively) was observed. $E_{1/2}$ was a good descriptor in Fenton reaction but fails in the photo-Fenton system. Thus the reaction Eq. 2.2 probably plays a less significant role in photo-Fenton process. The other electronic parameters described well the reactivity when excluding p-CHO (that reacted in a “regular way” in Fenton treatment). K_{ow} and pK_a were found to poorly correlate with r_0^{PF} . The deviation observed for p-Cl is justified by previous observations (part 2.3.1, 2.3.2); for p-COH the presence of a weak bond (Table 2.3) and the proposed mechanism in Eq. 2.3 might explain this deviation.

Table 2.3 Homolytic dissociation energy of different bonds of the *para*-substituted phenols.

Compound	Weakest bond	Homolytic dissociation energy (kJ/mol)
p-Cl	C ₆ H ₅ -Cl	394
p-COH	C ₆ H ₅ CO-H	377
Other p-Xs	C ₆ H ₅ -H	460

2.3.4 Evolution of biodegradability of photo-Fenton treated solutions

To couple the photo-Fenton process with a biological treatment, it is important to know the biodegradability of the solutions after the Fenton treatment (Bandara, 1997). The amount of oxygen consumed in 5 days by aerobic microorganisms (BOD_5) was measured to determine if the substituent nature induced significant changes in the biodegradability of the treated

solution. The experiments were performed using p-OH, p-Cl and p-NO₂ since these substances present a variety of electronic properties, toxicities and photo-Fenton degradation rates. The photo-Fenton treatment was stopped when 30% of TOC was mineralized.

The results presented in Table 2.4 show that before treatment, the BOD₅ values were low (around 5 mg/L). Consequently, these solutions were poorly biodegradable. After the photo-Fenton treatment, an increase in the biodegradability was observed since the BOD₅ values were higher than 150 mg/L. No important differences were observed between these three substituents. The ratio between BOD₅ and TOC was calculated (Table 2.4). This parameter varies from around 0.05 before treatment to 1.8, 1.7 and 1.6 for p-OH, p-Cl and p-NO₂ respectively after treatment. For easily biodegradable water (like urban wastewater), the ratio between BOD₅ and TOC being around 1.85, the results obtained show a substantial increase but poorly selective in the biodegradability due to photo-Fenton oxidation.

Table 2.4 BOD₅ (mg/L) and ratio between (BOD₅) and (TOC) before and after photo-Fenton treatment.

compound	BOD ₅	BOD ₅ /TOC	BOD ₅	BOD ₅ /TOC
	before treatment		after photo-Fenton	
p-OH	8	0.06	165	1.8
p-Cl	5	0.04	155	1.7
p-NO ₂	5	0.04	145	1.6

A possible explanation for this observation is that the degradation intermediates are similar once the aromatic ring has been broken (aliphatic acids) implying a similar biodegradability for the intermediates in solution.

2.4. Conclusions

Para-substituted phenol reactivity is a function of the electronic effects induced by the substituents. The Fenton and photo-Fenton degradation is faster when the electronic density of the aromatic ring is high favoring electrophilic radical attack on the ring. The degradation rates are higher when half wave potential is low. These results suggest different reactions occurring at different positions on the molecule on the aromatic ring, alcohol function, or on the substituent. The electronic descriptors (experimental and calculated) fit well with the kinetic parameters particularly with the Fenton rates (excluding p-Cl) but also with the photo-Fenton degradation rates (excluding p-Cl and p-CHO). The photo-Fenton rates can be non-linearly correlated with electronic descriptors especially when the reaction occurs rapidly at the substituents for p-CHO or p-Cl. This is possibly due to the presence of weak bonds. The increase in biodegradability induced by photo-Fenton treatment was significant but poorly selective regarding specific substituents. This is probably due to the similarity of the degradation kinetics of the intermediates.

2.5 References

- Amalric L., Guillard C., Blanc-Brude E., Pichat P. (1996) Correlation between the photocatalytic degradability over TiO₂ in water of meta and para substituted methoxybenzenes and their electron density, hydrophobicity and polarizability properties. *Water Research* 30: 1137-1142.
- Aptula A.O., Netzeva T.I., Valkova I.V., Cronin M.T.D., Schultz T.W., Khune R., Schurmann G. (2002) Multivariate discrimination between modes of toxic action of phenols. *Quantitative Structure-Activity Relationship* 21: 12-22.
- Arana J., Tello Rendon E., Dona Rodriguez J. M., Herrera Melian J.A., Gonzalez Diaz O., Perez Pena J. (2001a) High concentrated phenol and 1,2-propylene glycol water solutions treatment by photocatalysis: Catalyst recovery and re-use. *Applied Catalysis B: Environmental* 30: 1-10.
- Araña J., Tello-Rendón E., Doña-Rodríguez J.M., Valdés Do Campo C. (2001b) Highly concentrated phenolic wastewater treatment by heterogeneous and homogeneous photocatalysis: Mechanism study by FTIR-ATR. *Water Science and Technology* 44: 229-236.
- Assabane A., Ait Ichou Y., Tahiri H., Guillard C., Herrmann J.-M. (2000) Photocatalytic degradation of polycarboxylic benzoic acids in UV-irradiated aqueous suspensions of titania. Identification of intermediates and reaction pathway of the photomineralization of trimellitic acid (1,2,4-benzene tricarboxylic acid). *Applied Catalysis B: Environmental* 24: 71-87.

- Bandara J., Pulgarin C., Peringer P., (1997) Chemical (photo-activated) coupled biological homogeneous degradation of p-nitro-o-toluene-sulfonic acid in a flow reactor. *Journal of photochemistry and photobiology A: Chemical* 111: 253-263.
- Byung-Dae L., Mamoru I., Masaaki H. (2001) Prediction of Fenton oxidation positions in polycyclic aromatic hydrocarbons by Frontier electron density Prediction of Fenton oxidation positions in polycyclic aromatic hydrocarbons by Frontier electron density. *Chemosphere* 42: 431-435.
- Chun H., Yizhong W., Hongxiao T. (2000) Destruction of phenol aqueous solution by photocatalysis or direct photolysis. *Chemosphere* 41: 1205–1209.
- Colon G., Hidalgo M.C., Navio J. A. (2003) Photocatalytic behaviour of sulphated TiO₂ for phenol degradation. *Applied Catalysis B: Environmental* 45: 39–50.
- Colón G., Sánchez-España J.M., Hidalgo M.C., Navío J.A. (2006) Effect of TiO₂ acidic pre-treatment on the photocatalytic properties for phenol degradation. *Journal of Photochemistry and Photobiology A: Chemical* 179: 20-27.
- D'Oliveira J.-C., Guillard C., Maillard C., Pichat P. (1993) Photocatalytic destruction of hazardous chlorine- or nitrogen-containing aromatics in water. *Journal of Environmental Science and Health A: Environmental Science and Engineering* 28: 941-962.
- Gernjak W., Krutzler T., Glaser A., Malato S., Caceres J., Bauer R., Fernández-Alba A.R. (2003) Photo-Fenton treatment of water containing natural phenolic pollutants. *Chemosphere* 50:71-78.
- Goi A., Trapido M. (2002) Hydrogen peroxide photolysis, Fenton reagent and photo-Fenton for the degradation of nitrophenols: A comparative study. *Chemosphere* 46: 913-922.
- Gross K.C., Seybold P.G. (2001) Substituent Effects on the Physical Properties and pKa of Phenol. *International Journal of Quantum Chemistry* 85: 569–579.
- Hauser M.J.B., Olsen L.F. (1998) The role of naturally occurring phenols in inducing oscillations in the peroxidase-oxidase reaction. *Biochemistry* 37: 2458-2469.
- Herrera F., Pulgarin C., Nadtochenko V., Kiwi J. (1998) Accelerated photo-oxidation of concentrated p-coumaric acid in homogeneous solution. Mechanistic studies, intermediates and precursors formed in the dark. *Applied Catalysis B: Environmental* 17: 141-156.
- Karunakaran C., Dhanalakshmi R. (2006) Substituent Effect on Nano TiO₂- and ZnO-Catalyzed Phenol Photodegradation Rates. *International Journal of Chemical Kinetics* 41: 275-283.
- Kavitha V., Palanivelu K. (2004) The role of ferrous ion in Fenton and photo-Fenton processes for the degradation of phenol. *Chemosphere* 55: 1235-1243.
- Kavitha V., Palanivelu K. (2005) Degradation of nitrophenols by Fenton and photo-Fenton processes. *Journal of Photochemistry and Photobiology A: Chemical* 170 83-95.
- Kiwi J., Pulgarin C., Peringer P. (1994) Effect of Fenton and photo-Fenton reactions on the degradation and biodegradability of 2 and 4-nitrophenols in water treatment. *Applied Catalysis B: Environmental* 3: 335-350.
- Kusić H., Koprivanac N., Božić A.L., Selanec. *Journal of Hazardous Materials* 136: 632-644.

- Lapertot M., Pichat P., Parra S., Guillard C., Pulgarin C. (2006) Photocatalytic degradation of p-halophenols in TiO₂ aqueous suspensions: Halogen effect on removal rate, aromatic intermediates and toxicity variations. *Journal of Environmental Science and Health A: Environmental Science and Engineering* 41: 1009-1025.
- O'Shea K.E., Cardona C., (1994) Hammett study on the TiO₂-catalyzed photooxidation of para-substituted phenols. A kinetic and mechanistic analysis. *Journal of Organic Chemistry* 59: 5005-5009.
- Parra S., Olivero J., Pacheco L., Pulgarin C. (2003) Structural properties and photoreactivity relationships of substituted phenols in TiO₂ suspensions. *Applied Catalysis B: Environmental* 43: 293-301.
- Palmisano G., Addamo M., Augugliaro V., Caronna T., Di Paola A., García López E., Loddo V., Marci G., Palmisano L., Schiavello M. (2007) Selectivity of hydroxyl radical in the partial oxidation of aromatic compounds in heterogeneous photocatalysis. *Catalysis Today* 122: 118-127.
- Ruppert G., Bauer R., Heisler G., Novalic S. (1993) Mineralization of cyclic organic water contaminants by the Photo-Fenton reaction influence of structure and substituents, *Chemosphere* 27: 1339-1347.
- Serpone N. (1997) Relative photonic efficiencies and quantum yields in heterogeneous photocatalysis. *Journal of Photochemistry and Photobiology A: Chemical* 104: 1-12.
- Sobczynski A., Duczmal L., Zmudzinski W. (2004) Phenol destruction by photocatalysis on TiO₂: An attempt to solve the reaction mechanism. *Journal of Molecular Catalysis A: Chemical* 213: 225-230.
- Sun X., Sun T., Zhang Q. (2008) Degradation mechanism of PCDDs initiated by OH radical in Photo-Fenton oxidation technology: Quantum chemistry and quantitative structure-activity relationship, W. Wang. *Science of the total environment* 402: 123-129.
- Torres R.A., Torres W., Peringer P., Pulgarin C. (2002) Electrochemical degradation of p-substituted phenols of industrial interest on Pt electrodes. Attempt of a structure-reactivity relationship assessment. *Chemosphere* 50: 97-104.
- Tseng J.M., Huang C.P. (1991) Removal of chlorophenols from water by photocatalytic oxidation. *Water Science and Technology* 23: 377-387.
- Villasenor J., Reyes P., Pecchi G. (2002) Catalytic and photocatalytic ozonation of phenol on MnO₂ supported catalysts. *Catalysis Today* 76: 121-131.
- Vione D., Minero C., Maurino V., Carlotti M.E., Picatonott M.E.T., Pelizzetti E. (2005) Degradation of phenol and benzoic acid in the presence of a TiO₂-based heterogeneous photocatalyst. *Applied Catalysis B: Environmental* 58: 79-88.

3- SYNTHESIS OF IRON OXIDE COATED FUNCTIONALIZED POLYMER FILMS: EFFECT OF SURFACE TREATMENT ON PHOTOCATALYTIC ACTIVITY.

3.1. Introduction

Polymer films were used as supports for the deposition of iron oxides due to the wide range of applications possible with such materials. Among others, catalysts active under solar or UV light (such as self-cleaning surfaces or heterogeneous catalysts for water detoxification and disinfection, etc.) are attractive materials. However, the use of polymer films as substrate is a challenge as it induces several practical drawbacks that have to be overcome: (i) commercial polymer films surfaces are slick and intrinsically not very adhesionable (Mittal, 1996), limiting iron oxide crystal nucleation and its adhesion to the substrate; (ii) polymer films are destroyed under high temperature and are slowly degraded under solar irradiation which prevents from the proceeding of high temperature thermal treatment in preparation procedure. Although commercial available polymers have surface roughness, electron donor groups, relatively high melting points and a high stability under solar light, many commonly used polymers films such as polyethylene (PE), polyethylene terephthalate (PET) or fluorinated polymers etc. do not show such properties. Since those polymer films are widely used in packaging, bottles, coatings, etc., they can be recycled as photocatalyst supports, but a functionalization of their surface may be required.

The functionalization of polymer surfaces is recognized as a valuable tool to improve their adhesion properties. Surface functional groups like hydroxyl, ketone and carboxylic acids are introduced to adjust the surface free energy. Furthermore these groups are used to increase hydrogen binding and to create chemical bonds between the substrate and the

species to be deposited. Besides surface morphology changes are occurring increasing the surface roughness. During the modification, weak boundary layers and surface contaminants are removed. All these factors improve the adhesion properties of polymer surfaces.

The conventional methods for surface modification are mechanical and wet-chemical methods to produce either chemical or morphological changes in the surface. However, these processes have inherent problems of uniformity and reproducibility for plating products. Furthermore, they result in undesirable environmental pollution due to the aggressive acidic solutions such as chromic, sulfuric or potassium-permanganate solutions required to modify the surface of the polymer materials.

Alternative surface modification techniques include treatments by flame, corona, plasmas, photons, electron beams, ion beams, X-rays, γ -rays, reactive oxygen species (ROS).

In this chapter, radiative functionalization techniques (oxygen radio frequency plasma (RF-P), vacuum ultraviolet (VUV) and photocatalytic techniques (TiO₂ photocatalysis (Ti-PC and photo-Fenton oxidation (PF-O)) are used to functionalize polymer surfaces in order to improve iron oxide adhesion.

3.1.1 Radiative treatments of polymer surfaces

3.1.1.1 Plasma treatment

Plasma describes the state of partially ionized gas and sometimes referred as the fourth state of matter. Plasmas are generated by applying either high temperature or strong electric or magnetic field to a gas.

The plasmas used for polymer functionalization are produced by applying an electric field to a gas. The free electrons in this discharge are accelerated by the electric field and collide with neutral gas molecules or atoms. Due to these metastables collisions, positive ions, electrons and free radicals are generated (Terlingen, 2008).

Plasma treatment is one of the most versatile surface treatment techniques. Different types of gases such as argon, oxygen, nitrogen, fluorine, carbon dioxide, and water can produce the unique surface properties required by various applications. For example, oxygen-

plasma treatment can increase the surface energy of polymers, whereas fluorine-plasma treatment can decrease the surface energy and improve the chemical inertness. Cross-linking at a polymer surface can be introduced by an inert-gas plasma. Modification by plasma treatment is usually confined to the top several hundred Ångströms and does not affect the bulk properties. The main disadvantage of this technique is that it requires a vacuum system, which increases the cost of operation.

Oxygen and oxygen-containing plasmas are most commonly employed to modify polymer surfaces. It is well known that an oxygen plasma can react with a wide range of polymers to produce a variety of oxygen functional groups, including C-O, C=O, O-C=O, C-O-O, and CO₃ at the surface. In an oxygen plasma, two processes occur simultaneously: etching of the polymer surface through the reactions of atomic oxygen with the surface carbon atoms, giving volatile reaction products; and the formation of oxygen functional groups at the polymer surface through the reactions between the active species from the plasma and the surface atoms. (Chan, 1996).

3.1.1.2 Vacuum UV (V-UV) treatments

The VUV spectral region corresponds to light with wavelengths, λ , in the range from 200 nm (approximate threshold of light absorption in air) to about 1 nm (Samson et al 1987). Light with these wavelengths is present in the solar radiation spectrum above the terrestrial atmosphere and in radiation from gas discharge plasmas.

Most of the polymers strongly absorb the V-UV radiation. V-UV photons selectively excite electrons to high levels called Rydberg states (Vasilets, 2004) located near the threshold of ionization. In contrast to UV radiation, the energy of V-UV photons is high enough to cause the dissociation of various chemical bonds in polymer molecules including C-C, C-H, C-O, C-F and produce radicals. The recombination of radicals formed by V-UV photolysis leads to the formation of crosslinks. The detachment of hydrogen molecules H₂ induced by V-UV photolysis is responsible of the formation of double bonds in polymer matrix (Skurat, 2003). In presence of air or other gases, radicals may react with gas molecules as well as with activated species such as excited molecules, atoms, and radicals produced by V-UV gas photolysis in the reaction chamber. These reactions result in the

formation of specific groups on the polymer surface and provide selective functionalization of the polymers (Vasilets, 1994). The V-UV irradiation modifies a surface polymer layer without deterioration of the bulk mechanical properties.

Recently, plasma and V-UV treatments have been applied to polymers for medical applications or to prepare antibacterial material. These surface modifications enhance the adhesions of biomolecules (Vasilets, 2006), metals (Charbonnier, 2003; Yuranova, 2003) or oxides (Mejia, 2009) on polymer surfaces. However, methods using plasma or V-UV have the disadvantage of requiring vacuum conditions, electrical power, and the large investment costs for commercialization. These limitations have increased the demand for the development of new, efficient, and dependable processes.

3.1.3 Photocatalytic treatments of polymer surface

Due to the mild conditions required (atmospheric pressure, ambient temperature, water as solvent) and the possibility of using sunlight as the source of irradiation, the photocatalytic processes constitute attractive methods to functionalize polymer surfaces. Photo-Fenton and TiO₂ photocatalysis are based on the generation of ROS able to oxidize most of the organic compounds.

The functionalization of polymers surfaces by means of TiO₂ photocatalysis was recently proposed (Kim, 2006; Kim, 2007). This treatment was found to produce functional groups such as carboxylic acid or hydroxide on polymer surface and to improve the adhesion of a metallic layer. Photo-Fenton was not used yet to modify polymer surfaces to our knowledge. However, Fenton and photo-Fenton processes were applied to produce hydroxide and carboxylic acid groups on carbon nanotubes (Fan 2007, Escobar 2009) and diamond nanoparticles (Martín, 2009) surfaces.

This chapter is directed toward the fixation and photocatalytic performance of iron oxide on polyvinyl fluoride (PVF) films previously functionalized by different methods. The main objective is to compare the catalytic activity and stability of photocatalysts as a function of preparation procedure (different functionalization methods) toward hydroquinone degradation.

3.2. Materials and Method

3.2.1 Chemicals

Hydroquinone, NaOH, HNO₃, FeCl₃ anhydrous, FeSO₄·7H₂O, ferrozine, hydroxylamine hydrochloride, acetate buffer (pH = 4.65) were Fluka p.a. reagents (Buchs, Switzerland) and used as received. Hydrogen peroxide (35%) was supplied by Merck AG (Darmstadt, Germany). TiO₂ P25 powder (anastase to rutile ratio between 70:30 and 80:20) was supplied by Degussa. The polyvinyl fluoride (PVF) films were 72 μm thick and were supplied by Goodfellow (Cambridge Ltd. United Kingdom).

3.2.2 Photocatalyst preparation

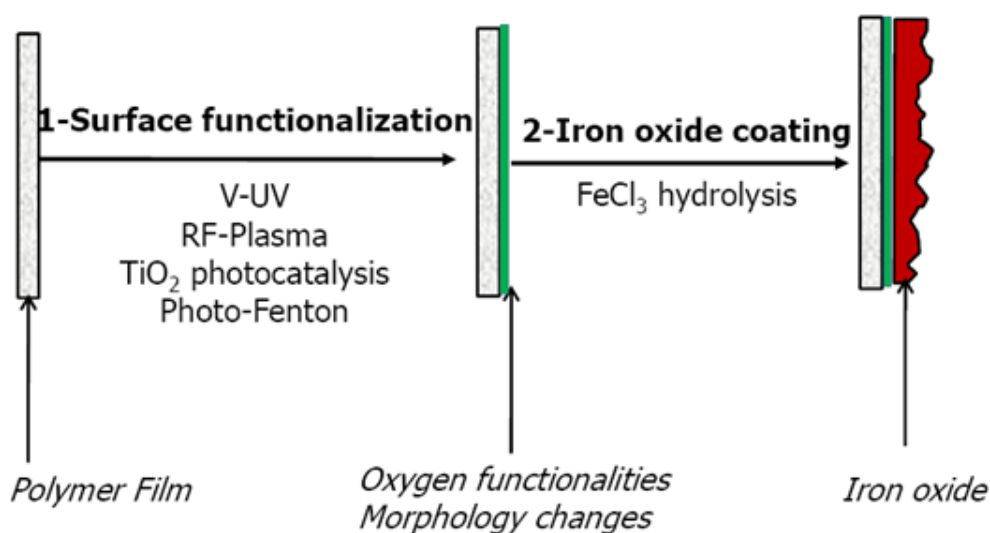


Figure 3.1 Scheme of catalyst preparation strategy (not to the scale).

Photoactive iron oxide was deposited on commercial polymer film substrates following the strategy presented in Figure 3.1. Before use, the films were washed in a diethyl ether: ethanol (1:1) mixture and in MilliQ water in order to eliminate surface contaminants. Then polymer films surfaces were functionalized by different methods described in the next paragraphs. Finally to immobilize iron oxide, functionalized polymer films (P^f) were immersed in a solution of FeCl₃ (anhydrous) 5 g/L and heated under stirring at 80 °C during one hour. Optionally, the composite material was heated in an oven at 100 °C for

one hour. The final films showed a brownish iron oxide coat probably constituted by akaganeite ($\beta\text{-FeOOH}\cdot\text{Cl}_n$) that will be characterized in chapter 4, by X-ray photoelectron spectroscopy (XPS).

3.2.2.1. Functionalization with radio frequency plasma (RF-P)

The polymers films were treated in a plasma cavity (Harricks Corp, 13.56 MHz, power 100 W), at a pressure of 1.0 mbar. The gas used for the plasma generation was air. The functionalization process occurs in the topmost layers and increases with longer treatment time, but remains constant with treatment time > 30 min (Yuranova, 2003). For this reason the latter time has been chosen for RF-P treatment. A previous report (Golub, 1989) presented a detail electron spectroscopy for chemical analysis (ESCA) study of the effect of oxygen RF-P treatment on PVF surface which was shown to produce C=O, fluorine loss and a slight loss of carbon atoms (by etching).

3.2.2.2. Functionalization with V-UV

The polymer film surface was also functionalized by V-UV irradiation using the 185 nm (6 W) line from a 25 W (254 + 185 nm) low pressure mercury lamp (Ebra Corp, Tokyo, Japan). The lamp was a synthetic silica tube. The polymer film was attached around the lamp tube. The gas used was air (0.8 mbar) and the treatment time was 30 minutes (condition selected from (Yuranova, 2003)). A detail investigation on the effect of V-UV radiation on PVF films was reported recently (Everett, 2006). It was found that with short treatment times (i.e. < 24 hours) the main effect induced by this treatment was a washing of surface contamination a decrease of fluorine surface concentration and an increase of carbon surface concentration.

3.2.2.3 Functionalization with photo-Fenton oxidation (P-FO)

The polymer films were attached on a cylindrical steal support and immersed in solutions of Fe^{2+} (50 mg/L) containing H_2O_2 (30 mM) at pH 3. The batch reactor was irradiated in a solar simulator CPS Suntest system (ATLAS). The polymer surface undergoes the photo-Fenton functionalization during two hours under magnetic stirring.

3.2.2.4 Functionalization with TiO_2 photocatalysis

The polymer films were attached on a cylindrical steal support and immersed in well dispersed solutions of TiO_2 0.2 g/L at initial natural pH. The batch reactor was irradiated in a solar simulator CPS Suntest system (ATLAS). The polymer surface underwent the TiO_2 photocatalytic functionalization under magnetic stirring during 2 hours. This treatment induced the deposition of a white layer constituted by TiO_2 particles (that will be characterized in chapter 4).

3.2.3 Photo-reactor and irradiation procedure

All the degradation experiments were carried out under simulated solar light, using thin film Pyrex glass reactors (Figure 3.2).

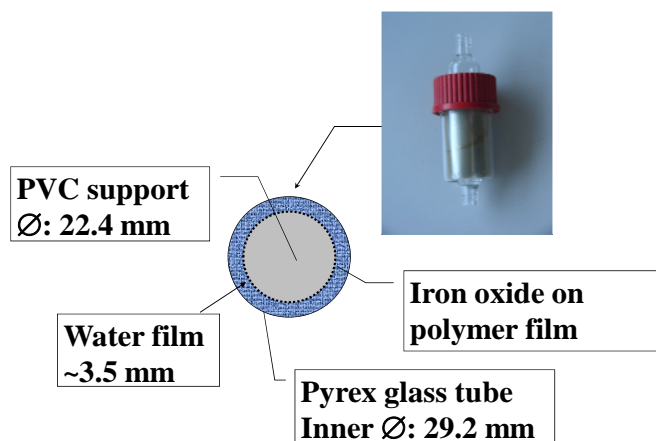


Figure 3.2 Transversal cut and characteristics of the photo-reactor.

A peristaltic pump allows circulation of water (flow rate of 100 mL/min) using an Erlenmeyer flask as a recirculation tank. The total volume of the system (110 mL) consists of two parts: 25 mL irradiated volume and the dead volume in connecting tubes and Erlenmeyer tank. Internal PVC supports were placed in the reactor to carry the photocatalyst films. The reactor was illuminated inside a solar simulator CPS Suntest

system (Atlas GmbH the details characteristics are reported point 2.2.2). The irradiation experiments were started at room temperature (20 °C) and progressively the temperature increased up to approximately 30 °C. Three reactors were placed in parallel inside the solar box. The degradation experiments were performed using solutions containing HQ (0.18 mM) and H₂O₂ (1.6 mM).

3.2.4 Analysis of the irradiated solutions

The quantitative determination of organic compounds was carried out by HPLC chromatography using a LC system HPLC-UV Shimadzu LC-2010A equipped with a UV detector. Samples, injected via an auto-sampler, were eluted at a flow rate of 1 mL/min through a column (Nucleosil C18 Marcherey Nagel) and using as mobile phase HPLC grade acetonitrile–acetic acid solution (10%) in a 40% - 60%. The total organic carbon (TOC) was monitored via an ASI automatic sample injector (Shimadzu 500). The peroxide concentrations were assessed by Merkoquant[®] paper at levels between 0.5 and 25 mg/L. The total iron concentration in the irradiated solutions was measured by complexation with Ferrozine[®] (Aldrich 16.060-1) in the presence of hydroxylamine hydrochloride and acetate buffer (pH=4.65) (Gibbs, 1979).

3.2.5 Catalyst characterization by UV-visible spectrophotometry

Conventional UV-Visible spectrophotometry is carried out in transmission mode with samples that allow the light beam to pass straight through without being diverted by refraction or spread out by scattering. Since the prepared materials let the light pass, but scatter the beam as it passes through, they were analyzed by placing them in front of the sphere and gathering the transmitted light as it emerges from the sample.

An integrating sphere is a type of Diffuse Reflectance Accessory. Diffuse reflectance refers to light being reflected off a matte surface – an effect that is sometimes referred to as *Lambertian* behavior.

The UV-Visible spectra of different photocatalysts were recorded on a Varian Cary 5 equipped with an integration sphere.

3.3 Results and discussions

3.3.1. Effect of functionalization on photocatalytic activity of PVF^f-Fe oxide

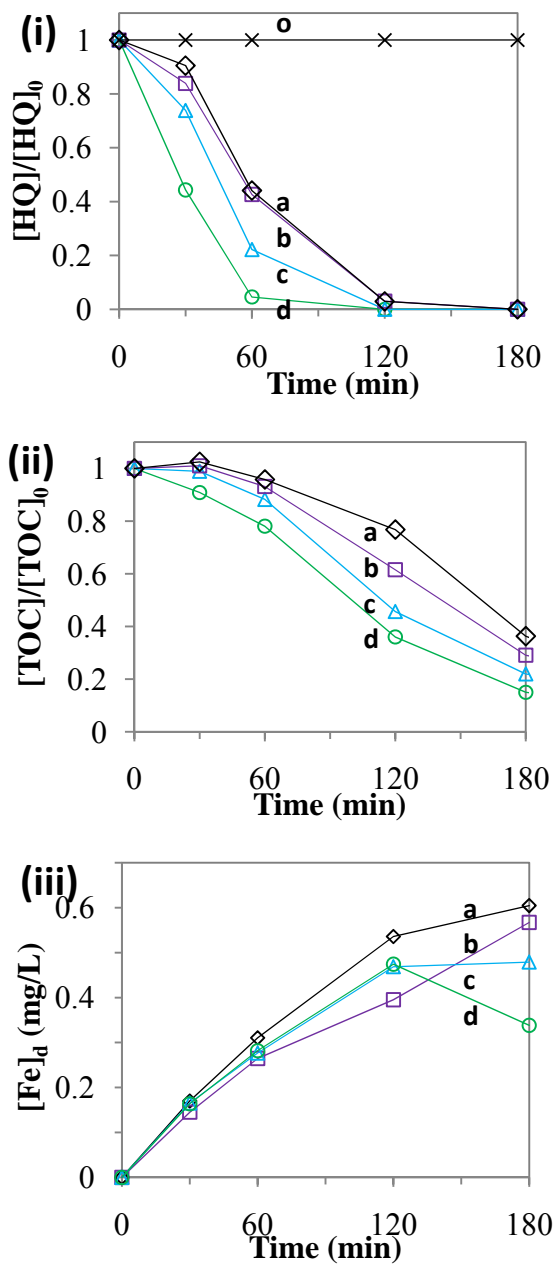


Figure 3.3. Evolution of (i) HQ concentration, (ii) TOC and (iii) [Fe]_d during degradation of 0.18 mM of HQ at initial pH 5.7, in presence of 1.6 mM H₂O₂, 75 cm² of catalyst under solar simulation (light): (o) photolysis; (a) PVF-Fe-oxide; (b) PVF^{V-UV}-Fe-oxide and PVF^{P-FO}-Fe oxide*; (c) PVF^{RF-P}-Fe oxide; (d) PVF^{Ti-PC}-Fe-oxide. The traces represent an average

over three runs. *Due to similar result obtained for PVF^{V-UV}-Fe-oxide and PVF^{P-FO}-Fe oxide trace (b) represent the results relative to these two catalysts.

Figure 3.3 shows (i) HQ, (ii) TOC and (iii) dissolved iron concentrations ($[Fe]_d$) over time during degradation experiments mediated by different photocatalysts in presence of H₂O₂ and light. The pH initially 5.7 decreased to 4.5 after 30 min mostly due to the formation of short acidic degradation intermediates.

Figure 3.3 (i) shows that HQ was resistant to direct photolysis by simulated solar light alone (trace o). During the degradation of HQ mediated by PVF-Fe oxide (trace a Figure 3.3(i)), PVF^{P-FO}-Fe oxide and PVF^{V-UV}-Fe oxide (both represented by trace b Figure 3.3(i)), the HQ degradation was low during the first 30 min of treatment but was complete at 120 min. The initial phase is slow and then fast degradation sets seems to be due to homogeneous photo-Fenton oxidation, since after 60 min the concentration of dissolved iron ($[Fe]_d$) detected is around 0.3 mg/L (Figure 3.3(iii)). For the photo-assisted degradations (Figure 3.3(i)) mediated by PVF^{RF-P}-Fe oxide (Trace c) and PVF^{Ti-PC}-Fe oxide (trace d), the initial degradation (first 30 min) was important with about 30 and 60 % of HQ degradation, respectively.

Figure 3.3 (ii) shows that during the first 30 min of irradiation, the TOC slightly increased for PVF-Fe oxide (trace a), PVF^{V-UV}-Fe oxide and PVF^{P-FO}-Fe oxide (both in trace b), due to a degradation of the polymer substrate, but remains constant for PVF^{RF-P}-Fe oxide. After that the TOC begins to decrease and about 25, 40 and 55% of mineralization was observed for PVF-Fe oxide, both PVF^{V-UV}-Fe oxide and PVF^{P-FO}-Fe oxide, and, PVF^{RF-P}-Fe oxide, respectively, after 120 min of treatment. In contrast, a significant TOC decrease was observed from the beginning, when PVF^{Ti-PC}-Fe oxide was used and 65% of TOC was mineralized after 120 min of treatment.

Figure 3.3 (iii) shows that the leaching of iron was similar for the five tested catalysts. Only for the PVF^{Ti-PC}-Fe oxide, the $[Fe]_d$ decreased slightly at the end of the treatment. This fact suggests that dissolved iron species were re-adsorbed on the catalyst surface possibly on TiO₂ particles. Thus the heterogeneous contribution seems to be involved in the observed differences as follows: no treatment \leq P-FO \approx V-UV $<$ RF-P \ll Ti-PC. The possible

heterogeneous reactions involved in the degradation and mineralization of HQ are Fenton and photo-Fenton oxidation (Eq. 1.55-1.56, 1.62-1.68) and iron oxide photocatalysis (Eq. 1.57-1.61). In the case of catalyst prepared by Ti-PC, TiO₂ photocatalysis (Eq. 1.6-1.12) may also contribute to the processes as TiO₂ particles were deposited on polymer surface. Besides synergistic effects between Fenton and semiconductor (iron oxide and/or TiO₂) photocatalysis are likely to occur which will be discussed in more details in chapter 4.

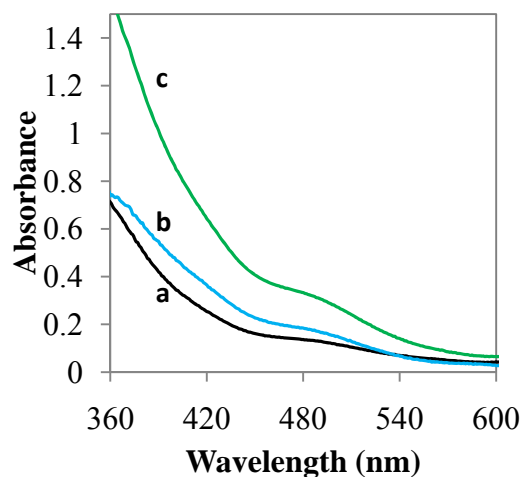


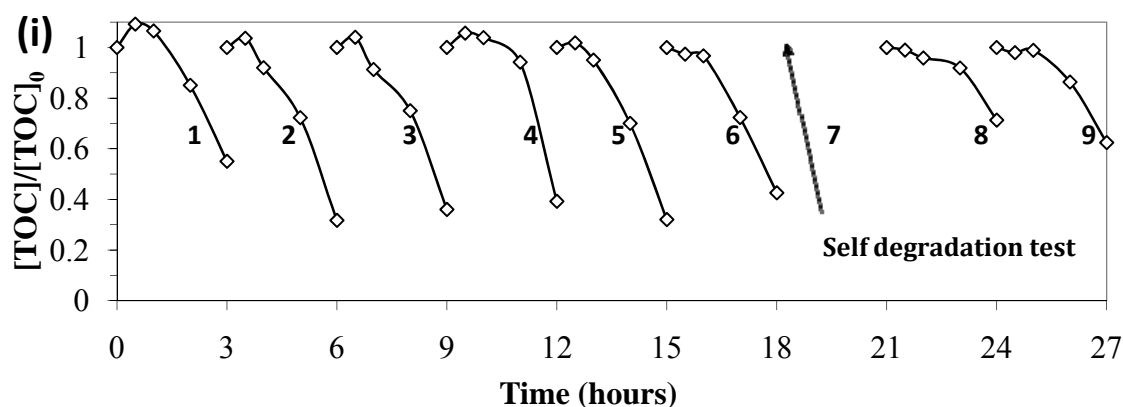
Figure 3.4. UV-vis absorption spectrum of (a) PVF-Fe oxide, PVF^{V-UV}-Fe oxide, PVF^{P-FO}-Fe oxide; (b) PVF^{RF-P}-Fe oxide; (c) PVF^{Ti-PC}-Fe oxide.

Figure 3.4 shows the UV-Vis absorption spectrum of several photocatalysts between 360 and 700 nm before their first use. The absorbance of PVF film in this region was negligible. The spectra of PVF-Fe oxide, PVF^{V-UV}-Fe oxide and PVF^{P-FO}-Fe oxide were similar and are thus represented by trace a. In contrast, PVF^{RF-P}-Fe oxide (trace b), and more markedly PVF^{Ti-PC}-Fe oxide (trace c) spectra show that the absorption was higher. The iron oxide on the polymer surface is responsible for the absorption of light. Hence the absorbance can be correlated with the thickness of iron oxide coating. These results show that RF-P and Ti-PC treatments favor iron oxide nucleation and/or deposition on the functionalized film. On the contrary, P-FO and V-UV treatments did not improve significantly iron oxide deposition on polymers if compared to not treated ones.

Several causes could explain the beneficial effects induced by the functionalization of PVF surface: (i) a chemical functionalization where oxygen surface functionalities increase the surface polarity; (ii) the modification of polymer surface morphology induced by RF-P (etching) and by Ti-PC (deposition of particles); and (iii) the additional photocatalytic activity induced by the deposition of TiO₂ particles. The fact that V-UV and P-FO pre-treatments did not increase the photocatalytic activity of as prepared material (and by extension iron oxide deposition) can be explained by: (i) Short V-UV treatment does not allow the production of polar groups on polymer surface and thus will not enhance iron oxide deposition; (ii) P-FO treatment may produce polar groups susceptible to bind iron oxide particles, however iron aquacomplexes might immediately bind with these freshly formed polar moieties during the pre-treatment process.

3.3.2. Effect of functionalization on long-term stability of PVF^f-Fe oxide

The long term stability of several photocatalysts was tested repeating photo-Fenton HQ degradations experiments and applying a self-degradation test (SDT) that involved irradiation of the photocatalysts in absence of dissolved organic substance but in presence of H₂O₂. SDT simulates highly reactive conditions and aims to assess if the polymer substrate as well as overall photocatalytic activity are altered by radicals produced in absence of any organic compounds.



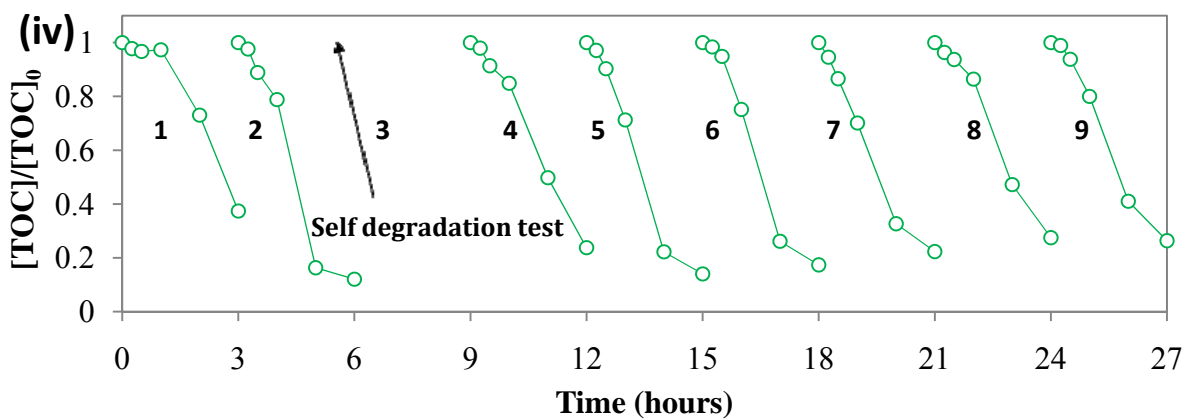
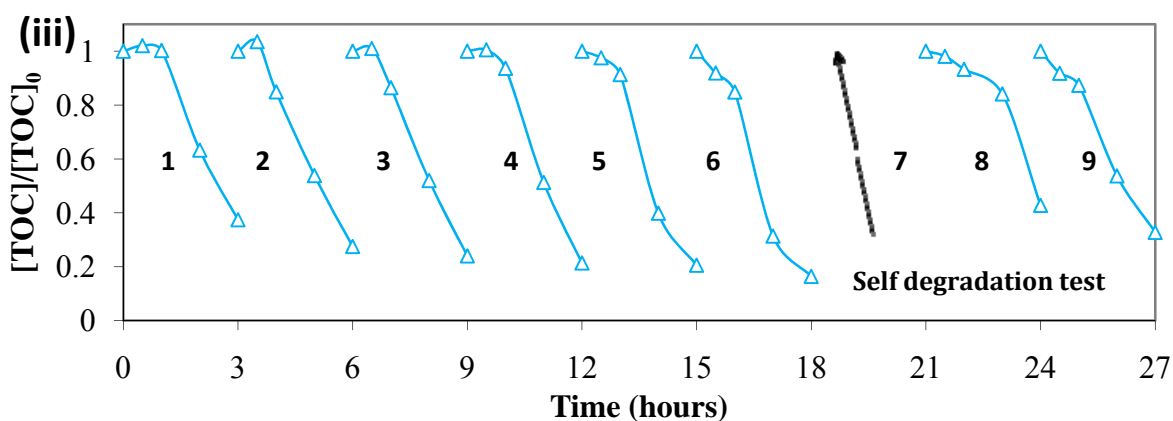
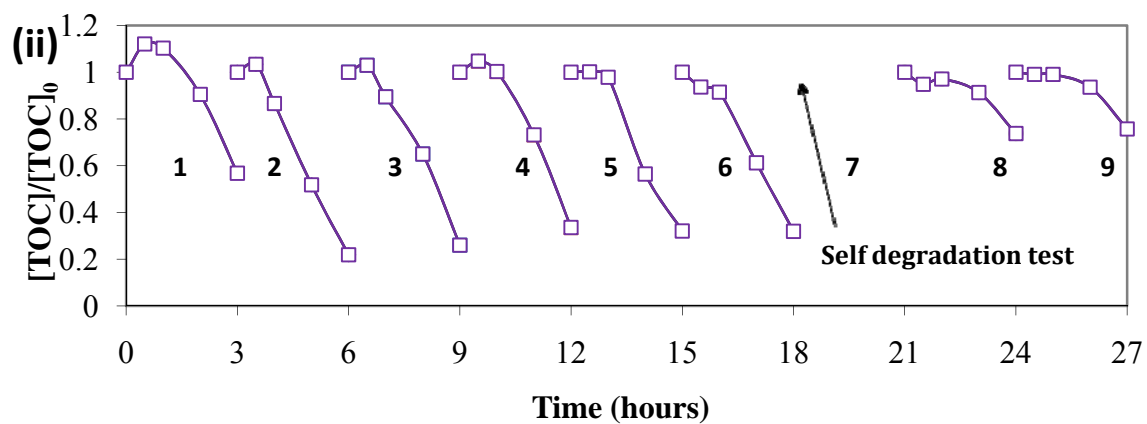


Figure 3.5 TOC removal during repetitive HQ photocatalytic degradations by (i) PVF-Fe oxide, (ii) PVF^{V-UV}-Fe oxide, (iii) PVF^{RF-P}-Fe oxide and (iv) PVF^{Ti-PC}-Fe oxide (experimental conditions: 0.18 mM of HQ, solar simulation, initial pH 5.7, H₂O₂ 1.6 mM).

Figure 3.5 shows repetitive HQ mineralization (eight cycles and a self degradation test). Between two runs, the catalyst and reactor system were thoroughly washed with distilled

water. In Figure 3.5 (i) and (ii) (corresponding to PVF-Fe oxide and PVF^{V-UV}-Fe oxide, respectively) the photocatalytic activity remained constant during five cycles with about 60 and 70% TOC removal after 3 hours of treatment. The SDT (after 18h) induced an important and irreversible loss of 50% of photocatalytic activity (runs 8-9). For the PVF^{RF-P}-Fe oxide presented in Figure 3.5 (iii), irreversible catalytic activity loss of about 25% was observed after the SDT. In contrast, Figure 3.5 (iv) shows that for the PVF^{Ti-PC}-Fe oxide, the catalytic activity was recovered after the SDT (runs 4-5) and then decreases slowly as shown by trace h. This recovery can be due to the presence of a thicker iron oxide shell (Figure 3.4) and/or to a more solid binding of iron oxide particles to the polymer surface in the case of PVF^{Ti-PC}-Fe oxide than for the other catalysts.

These results show that the V-UV functionalization was not beneficial in term of final photocatalyst activity and long-term stability. In contrast, RF-P and Ti-PC functionalized materials shows higher stability and catalytic activity than not functionalized ones. Thus the formation of polar oxygen functionality on polymer surface as well as the increase of roughness allows the solid binding of iron oxide particles leading to stable photocatalysts. Besides for Ti-PC functionalization the presence of significant amount of TiO₂ particles on polymer surface could stabilize the photocatalyst acting as charge trap.

Because the Ti-PC functionalization led to the photocatalyst with the highest HQ degradation rates and long-term stability, this method was studied in the following chapters.

3.5 Conclusions

Iron oxide coated functionalized polymer films are suitable materials to degrade and mineralize hydroquinone under simulated solar irradiation. During the process relatively low amount (e.g. 0.3-0.5 mg/L) of leached iron was detected in solution.

To implement a functionalization of polymer surface is an efficient strategy to improve the attraction between iron oxide and polymer film supports. As a result, a higher amount of iron oxide is immobilized on the catalyst surface leading to more efficient photocatalysts. Besides functionalization process such as Ti-PC can concomitantly lead to the deposition of

additional active specie (TiO₂ particles). RF-P and more markedly Ti-PC treatments were useful to improve material photocatalytic activity. The prepared materials studied here were stable toward repetitive hydroquinone degradation, nevertheless only RF-P and Ti-PC functionalization led to catalysts keeping activity after a self degradation test.

3.6 References

- Chan C., Ko -M., T. -M, Hiraoka H. (1996) Polymer surface modification by plasmas and photons. *Surface Science Reports* 24: 1-54.
- Charbonnier M., Romand M. (2003) Polymer pretreatments for enhanced adhesion of metals deposited by the electroless process. *International Journal of Adhesion and Adhesives* 23: 277-2853.
- Escobar M., Goyanes S., Corcuera M.A., Eceiza A., Mondragon I., Rubiolo G.H., Candal R.J. (2009) Purification and functionalization of carbon nanotubes by classical and advanced oxidation processes. *Journal of Nanoscience and Nanotechnology* 9: 6228-6233.
- Everett M.L., Hoflund G.B. (2006) Chemical alteration of poly(vinyl fluoride) Tedlar® induced by exposure to vacuum ultraviolet radiation *Applied Surface Science* 252: 3789-3798.
- Fan C., Li W., Li X., Zhao S., Zhang L., Mo Y., Cheng R. (2007) Efficient photo-assisted Fenton oxidation treatment of multi-walled carbon nanotubes. *Chinese Science Bulletin* 52: 2054-2062.
- Gibbs M.M., (1979) A simple method for the rapid determination of iron in natural waters. *Water Research* 13: 295-297.
- Golub M.A., Wydeven T., Cormia R.D. (1989) ESCA study of several fluorocarbon polymers exposed to atomic oxygen in low Earth orbit or within or downstream from a radio-frequency oxygen plasma. *Polymer* 30: 1571-1575.
- Kim G.G., Kang J.A., Kim J.H., Kim S.J., Lee N.H., Kim S.J. (2006) Metallization of polymer through a novel surface modification applying a photocatalytic reaction. *Surface and Coating Technology* 201:3761–3766.
- Kim G.G., Kang J.A., Kim J.H., Lee K.-y., Kim S.J., Kim S.-J. (2007) Photocatalytic pretreatment of acrylonitrile-butadiene-styrene polymer for electroless plating. *Scripta Materialia* 56: 349-351.
- Martín R., Heydorn P.C., Alvaro M., Garcia H. (2009) General strategy for high-density covalent functionalization of diamond nanoparticles using Fenton chemistry. *Chemistry of Materials* 21: 4505-4514.
- Mejía M.I., Marín J.M., Restrepo G., Pulgarín C., Mielczarski E., Mielczarski J., Arroyo Y., Lavanchy J.-C., Kiwi J. (2009), Self-cleaning modified TiO₂-cotton pretreated by UVC-light (185 nm) and RF-plasma in vacuum and also under atmospheric pressure. *Applied Catalysis B: Environmental* 91:481–488.
- Mittal K.L., (1996) Polymer Surface Modification: Relevance to Adhesion. VSP Utrecht, The Nederland.
- Samson J.A.R. (1967) Techniques of Vacuum Ultraviolet Spectroscopy, Wiley, New York.

- Skurat V. (2003) Vacuum ultraviolet photochemistry of polymers. *Nuclear Instruments and Methods in Physics Research, Section B: Beam Interactions with Materials and Atoms* 208: 27-34.
- Terlingen J.G.A. (2008). Introduction of functional groups at polymer surfaces by glow discharge techniques. Functionalization of Polymer Surfaces: Chapter 2. *Europlasma Technical Paper* p 29.
- Vasilets VN, Yuranova TI, Ponomarev AN. (1994) The changes of structure and wettability of siloxane polymers under vacuum ultraviolet action. *Journal of Photopolymer Science and Technology* 7:309 –314.
- Vasilets V.N., Kuznetsov A.V., Sevastianov V.I. (2004) Vacuum ultraviolet treatment of polyethylene to change surface properties and characteristics of protein adsorption. *Journal of Biomedical Materials Research - Part A* 69: 428-435.
- Vasilets V.N., Kuznetsov A.V., Sevast'yanov V.I. (2006) Regulation of the biological properties of medical polymer materials with the use of a gas-discharge plasma and vacuum ultraviolet radiation. *High Energy Chemistry* 40: 79-85.
- Yuranova T., Rincon A.G., Bozzi A., S. Parra S., C. Pulgarin, C. P. Albers P., J. Kiwi J. (2003) Antibacterial textiles prepared by RF-plasma and vacuum-UV mediated deposition of silver. *Journal of Photochemistry and Photobiology A: Chemical* 161: 27–34.

4- TiO₂ AND IRON OXIDE COATED POLYMER FILMS: CHARACTERIZATION, OPTIMISATION AND SYNERGISTIC PHOTO-ACTIVITY

4.1 Introduction

The preparation of catalysts containing iron oxide and TiO₂ is an attractive option since these materials could be bi-functional (i.e. combining TiO₂ and iron oxide properties Zhou, 2008) and because synergistic effects are likely to occur. Some recent studies described Fe₂O₃-TiO₂ coatings on glass (Celik, 2006) and activated carbon fiber (Zhang, 2008b).

Synergistic effects refer to the phenomena when the degradation rate of combined system is greater than the sum of its parts. These non-additive effects have recently been observed for the combination of suspended TiO₂ mediated photocatalysis with high frequency ultrasound (Torres, 2008), with ozonization (Zou, 2008) and when combining supported TiO₂ with homogeneous photo-Fenton oxidation (Bouras, 2008).

This chapter presents a detailed investigation of an innovative method to bind TiO₂ and iron oxide on polymer film. The procedure to bind TiO₂ on polymers employs solar light, low temperature, needs short preparation time in aqueous solution and generates C=O, C-OH, COOH groups on the polymer surface by TiO₂ photocatalysis (Kim, 2006). The photocatalysts are characterized by scanning electron microscopy (SEM), X-ray photoelectron spectroscopy (XPS) and UV-visible spectroscopy.

The objective of this chapter is to evaluate the photocatalytic performance of TiO₂ and iron oxide coated functionalized polymer films (P^f-TiO₂-Fe oxide) toward the degradation of hydroquinone (HQ), and inactivation of *E. Coli*.

4.2 Experimental

4.2.1 Chemicals

Hydroquinone, NaOH, HNO₃, FeCl₃ anhydrous, FeSO₄·7H₂O, ferrozine, hydroxylamine hydrochloride, acetate buffer (pH = 4.65) were Flucka p.a. reagent and used as receive. Hydrogen peroxide (35%) was supplied by Merck AG (Darmstadt, Germany) TiO₂ P25 powder (anastase to rutile ratio between 70:30 and 80:20) was supplied by Degussa. The polyvinyl fluoride (PVF), polyethylene (PE) and polyethylene terephthalate (PET) films were 72 μm thick and supplied by Goodfellow (Cambridge Ltd. United Kingdom). The PET bottles (Polypropylene cover, 100 mL, diameter: 4.8 cm, heighth: 9.5 cm) were supplied by Reactolab SA, (Servion, Switzerland). Solutions were prepared with Millipore water (18.2 MΩ.cm at 25 °C).

4.2.2 Photocatalyst preparation

Photoactive TiO₂ and/or iron oxide were deposited on commercial polymer films as polymeric substrate. Before use, the polymer films were washed in diethyl ether ethanol (1:1) mixture and in MilliQ water in order to eliminate surface contaminants. Three different preparation methods have been used:

(1) The first preparation method consisted in the application of a single TiO₂ photocatalytic surface functionalization-deposition (PSFD) treatment: the clean polymer substrates (PVF, PE or PET) were attached around a cylindrical steel support and immersed in a photo-reactor containing well dispersed suspensions of TiO₂ (0.2-1.7 g/L) at different pH (3, natural, 7, 11). The photo-reactor was irradiated in a CPS Suntest system (ATLAS GmbH) during two hours under magnetic stirring. Steel support was dimensioned to maintain the PVF film close to the surface of the photo-reactor. This treatment led to the immobilization of TiO₂ particles on the functionalized polymer surface (P^f-TiO₂). The possible nature of polymer-TiO₂ bonding is proposed in point 4.3.1.1.

(2) In the second preparation method, the iron oxide was immobilized on polymer substrates. Commercial polymer films were immersed in a 5 g/L solution of FeCl₃ and heated under stirring at 70, 80 or 90 °C during one hour. Optionally, the composite material

was heated in an oven at 100 °C for one hour. The final film showed an iron oxide coat (P-Fe oxide).

(3) The third preparation method consisted in applying a TiO₂ PSFD treatment followed by iron oxide coating as described in method (1) and (2) to immobilize the TiO₂ and iron oxide on the polymer film leading to P^f-TiO₂-Fe oxide.

For the bacteria inactivation tests, the photoactive TiO₂ and iron oxide were deposited on commercial PET bottles (100 mL) in a similar way like described previously. Briefly, clean PET bottles were filled up with a 60 mL dispersed suspension of TiO₂ (1g/L). The bottles were then irradiated in a CPS Suntest system for 2.5 hours under magnetic stirring. The functionalized bottles were then emptied, rinsed with miliQ water and filled up with 60mL of a FeCl₃ solution (5 g/L) to carry out forced hydrolysis at 60 °C during 1.5 hours. Heating at 95 °C during half an hour in an oven was performed to anneal TiO₂ and iron oxide particles on the PET surface.

4.2.3 Photo-reactor and irradiation procedure

The photo-reactor and irradiation procedure used for organic compounds degradation is described in detail point 3.2.3.

For bacterial inactivation, experiments were carried out in PET bottles reactors placed in parallel inside the solar box. PET bottles were used both as reactor and photocatalyst substrate. The temperatures during the experiments were always below 38 °C then thermal inactivation of micro-organisms can be excluded.

4.2.4 Analysis of the irradiated solutions

The methods are described in detail in point 3.2.4.

4.2.5 Bacterial strain and growth media

Bacterial strains. The *E. coli* strain K-12 (MG1655) was used for all the disinfection experiments and supplied by DSMZ (German Collection for Microorganisms and Cell

cultures, Darmstadt, Germany). *E. coli* K-12 is a non-pathogenic and close to the wild-type *Eschecheria coli*, typical indicator bacteria for enteric pathogens.

Sample preparation. Strain samples were stored in cryo-vials containing 20% glycerol at -20 °C. Bacterial pre-cultures were prepared for each experimental series by streaking out a loopfull from the strain sample onto Plate Count Agar (PCA) and subsequent incubation of these plates for 24 hours at 37 °C (Heraeus incubator B 5060 EK-CO2, Heraeus Instruments, Hanau, Germany). From the growing colonies, one was re-plated on a separate PCA and incubated again for 24 hours at 37 °C.

Luria-Bertani (LB) broth (10 g Bacto™ Trypton, 5 g Yeast extract, 10 g NaCl per liter) was prepared for each experimental series by suspension in MilliQ and heat-sterilization by autoclave (121 °C, 20 min, VST 500A, LS SECFROID, Blanc Labo, Lonay, Switzerland).

To prepare the bacterial pellet for the photo-inactivation experiments, one colony was picked from the pre-cultures and loop-inoculated into a 50 mL sterile PE Eppendorf flask containing 5 mL of LB broth. The flask was then incubated at 37 °C and 180 rpm in a shaker incubator (Minitron AI 71, IN- 3 FORS AG, Bottmingen, Switzerland). After 8 hours, the cells were diluted (1% v/v) in a 250 mL Erlenmeyer flask containing 25 mL of pre-warmed LB broth and incubated at 37 °C for 15 hours in Heraeus Incubator until stationary physiological phase was reached. Bacterial growth and stationary phase was monitored by the optical density at 600 nm. Cells were harvested during stationary growth phase by centrifugation (15 minutes at 5000 x g (RCF) and 4 °C) in a universal centrifuge (HERMLE Z 323 K, Renggli Laboratory Systems, Renens, Switzerland). The bacterial pellet was re-suspended and washed for 10 minutes in the centrifuge.

Washing was repeated twice and the bacterial pellet was re-suspended to the initial volume. This procedure resulted in a bacterial pellet containing $1.5 \cdot 10^8$ CFU/mL. Washing and re-suspension was done either in heat sterilized MilliQ water or in a nutritional solution containing Bacto™ Trypton. At the beginning of each experiment the reactors containing the bacterial suspension were placed in the solar simulator in the dark under magnetic stirring for at least one hour in order to let bacteria adapt themselves to the new matrix and to allow die-off of the most stress sensitive species. After stabilization of the population, H₂O₂ was added before turning on the lamp.

Plating. Colony forming units (CFU) were monitored by pour plating on PCA. At each data point 1 mL of sample was withdrawn. Exceeding H₂O₂ was neutralized with catalase, aliquots were diluted in 10% steps and pour plated on PCA. Plates were incubated for 24 hours at 37 °C and CFU were counted manually.

4.2.6 Photocatalyst characterization

4.2.6.1 X-ray photoelectron spectroscopy (XPS)

X-ray photoelectron-Spectroscopy is a non-destructive technique that can be used to analyze the surface chemistry of a material (Moulder 1996). It provides elemental analysis and the chemical and electronic state of the elements. XPS spectra are obtained by irradiating a material with a beam of X-rays while simultaneously measuring the kinetic energy (KE) and the number of electrons that escape from the top 1 to 10 nm of the material being analyzed.

Because the energy of a particular X-ray wavelength equals a known quantity, we can determine the electron binding energy (BE) of each emitted electrons according to:

$$E_{\text{binding}} = E_{\text{photon}} - E_{\text{kinetic}} - \phi$$

Where E_{binding} is the energy of the emitted electron, E_{photon} is the energy of the X-ray photons; E_{kinetic} is the energy of the emitted electron as measured by the instrument and ϕ is the work function of the spectrometer. A typical XPS spectrum is a plot of a number of electrons detected as a function of their binding energy. Each element produces a characteristic set of XPS peaks at defined binding energy values; thus it is possible to detect each element on the surface or the top layers of the material. These characteristic peaks correspond to the electron configuration of the electrons within the atoms e.g. 1s, 2s, 2p, 3s etc. The number of electrons in each peak is related to the amount of the element within the irradiated area (volume). To generate atomic percentage values, each raw XPS signal must be normalized over all the elements detected.

It is important to note that XPS detects only the electrons that have actually escaped into the vacuum of the instrument from the top 10 to 12 nm of the material. The deeper photo-

emitted electrons, which were generated as the X-rays penetrated 1-5 μm of the material, are either recaptured or trapped in various excited states within the material.

X-ray photoelectron spectroscopy data were collected by Axis Ultra system (Kratos analytical, Manchester, UK) under ultra-high vacuum condition ($<10^{-8}$ Torr), using a monochromatic Al K_{α} X-ray source (1486.6 eV) at the laboratory of Chemical Metallurgy at EPFL. The source power was maintained at 150 W (10 mA, 15 kV). The emitted photoelectrons were sampled from a square area of $750 \times 350 \mu\text{m}^2$. The gold (Au $4f_{7/2}$) and copper (Cu $2p_{3/2}$) lines at 84.0 and 932.6 eV respectively, were used for calibration, and the adventitious carbon 1s peak at 285 eV was used as an internal standard to compensate for charging effects.

4.2.6.2 Scanning electron microscopy (SEM)

The scanning electron microscope images the sample surface by scanning it with a high-energy beam of electrons. The electrons interact with the atoms that make up the sample producing signals that contain information about the sample's surface topography, composition and other properties such as electrical conductivity.

The types of signals produced by SEM include among others secondary electrons, back-scattered electrons, characteristic X-rays, specimen current and transmitted electrons.

The signals result from interactions of the electron beam with atoms at or near the surface of the sample. In the most common or standard detection mode (secondary electron imaging) the SEM can produce very high-resolution images of a sample surface, revealing details about less than 1 to 5 nm in size. Due to the very narrow electron beam, SEM micrographs have a large depth of field yielding a characteristic three-dimensional appearance useful for understanding the surface structure of a sample. Characteristic X-rays are emitted when the electron beam removes an inner shell electron from the sample, causing a higher energy electron to fill the shell and release energy. These characteristic X-rays are used to identify the composition and measure the abundance of elements in the sample.

The surface morphology of the catalysts were investigated using a scanning electron microscope (Phillips XL30 SFEG) equipped with X-ray detector.

4.2.6.3 UV-Visible spectrophotometry

This technique and the characteristics of the apparatus used were described in point 3.2.5.

4.3 Results

4.3.1 Photocatalyst characterization

The XPS spectroscopy allows determining surface composition of the thin outermost surface layers. It also allows obtaining the elemental depth profile. XPS measurements were performed on PVF^f-TiO₂ and PVF^f-TiO₂-Fe oxide prepared under different pH condition. An energy shift to lower binding energies (BE) of about 3 eV was observed due to the low conductivity of the samples. In the present study, the corrected BEs are reported.

4.3.1.1 XPS study of the influence of pH on TiO₂ photocatalytic surface functionalization-deposition (PSFD) treatment of polyvinyl fluoride film

Different PVF^f-TiO₂ and PVF^f-TiO₂-Fe oxide samples have been produced by functionalization at various pHs. Figure 4.1(i) presents the C (1s) carbon peaks at each preparation step. For the non-modified PVF film (trace a), there are two peaks: the higher peak centered at BE = 284.6 eV corresponding to (CH₂)_n groups, the second centered at BE = 286.6 eV corresponding to C-F bond. The F/C atomic ratio for the PVF was 0.46, which is less than the theoretical stoichiometric value of 0.5 (Table 4.1). This slight difference can be attributed to hydrocarbon contamination and the presence of surface oxygen. After the TiO₂ PSFD treatment of PVF at pH 11, (trace b), the XPS spectrum changes with the appearance of C (1s) peaks at a BE of 287.2 and 289 eV corresponding to the formation of C=O bond of ketones and carboxylic acids respectively. This observation confirms that the TiO₂ PSFD treatment induces the formation of oxygen functional groups in agreement with a recent study (Kim, 2006). After TiO₂ PSFD treatment at pH 3 (trace c), the XPS spectrum

was similar to the trace b excepting that the carboxylic acid peak at 289 eV is not visible and that the ratio C-H/C=O is considerably lower, indicating a larger formation of oxygen-based groups at the Tedlar[®] surface at acidic pH.

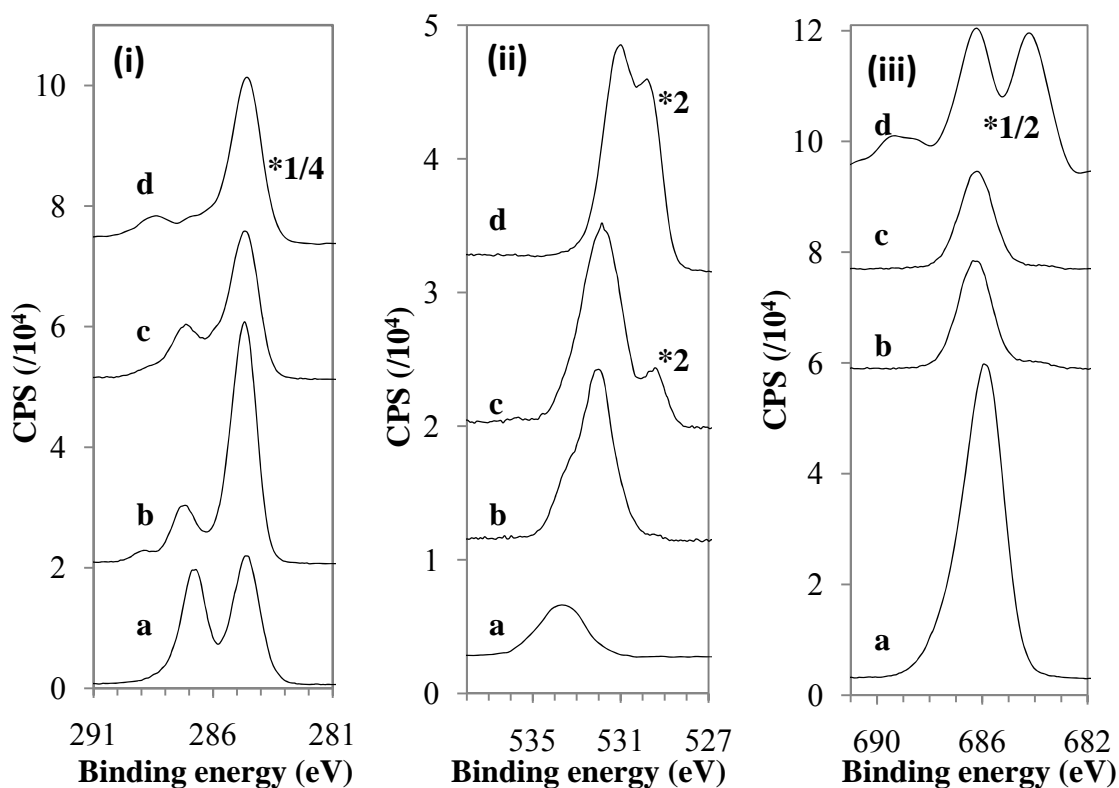


Figure 4.1 X-ray photoelectron spectra of: (i) C (1s); (ii) O (1s); (iii) F (1s) core level photoelectron spectra of (a) PVF; (b) PVF after a TiO₂-PSFD treatment at pH 11; (c) PVF after a TiO₂ PSFD treatment at pH 3; (d) PVF^f-TiO₂-Fe-oxide (TiO₂ PSFD treatment at pH 3).

Figure 4.1(ii) shows the evolution of PVF surface oxygen peak O (1s) for different preparation steps. In trace a, the O (1s) peak is centered at BE = 533.7 eV corresponding to the oxygen contained in hydrocarbon contamination on the polymeric surface. After a TiO₂ PSFD treatment at pH 11, (trace b) the O (1s) peak is shifted to 532 eV, corresponding to the formation of C=O and COOH groups on the PVF surface. Trace b shows as well a small peak at 529.4 eV which corresponds to the oxygen in TiO₂ suggesting the presence of traces of this oxide on PVF surface. After a TiO₂ PSFD treatment at pH 3 (trace c), a significant O (1s) peak appears at BE = 529.4 eV corresponding to the oxygen of the TiO₂

while the next peak at BE = 531.8 eV corresponds to O (1s) in C=O, COOH groups.

Figure 4.1(iii) shows the changes in the F (1s) XPS spectrum due to TiO₂ PSFD treatment. For the non-modified PVF, the F (1s) signal consists of a single peak located at a BE of 685.9 eV. The main differences between non-modified PVF (trace a) and TiO₂ PSFD treated polymers (trace b, c) are a shift (of 0.3 eV) of F (1s) BE to the higher energy possibly due to the changes in the fluorine chemical environment and a decrease of the peak due to fluorine substitution.

Table 4.1 shows the atomic composition of PVF surface before and after TiO₂ PSFD treatment. From a semi-quantitative comparison of relative atomic percentage of oxygen, carbon, fluorine and titanium on the surface before and after TiO₂ PSFD treatment, it was found that this treatment led to an important increase in relative oxygen and carbon surface concentration and a concomitant decrease in the fluorine concentration. In Table 1 can be seen that the pH during TiO₂ PSFD treatment influences the surface modification. The surface O/C ratio changes from 0.06 in the non-modified PVF to 0.24 after a TiO₂ PSFD treatment at pH 3 and to 0.12 at pH 11. The surface F/C ratio changed from 0.46 in the non-modified PVF to 0.13 and 0.11 after a TiO₂ PSFD treatment at pH 3 and 11 respectively. Thus photocatalytic oxidation of the polymer surface induces the formation of oxygenic functional groups along the elimination of bounded fluorine.

Table 4.1. Composition of original polymer surface (PVF), TiO₂ PSFD treated polymer (PVF^f-TiO₂) at pH 3 and 11 (in atomic %; only principal constituents).

Samples	C	O	F	Ti	F/C	O/C
PVF	66.0	3.7	30.3	0	0.46	0.06
PVF ^f -TiO ₂ pH 11	80.4	10.3	9.3	0	0.11	0.12
PVF ^f -TiO ₂ pH 3	72.6	16.9	9.3	1.2	0.13	0.24

Simultaneously, when submitting PVF to a TiO₂ PSFD treatment, the immobilization of the TiO₂ assisted by polymer surface functionalization occurs. Figure 4.2 (trace a) shows the Ti (2p) core level photoelectron spectrum characteristic of Ti in TiO₂ (handbook, 1992) after TiO₂ PSFD treatment at pH 3 and 11. Thus after the treatment performed at pH 3, the

polymer is partially covered with TiO_2 (1.2% atomic percentage of the surface) whereas after treatment at pH 11, Titanium was not detected. These results show that it is possible to control the extent of TiO_2 deposition by varying the pH.

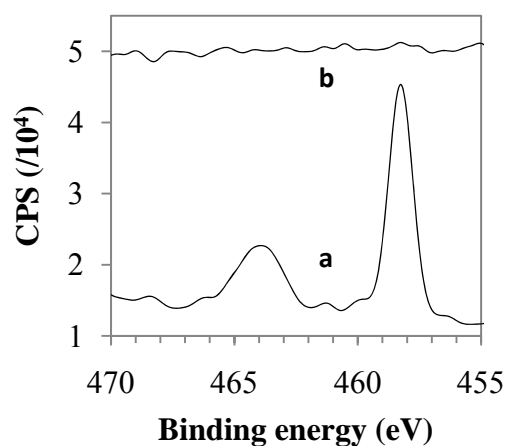


Figure 4.2 X-ray photoelectron spectra of Ti (2p) in (a) PVF after a TiO_2 PSFD treatment at pH 3; (b) PVF after a TiO_2 PSFD treatment at pH 11.

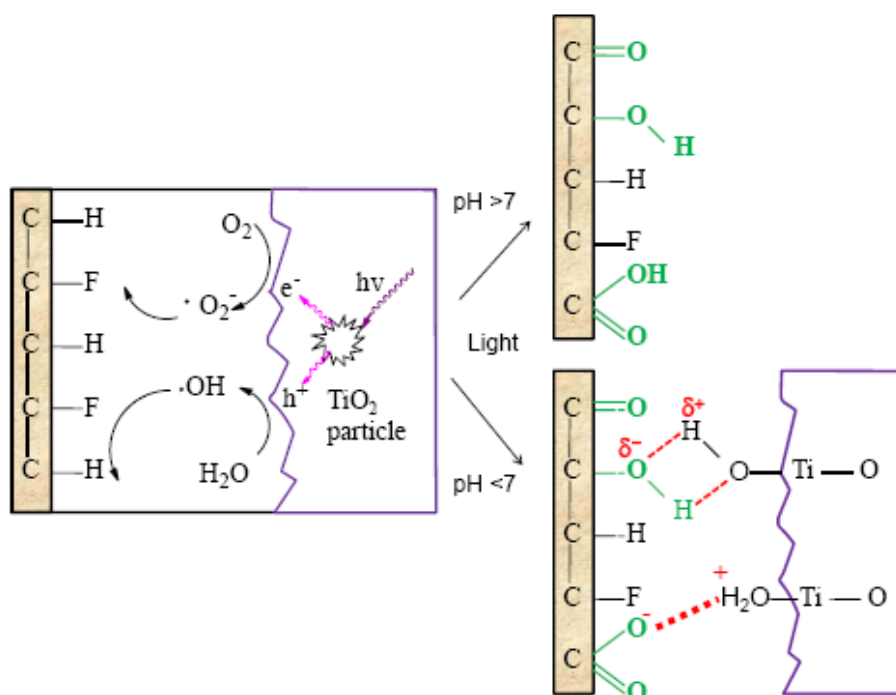


Figure 4.3 Mechanistic proposition for TiO_2 photocatalytic surface functionalization-deposition as a function of pH.

The simultaneous photocatalytic functionalization of PVF surface and a deposition of TiO₂ are illustrated in Figure 4.3. As a matter of fact, under irradiation in aqueous TiO₂ suspension in equilibrium with air, PVF film suffers photocatalytic attacks leading to C=O, COOH groups and to the elimination of fluorine. When the pH of the aqueous solution is acidic, (i) The polymer surface is negatively charged since the TiO₂ PSFD treatment induced the formation of functional groups like COO⁻ and (ii) The superficial charge of TiO₂ P25 is positive since its isoelectric point is near to 7. Consequently an electrostatic attraction binds the TiO₂ particles to the polymer surface.

4.3.1.2 XPS studies of iron species and overall atomic profile of the PVF^f-TiO₂-Fe oxide photocatalyst

The deposition of iron oxide on PVF^f-TiO₂ surfaces was described under point 4.2.2. The determination of the chemical nature of the iron coating was investigated by XPS.

In Figure 4.4, the iron peak was located at a BE of 711 eV which is characteristic of Fe³⁺ ions in akaganeite (Deliyanni, 2006). Nevertheless, the XPS results are not sufficient to determine with accuracy the nature of iron oxide present at polymer surface. However, various reports confirm this hypothesis, as the thermal hydrolysis of FeCl₃ solutions leads mainly to the formation of akaganeite (Music, 2003).

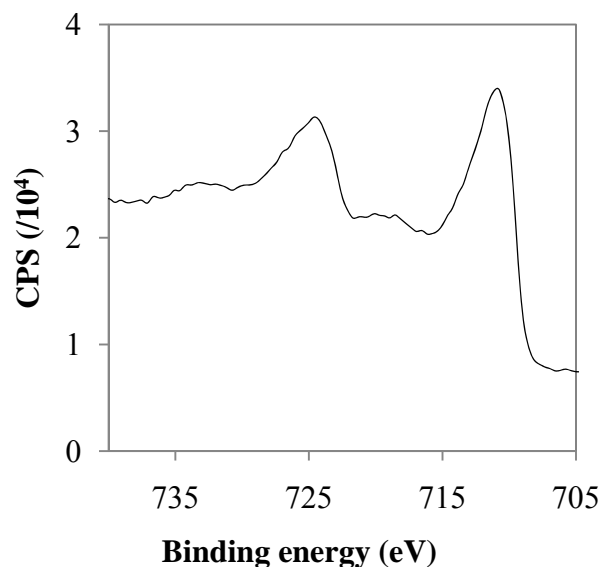


Figure 4.4. Fe (2p) core level photoelectron spectrum of PVF^f-TiO₂-Fe oxide.

In Figure 4.1(iii), the XPS spectrum of F (1s) core level is presented. The PVF^f-TiO₂-Fe oxide spectrum (trace d) includes the triplet F (1s) peak with two predominant components at a BE of 684.2 and 686.3 eV. These two peaks correspond respectively to fluorine incorporated into iron oxide (FeOF), due to the anion exchange properties of akaganeite (Cai, 2001), and to the polymeric C-F bond. The smaller F (1s) peak is centered at a BE = 689 eV corresponding to F⁻ ions adsorbed on the iron oxide surface.

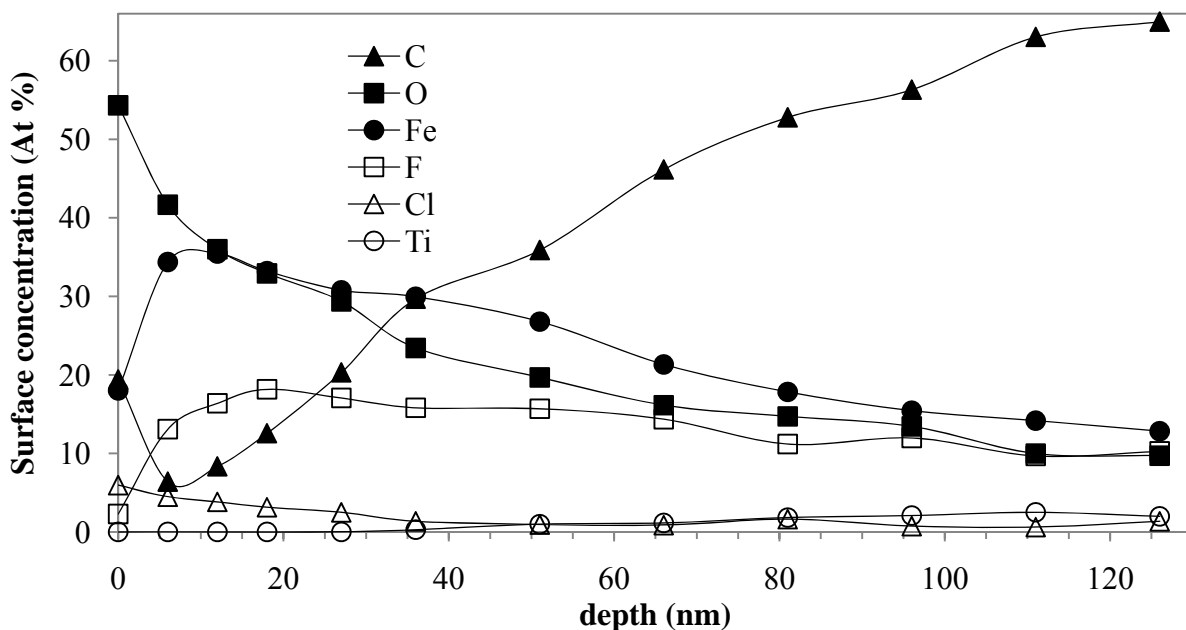


Figure 4.5. Depth profile of PVF^f-TiO₂-Fe oxide (PSFD treatment at pH 3).

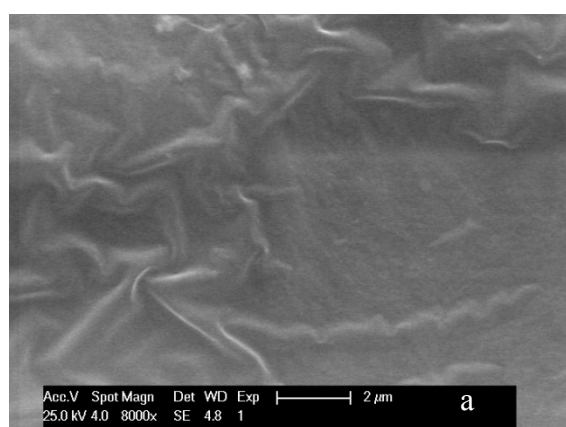
Figure 4.5 shows the XPS depth profile of PVF^f-TiO₂-Fe oxide surface indicating the atomic composition as a function of depth. Each minute, the topmost layer of about 2 nm depth was eroded by the Ar⁺-ions sputtering. The reported values are approximations, since preferential sputtering effects cannot be excluded because the sputter rate for each investigated element is different and depends on its particular sensitivity factor. Figure 7 shows the contamination of the first layer (about 5 nm) with hydrocarbons and oxygen. In the next layer of about 15 nm, iron, oxygen, fluorine and chlorine atomic concentration were seen to be close to their maximum value (35, 35, 18, and 6% respectively) decreasing continuously with increasing depth. The atomic concentration of carbon follows an

opposite tendency i.e. has its minimum value (10%) between 5 and 20 nm and then increases. Atomic concentration of Ti is zero until ~35 nm and then increases to reach a maximum value of 2.5% at ~100 nm. This result indicates that TiO₂ particles are located close enough to the surface of the catalyst to play a role in the degradation processes particularly if the photocatalyst has been reused several times and the iron oxide coat has been partially dissolved allowing the TiO₂ to diffuse to the surface. An XPS study of PVF^fTiO₂-Fe oxide surface changes after reuse will be presented in chapter 5.

4.3.1.3 Scanning electron microscopy (SEM)

Figure 4.6 shows the SEM micrograph of polymer surface before and after the sequential TiO₂ PSFD and iron oxide coating.

The non-modified PVF surface, Figure 4.6a, is predominantly smooth. After a TiO₂ PSFD treatment at pH 5, aggregated TiO₂ particles cover a significant part of the surface exposed to the light irradiation (Figure 4.6b) and to a lesser degree in the back side (Figure 4.6c). This TiO₂ coating seems to increase the surface roughness favoring subsequent iron oxide nucleation around the TiO₂ particles. TiO₂ decrease the interfacial energy which is a limiting factor for the crystallization of iron oxide (Greer, 2006). Figure 4.6d shows the PVF^f-TiO₂-Fe oxide catalyst surface loaded with iron oxide aggregates of about 1 μm. These aggregates are composed of nanoparticles of approximately 50 nm, which seem to cover the polymer surface (Figure 4.6e).



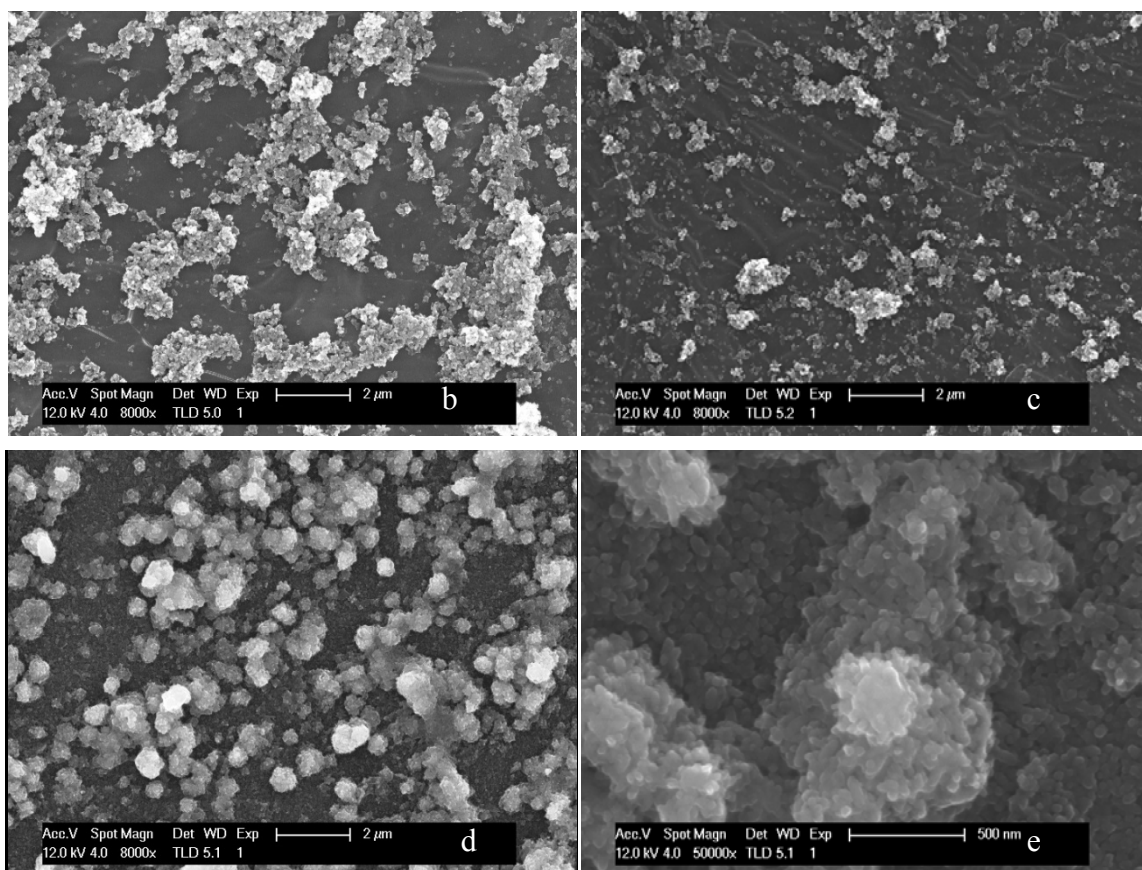


Figure 4.6. Scanning electron microscopic images of: (a) PVF; (b) PVF^f-TiO₂ prepared at pH 5 (external side); (c) PVF^f-TiO₂ prepared at pH 5 (internal side); (d)-(e) PVF^f-TiO₂-Fe oxide prepared at pH 5.

4.3.1.4 UV-Visible absorbance study

Figure 4.7 presents the UV-visible absorption of PVF^f-TiO₂, PVF-Fe oxide and PVF^f-TiO₂-Fe oxide composites between 350 and 700 nm. The absorbance of PVF in this region was negligible. For The PVF^f-TiO₂ (trace a) the UV-visible spectrum shows that this material only absorbs light below 400 nm, characteristic for TiO₂ particles. In contrast, PVF-Fe-oxide (trace b) absorbs visible light. Its spectrum shows an important absorption for low wavelength (violet and UV light) and a shoulder between 550 and 450 nm (green-blue light). PVF^f-TiO₂-Fe oxide spectrum (trace c) presented a similar spectrum shape to trace b but the observed absorption was 2 times higher. Thus, the PVF^f-TiO₂-Fe oxide UV-visible spectrum does not correspond to the sum of PVF^f-TiO₂ and PVF-Fe oxide spectra, which is

due to a more significant iron oxide presence on the rough PVF^f-TiO₂ surface than on smooth PVF. The photography shows the visual appearance of these materials.

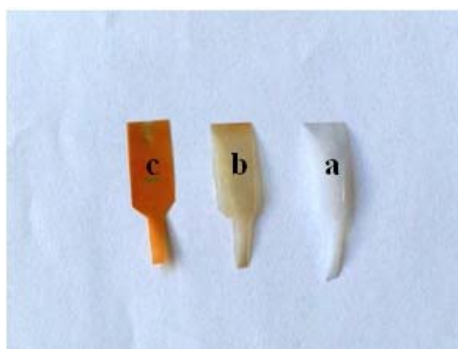
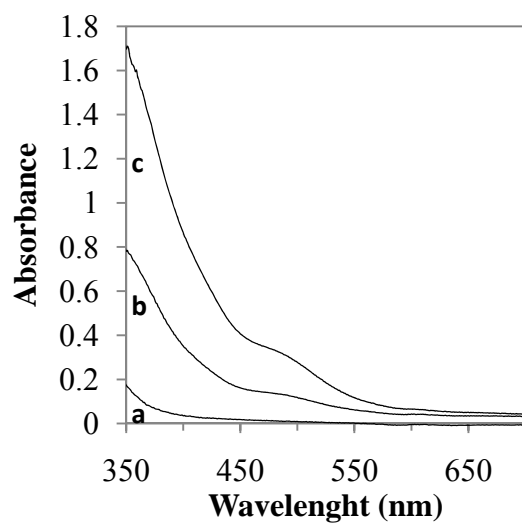


Figure 4.7 UV-Visible absorption spectrum of: (a) PVF^f-TiO₂; (b) PVF-Fe oxide; (c) PVF^f-TiO₂-Fe oxide; and photography of the three materials.

4.3.2 Photocatalytic activity

Figure 4.8 presents the evolution of hydroquinone (HQ) within 240 min under different conditions. During photolysis and dark runs (both represented by trace a), HQ concentration remained constant: (i) HQ was resistant to direct photolysis by simulated solar light and (ii) No adsorption of HQ on PVF^f-TiO₂-Fe oxide was detectable. For photo-assisted reaction on PVF^f-TiO₂ (trace b) and on PVF^f-TiO₂-Fe oxide (trace c), 7 and 15 % of HQ was degraded in 240 min of treatment. HQ degradation by the system PVF^f-TiO₂/H₂O₂/light (trace d) reached almost 40% whereas the system PVF^f-TiO₂-Fe

oxide/H₂O₂ under dark (trace e) reached 50% of HQ degradation in 240 min by heterogeneous Fenton-like oxidation. For the system PVF-Fe oxide/H₂O₂/light (trace f), the HQ degradation rate remained low during an activation period of 30 minutes, but increased between 30 and 120 min of treatment with 10% and 97% degradation efficiency. This behavior is typical for iron photo-leaching during the first step of the reaction leading to a subsequent important contribution of the homogeneous process to HQ degradation after the first 60 min of treatment since 0.5 mg/L of dissolved iron ions have been detected by the ferrozine method. For heterogeneous reaction with the system PVF^f-TiO₂-Fe-oxide/H₂O₂/light (trace g), HQ decreased very fast (91%) and with a constant slope typical of heterogeneous processes during the first 60 min. Only 0.2 mg/L of dissolved iron ions were detected at the end of this process. Consequently, the influence of homogeneous photo-Fenton processes on HQ degradation is probably small. A more accurate estimation of homogeneous contribution will be proposed in Chapter 5.

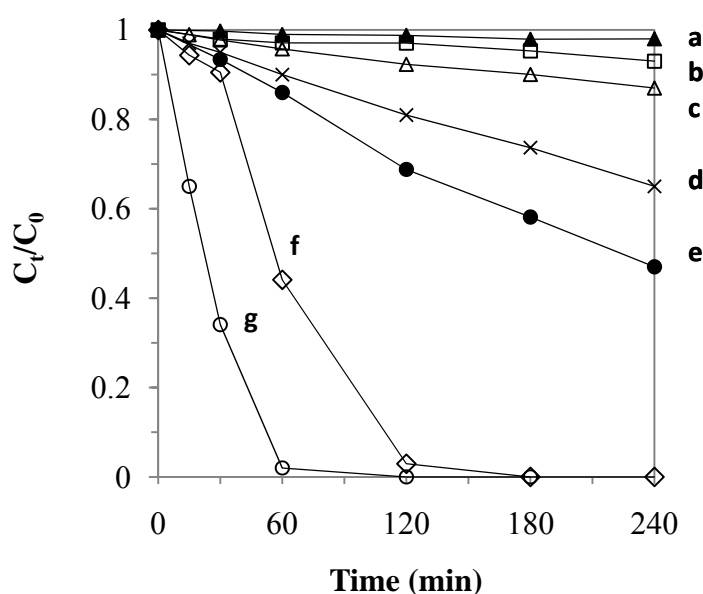


Figure 4.8 Degradation of 0.18 mM of HQ, initial pH 5.7, 75 cm² of heterogeneous photocatalyst 1.6 mM H₂O₂ under solar simulation: (a) bare light/dark adsorption; (b) PVF-TiO₂/light; (c) PVF^f-TiO₂-Fe oxide/light; (d) PVF^f-TiO₂/H₂O₂/light; (e) PVF^f-TiO₂-Fe-oxide/H₂O₂; (f) PVF-Fe oxide/H₂O₂/light; (g) PVF^f-TiO₂-Fe oxide/H₂O₂/light. The traces represent an average of three consecutive runs using the same photocatalysts (first run not included).

The evolution of the TOC versus time for some processes is illustrated in Figure 4.9. For the system PVF^f-TiO₂-Fe oxide/H₂O₂, under dark, no mineralization was observed (trace a). Homogeneous photo-Fenton process (Fe²⁺ (0.3 mg/L)/H₂O₂/light) mineralized about 60% of TOC after 240 min (trace b). Using PVF-Fe oxide/H₂O₂/light system (trace c), the TOC increased during the first 30 min, due to a degradation of the polymer substrate by generated radicals. Thereafter, the TOC concentration decreased rapidly up to 80% within 240 min (essentially due to mineralization caused by dissolved iron ions). TOC removal by the system PVF^f-TiO₂-Fe oxide/H₂O₂/light (trace d) was the fastest achieving a mineralization of 95% after 240 min. For each process, the residual H₂O₂ concentrations were measured; in no case the initially added H₂O₂ was totally consumed. The decrease of mineralization rates between 180 and 240 min (trace c-d) is therefore limited by diffusion.

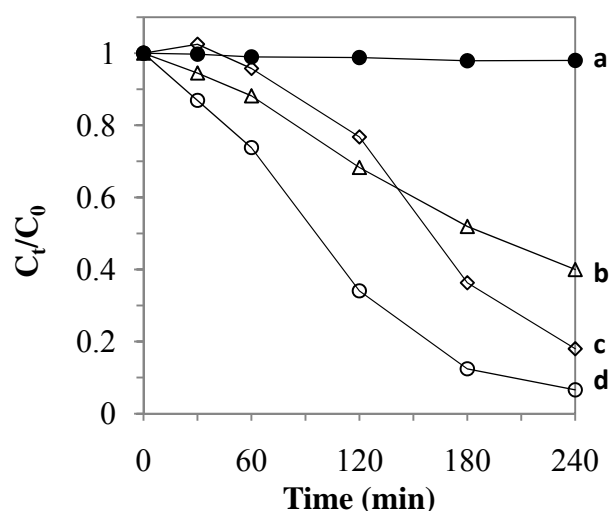
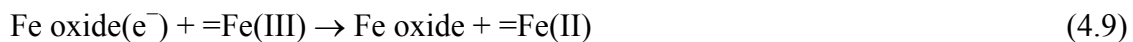


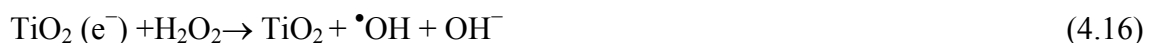
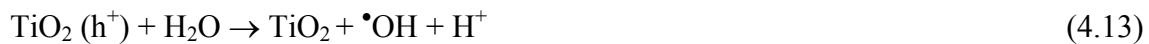
Figure 4.9 TOC removal of 0.18 mM of HQ, initial pH: 5.7, 75 cm² of heterogeneous photocatalyst 1.6 mM H₂O₂ under solar simulation: (a) PVF^f-TiO₂-Fe oxide/H₂O₂; (b) Fe²⁺ (0.3 mg/L)/H₂O₂/light; (c) PVF-Fe oxide/H₂O₂/light; (d) PVF^f-TiO₂-Fe oxide/H₂O₂/light. The traces represent an average of three consecutive runs using the same photocatalysts (first run not included).

During the photo-assisted reaction on PVF^f-TiO₂-Fe oxide in presence of H₂O₂, besides Eq. 4.2-4.3, the =Fe(II) regeneration (which is the rate determinant step of Fenton reaction) could occur via the photo-reduction of =Fe(III) species including hydroxy- or organo-

complexes (Eq. 4.5-4.6). Additionally photo-induced reactive species (electron-hole pair) are probably formed on iron oxide under illumination, enhancing HQ degradation rates (Eq.4.7). Conduction band electrons could react with H₂O₂ to form hydroxyl radicals (Eq.4.8) or could participate in the regeneration of =Fe(II) species (Eq. 4.9). Valence band holes may oxidize the pollutant (Eq.4.10, Bandara, 2007) (=Fe(II) and =Fe(III) represent the Fe(II)/Fe(III) species in solid or solution phase).



Beside photo-Fenton oxidation (Eq. 4.1-4.6) and iron oxide photocatalysis (Eq. 4.7-4.10), other reactions may occur mediated by PVF^f-TiO₂-Fe oxide/H₂O₂/light involving electron-hole pair formation by TiO₂ band-gap illumination ($\lambda < 400\text{nm}$). These reactions lead to radicals active in the degradation process as described in Eq. 4.11-4.16.



Furthermore, synergistic effects are likely to occur between TiO₂, iron oxide, dissolved iron ions and functionalized polymer surface, accelerating HQ degradation in presence of H₂O₂ as the electron acceptor.

4.3.3 Synergistic effects

Synergistic effects can be quantified by the synergistic factor S defined in Eq. 4.17, where R₀ represents the initial rate of degradation for a given process (Eq. 4.18).

$$S = R_0(AB)/(R_0(A)+R_0(B)) \quad (4.17)$$

$$R_0 = ([HQ]_0-[HQ]_{30})/30 \quad (4.18)$$

In the system PVF^f-TiO₂-Fe oxide/H₂O₂/light, the overall process is a combination of polymer supported TiO₂ and iron oxide photocatalysis associated with heterogeneous and homogeneous photo-Fenton oxidation. The exact assessment of synergistic effects in this system is not easy due to the difficulty to prepare PVF-Fe oxide and PVF^f-TiO₂-Fe oxide samples with the same iron oxide load. An approximated synergistic factor can be estimated assuming that (1) The photocatalyst UV-visible extinction coefficients between 450-550 nm (Figure 4.7) are proportional to the amount of iron oxide present on the PVF surface and (2) The photocatalytic activity of PVF-Fe oxide increases linearly with the amount of immobilized iron oxide.

The initial HQ degradation rates (R₀) have been calculated during the first 30 minutes for different photo-assisted processes (Eq. 4.18) from the decay curve b, d, e, f, g in Figure 4.8 and are represented in Table 4.2.

These rates are representative for the heterogeneous reactions since a low amount of iron is dissolved (<0.1 mg/L) at the beginning of the process. The rate R₀ corresponding to a virtual PVF-Fe oxide containing the same amount of iron oxide as a PVF^f-TiO₂-Fe oxide was estimated according to assumptions (1) and (2). A correction factor C, defined in Eq. 4.19 as the integrated absorbance of PVF^f-TiO₂-Fe oxide (trace c) over the integrated absorbance of PVF-Fe oxide (trace b) from 450 to 550 nm (where the TiO₂ absorbance is insignificant), was calculated from Figure 4.7.

$$C =_{450} \int^{550} [A(\text{PVF}^{\text{f}}\text{-TiO}_2\text{-Fe oxide})/A(\text{PVF-Fe oxide})] d\lambda = 2.2 \quad (4.19)$$

Multiplying $R_0(\text{PVF-Fe oxide}/\text{H}_2\text{O}_2/\text{light})$ by C we can estimate $R_0(\text{PVF-Fe oxide}/\text{H}_2\text{O}_2/\text{light})_{\text{VIRTUAL}}$ corresponding to the degradation rate relative to a PVF-Fe oxide with an iron oxide load as $\text{PVF}^{\text{f}}\text{-TiO}_2\text{-Fe oxide}$ (Eq. 4.20):

$$R_0(\text{PVF-Fe oxide}/\text{H}_2\text{O}_2/\text{light})_{\text{VIRTUAL}} = C * R_0(\text{PVF-Fe oxide}/\text{H}_2\text{O}_2/\text{light}) \quad (4.20)$$

Replacing $R_0(A)$, $R_0(B)$ and $R_0(AB)$ in Eq. 4.17 by the values of $R_0(\text{PVF}^{\text{f}}\text{-TiO}_2/\text{H}_2\text{O}_2/\text{light})$, $R_0(\text{PVF-Fe oxide}/\text{H}_2\text{O}_2/\text{light})_{\text{VIRTUAL}}$ and $R_0(\text{PVF}^{\text{f}}\text{-TiO}_2\text{-Fe oxide}/\text{H}_2\text{O}_2/\text{light})$ (from Table 4.2) respectively, the synergistic factor S can be calculated. A value of $S \approx 2.5$ was obtained, meaning that the rate relative to the combined processes is 2.5 times faster than the sum of rates relative to the separated processes. Compared to previous studies (Torres, 2008, Zou, 2008, Bouras, 2008), this result suggests the presence of a significant synergistic effect in the system $\text{PVF}^{\text{f}}\text{-TiO}_2\text{-Fe oxide}/\text{H}_2\text{O}_2/\text{light}$.

Table 4.2. Initial HQ degradation rates relative to different photo-assisted processes.

Photo-Process	$R_0(\mu\text{mol}/\text{min})$
H_2O_2	0.14
$\text{PVF}^{\text{f}}\text{-TiO}_2$	0.08
$(\text{PVF}^{\text{f}}\text{-TiO}_2)/\text{H}_2\text{O}_2$	0.29 ^a
$(\text{PVF-Fe oxide})/\text{H}_2\text{O}_2$	0.57 ^b
$(\text{PVF-Fe oxide})_{\text{Virtual}}^{\text{c}}/\text{H}_2\text{O}_2$	1.3 ^d
$(\text{PVF}^{\text{f}}\text{-TiO}_2\text{-Fe oxide})/\text{H}_2\text{O}_2$	4.0 ^e

^a Value calculated from decay curve d of Figure 4.8.

^b Value calculated from decay curve f of Figure 4.8.

^c Virtual photocatalyst containing the same amount of iron oxide as $\text{PVF}^{\text{f}}\text{-TiO}_2\text{-Fe oxide}$.

^d Rate estimated from ^a and from Eq. 19-20 and Figure 4.7.

^e Value calculated from decay curve g of Figure 4.8.

At the beginning of the treatment (for which S factor has been calculated), the combination of homogeneous photo-Fenton and TiO₂ photocatalysis is probably not the essential interaction. Indeed the concentration of dissolved iron ions is low (about 0.1 mg/L) as well as the relative atomic surface concentration of titanium (0.3%) obtained by XPS after utilization of PVF^f-TiO₂-Fe oxide. A more plausible suggestion would be that heterogeneous interactions between supported iron oxide and TiO₂ under irradiation are responsible of a significant part of the observed synergistic effects. This interaction has been investigated recently by double-beam photoacoustic spectroscopy (Murakami, 2008) and was suggested to depend on the irradiation wavelength:

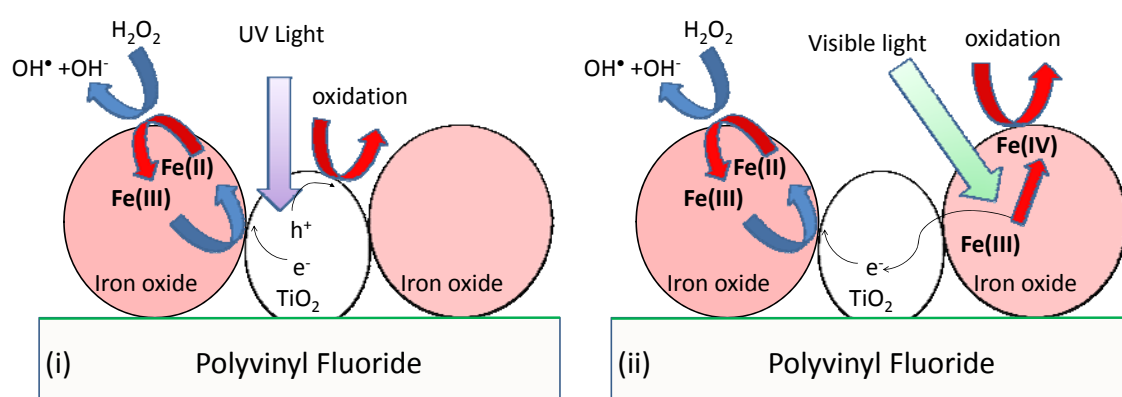
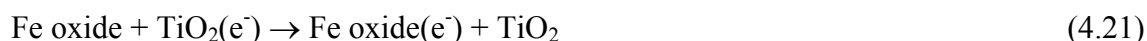


Figure 4.10 Schematic representation of possible synergistic photocatalytic action in the system PVF^f-TiO₂-Fe oxide/H₂O₂/light: (i) under ultraviolet light irradiation and (ii) under visible light irradiation.

(i) Under ultraviolet irradiation, photo-excited electrons generated in TiO₂ catalyst (Eq. 4.11) could be trapped into iron oxide particles (Eq. 4.21) resulting in improvement of charge separation on TiO₂ (completed by an oxidation reaction performed by remaining hole Eq. 4.12-4.13) and in regeneration of =Fe(II) sites (Eq. 4.9) (accelerating photo-Fenton reaction rates) by reduction of Fe(III) species.



This electron transfer is possible since the electrochemical potential position of TiO₂ bands relative to those of iron oxides (Zhang 2008a) allows electron transfer from excited TiO₂

valence band to iron oxide valence band by formation of a hetero-junction. This mechanism is represented in Figure 4.10(i).

(ii) Under visible light irradiation, iron oxide (or complex) could act as a sensitizer for TiO₂. First, a photo-excited iron species would inject an electron into TiO₂ and become oxidized. Then, the oxidized iron species (Fe(IV)) oxidize hydroquinone (polymer surface or ligand) to go back to their initial state (Fe(III)), whereas the electron injected in TiO₂ is transferred to iron oxide regenerating Fe(II). This mechanism which is described in Figure 4.10 (ii) needs further confirmation and solid evidence, due to the involvement of Fe(IV) oxidized species.

4.3.4 Optimization: effect of preparation parameters on the activity of catalysts

4.3.4.1 Effect of polymer film nature

The different polymeric substrates used to support iron oxide are represented in Figure 4.11.

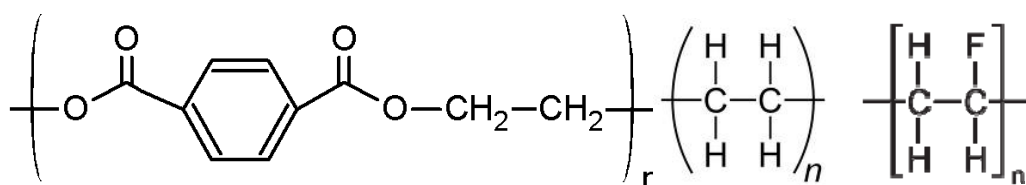


Figure 4.11 Structure of polymer substrate used: from left to right polyethylene terephthalate (PET), polyethylene (PE) and polyvinyl fluoride (PVF)

Figure 4.12 shows (i) TOC, (ii) HQ and (iii) [Fe]_d over time during the HQ degradations experiments mediated by photocatalysts composed of three types of polymeric substrates (PVF, PE, PET) prepared under conditions slightly different than previously (i.e. TiO₂ 1g/L in the Ti PSFD treatment and FeCl₃ 2 g/L in the hydrolysis step).

During the photocatalytic experiment mediated by the supported iron oxide on TiO₂ PSFD treated PE, PET and PVF, HQ and TOC reduction were similar, reaching HQ total degradation between 60-90 minutes, and around 80 % TOC decrease in 120 min. This fact indicates the negligible effect of the nature of polymer substrate on catalyst performance.

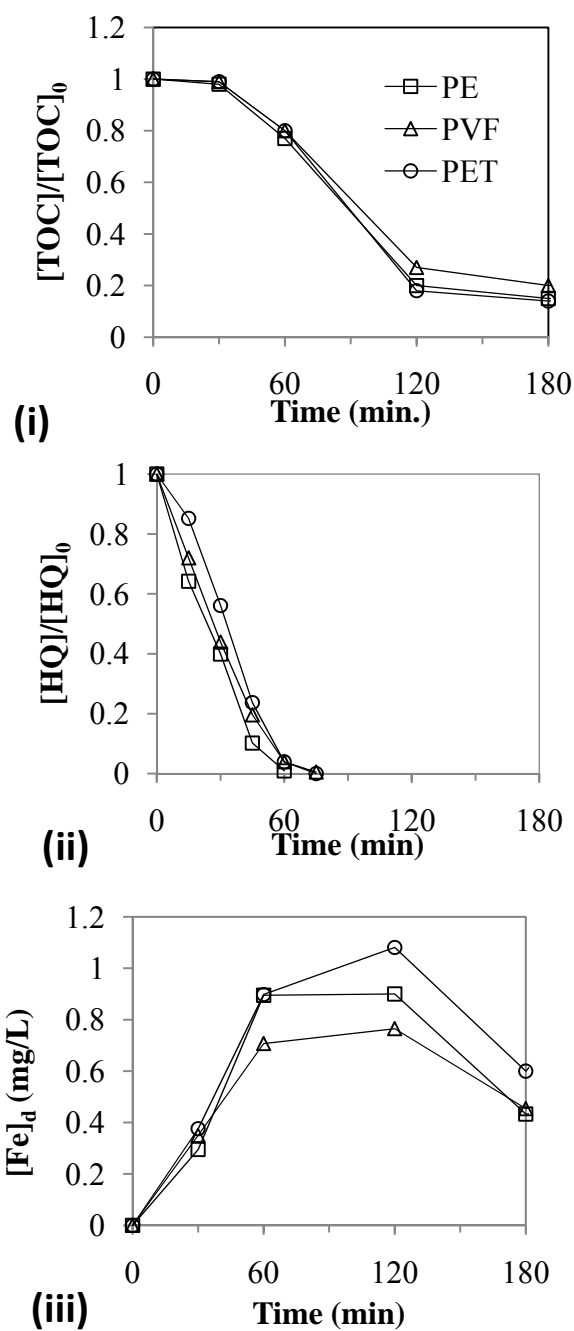


Figure 4.12 Evolution of (i) TOC, (ii) HQ concentration and (iii) $[Fe]_d$ during degradation of 0.18 mM of HQ at initial pH 5.7, in presence of 1.6 mM H_2O_2 , 75 cm² of catalyst (PE^f-TiO₂-Fe oxide, PVF^f-TiO₂-Fe oxide, PET^f-TiO₂-Fe oxide) under solar simulation for different polymeric substrates. The traces represent an average over three runs.

In contrast, Figure 4.12 (iii) shows that the amount of leached iron ions was dependant on the polymer nature with a maximum around 1.1, 0.9 and 0.7 mg/L after 120 min of treatment for PET, PVF and PE, respectively. A larger iron leaching could be linked to larger iron oxides quantities adsorbed on the substrate and, by extension, to the achievement of more surface functionalization in the pre-treatment, and to the own nature of the substrate (higher polarized surface).

The latter results suggest that different polymer substrate can be used depending on the application required. PET bottles could be used as catalyst support for drinking water production by modified solar water disinfection (SODIS). SODIS is a low cost method for treating microbial contaminated drinking water in transparent plastic bottles (Sommer, 1997). Nevertheless this method presents some disadvantages such as temperature dependency and re-growth of microorganism. The application of supported photo-Fenton could solve the SODIS limitations and lead to the simultaneous disinfection and degradation of xenobiotics and natural organic matter. The inactivation of *E. coli* in modified PET bottles is discussed section 4.3.4.5.

4.3.4.2 Effect of the pH during TiO₂ PSFD treatment

The initial pH of the aqueous medium during the TiO₂ PSFD treatment determines the amount of oxygenated groups formed and the superficial charge of TiO₂ nanoparticles. The extent of TiO₂ photo-deposition depends on the pH as well (Table 4.1). At acidic pH, the TiO₂ being positively charged can be stably deposited on electronegative oxygenated groups on the polymer surface. At basic pH, the TiO₂ and polymer are both negatively charged and the interaction is repulsive, limiting the polymer functionalization and the TiO₂ deposition. Consequently, since iron oxide crystallization is favored by TiO₂ presence, less iron oxide is deposited on its surface leading to a less efficient PVF^f-TiO₂-Fe oxide photocatalyst. HQ mineralization rates by PVF^f-TiO₂-Fe oxide/H₂O₂/light decrease as the pH for TiO₂ PSFD treatment increased with 73, 68 and 46% of HQ mineralized after 120 minutes for pH 3, 7 and 11 respectively. Figure 4.13 represents TOC removal by different photocatalyst during HQ degradation in presence of H₂O₂ under light. The disparity between PVF-Fe-oxide (trace a) and PVF^f-TiO₂-Fe oxide prepared at pH 11 and 3 (trace b-

c) shows the advantage of applying the TiO₂ PSFD treatment before iron oxide coating. Indeed at pH 3, more TiO₂ fixation induces as well more iron oxide coating. The TiO₂ PSFD treatment also avoids the initial TOC increase by the PVF-Fe oxide /H₂O₂/light system as the polymer already was degraded to a stable state under this treatment. In general, TOC removal is faster for the TiO₂ PSFD treated polymers particularly when the PSFD was carried out at acidic pHs.

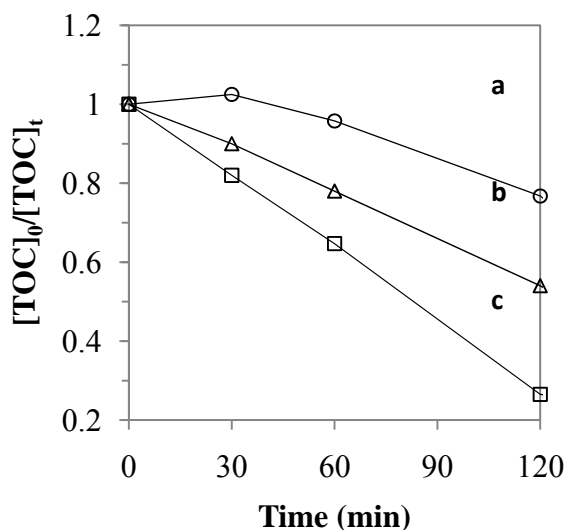


Figure 4.13 TOC removal of 0.18 mM of HQ, initial pH: 5.7, 75 cm² of heterogeneous photocatalyst 1.6 mM H₂O₂ under solar simulation: (a) PVF-Fe-oxide/H₂O₂/light; (b) PVF^f-TiO₂-Fe oxide (PSFD treatment at pH 11)/H₂O₂/light; (c) PVF^f-TiO₂ Fe oxide (PSFD treatment at pH 3)/H₂O₂/light.

4.3.4.3 Effect of TiO₂ concentration used for the TiO₂ PSFD treatment on HQ mineralization by the system PVF^f-TiO₂-Fe oxide/H₂O₂/light

Figure 4.14 shows that maximum HQ mineralization under light is reached when TiO₂ concentration used during PSFD treatment is ~1 g/L. The TiO₂ concentration influences both the extent of polymer surface functionalization and the amount of deposited TiO₂. Figure 4.14 shows that during PSFD treatment, the first run (curve a) of photocatalytic

mineralization is less efficient than following one (curve b). Thus, the first photocatalytic run enhances the photocatalyst performance for subsequent runs.

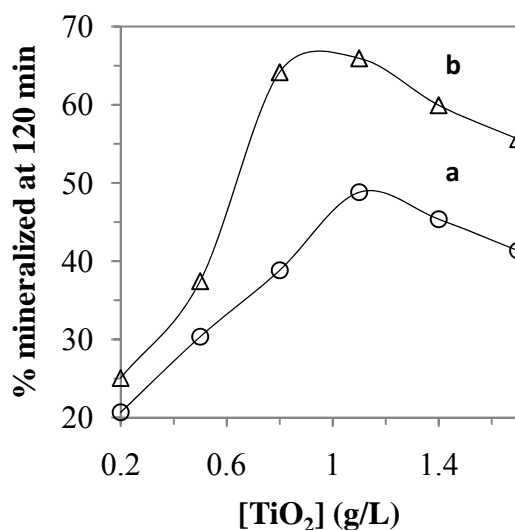


Figure 4.14 Effect of TiO₂ concentration (used for previous PSFD treatment of PVF) on HQ mineralization (of 0.18 mM HQ, initial pH = 5.7, PVF^f-TiO₂-Fe oxide 75 cm², H₂O₂ 1.6 mM under solar simulation): (a) first; (b) second consecutive HQ degradation.

4.3.4.4 Effect of iron oxide coating conditions

FeCl₃ hydrolysis was carried out at different temperatures (70, 80 and 90 °C) for the iron oxide generation and deposition. Applied temperatures during hydrolysis were found to play a significant role only for mineralization efficiency during the first degradation run: as temperature during hydrolysis was increased the mineralization rate during the first run increased. During the following runs, HQ mineralization was similar for photocatalysts prepared at 70, 80 or 90 °C. This may be due to the formation of oxide during the hydrolysis at low temperatures, which is stabilized during the first run. This adaptation phase as well as PVF-TiO₂-Fe oxide long-term stability will be discussed separately in chapter 5.

An additional thermal treatment at 100 °C during one hour after hydrolysis was applied to PVF^f-TiO₂-Fe oxide. The results obtained concerning HQ degradation suggested that this additional treatment was unnecessary. Actually a temperature of 100 °C is not sufficiently high to induce phase changes of iron oxide or to melt PVF substrate.

4.3.4.5 Effect of preparation on Bacterial inactivation

The ability of PET-TiO₂-Fe oxide to inactivate the indicator bacteria *E. coli* in presence of H₂O₂ and light was investigated in batch reactor. However, this material was found to constitute a light filter to the incoming light, protecting bacteria suspension from direct radiation. The protective effect was not observed in the case of HQ degradation because the reactor setup was different (the internal opaque PVC support make the photochemical reaction possible only between internal surface of Pyrex reactor and the surface of photocatalyst films) and because in contrast with *E. coli*, HQ is resistant to photolysis.

Then PET bottles (PET_b) were used as catalyst support and their bottom were functionalized and coated with iron oxide (to let the light pass through the suspension) leading to PET_b^f-TiO₂ Fe oxide (see Figure 4.15).



Figure 4.15 Photography of PET_b^f-TiO₂-Fe oxide used in this study

The inactivation of *E. coli* suspended in pure water under simulated solar light was measured in PET_b reactor in presence of Fe³⁺ and H₂O₂. Simultaneously, inactivation mediated by PET_b-TiO₂-Fe oxide in presence of H₂O₂ and the photolytic inactivation were measured. Figure 4.15 shows first order exponential fittings (lines) calculated in Matlab ($N_t = N_0 e^{-k_{obs} t}$). Table 4.3 shows the composition of the suspension matrices, the experimental conditions for the different systems and observed inactivation rates (k_{obs} (min⁻¹)).

Table 4.3 Experimental conditions and observed rate constants for the bacterial inactivation tests in PET bottle reactors under simulated solar radiation.

	Photocatalyst	H ₂ O ₂ (mM)	k _{obs} (min ⁻¹)
a (o)	-	-	0.024 ± 0.004
b (▼)	Fe ³⁺ (0.6 mg/L)	0.3	0.053 ± 0.008
c (x)	PET _b ^f -TiO ₂ -Fe oxide	0.3	0.060 ± 0.004

Figure 4.16 shows that the heterogeneous system (PET_b^f-TiO₂-Fe oxide /H₂O₂/light) has a similar bactericidal effect as the homogenous system (Fe³⁺/H₂O₂/light) in PET bottles (both k_{obs} ≈ 0.6 min⁻¹). Additional experiments using H₂O₂ (0.3mM) and light have shown that bacterial inactivation rates were similar to those when using light only (Spuhler, 2010). Iron ions concentrations in the filtered samples was below the detection limit (<0.1 mg/L) for both heterogeneous and homogeneous systems.

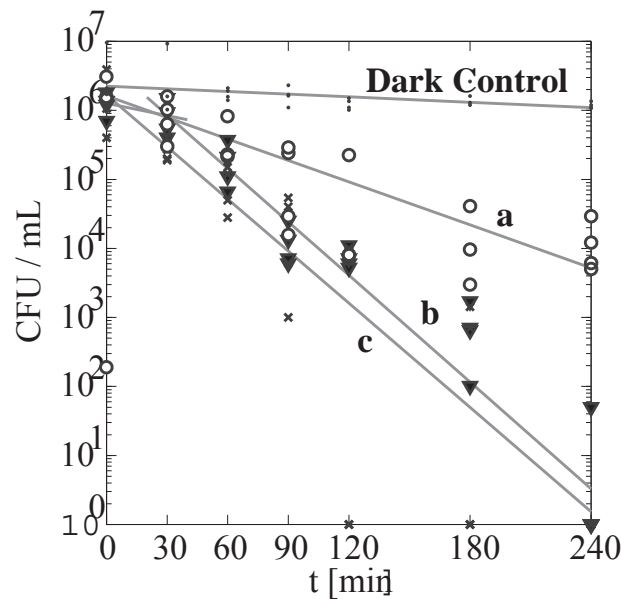


Figure 4.16 Inactivation of *E. coli* on PET bottle reactors (experimental conditions presented in Table 4.3)

Different explanations can justify the absence of detectable dissolved iron when using PET bottles: (i) the inactivation may take place on bottle surface (on iron or titanium oxide for heterogeneous system, and eventually iron complexes adsorbed on bottle surface for homogeneous system); (ii) the dissolved iron species may also be adsorbed on bacteria surface or even enter the intracellular medium and this contact could significantly contribute to the effective photo-inactivation (Spuhler, 2010).

4.4 Conclusions

- This work presents an innovative and simple way to prepare a highly photoactive catalyst combining TiO₂ and iron oxide fixed on PVF films.
- The surface characterization of photocatalyst shows that the PSFD treatment induced simultaneous surface functionalization involving oxygen-surface species formation and deposition of TiO₂ on carboxylic groups due to an electrostatic attraction.
- The TiO₂ deposition occurred preferentially when $\text{pH} \leq 7$ and the activity of photocatalysts increased with acidity during PSFD treatment.
- The TiO₂ and iron oxide on PVF was an efficient material toward HQ degradation and mineralization under light in presence of H₂O₂, at ambient temperature and neutral initial pH.
- Synergistic effects between TiO₂ and iron oxide for the system PVF^f-TiO₂-Fe oxide/H₂O₂/light were found to be significant and a synergistic factor S around 2.5 was estimated. These synergistic effects were assigned to the regeneration of =Fe(II) which is the rate-limiting step in Fenton processes.
- PVF, PE or PET supports led to catalysts showing similar photoactivity ruling out the possibility that the polymer nature influences significantly the catalyst efficiency.
- PET bottle employed as reactors and catalysts support (PET_b^{Ti-PC}-Fe oxide) was an efficient heterogeneous photocatalyst to inactivate bacteria and no dissolved iron ions were detected in the filtered solution opening perspectives for SODIS applications.

4.5 References

- Bandara J., Klehm U., Kiwi J. (2007) Raschig rings-Fe₂O₃ composite photocatalyst activate in the degradation of 4-chlorophenol and Orange II under daylight irradiation. *Applied Catalysis B: Environmental* 76: 73-81.
- Bouras P., Lianos P. (2008) Synergy effect in the combined photodegradation of an azo dye by titanium dioxide photocatalysis and photo-fenton oxidation. *Catalysis Letters* 123: 220-22.
- Cai J., Liu J., Gao Z., Navrotsky A., Suib S.L. (2001) Synthesis and anion exchange of tunnel structure akaganeite. *Chemistry of Materials* 13: 4595-4602.
- Celik E., Yildiz A.Y., Ak Azem N.F., Tanoglu M., Toparli M., Emrullahoglu O.F., Ozdemir I. (2006) Preparation and characterization of Fe₂O₃-TiO₂ thin films on glass substrate for photocatalytic applications. *Materials Science and Engineering B: Solid-State Materials for Advanced Technology* 129: 193-199.
- Deliyanni E.A., Nalbandian L., Matis K.A. (2006) Adsorptive removal of arsenites by a nanocrystalline hybrid surfactant-akaganeite sorbent. *Journal of Colloid and Interface Science* 302: 458-466.
- Greer A.L., Quedstedt T.E. (2006) Heterogeneous grain initiation in solidification. *Philosophical Magazine* 86: 3665-3680.
- Handbook of X-ray photoelectron spectroscopy, Perkin Elmer Corporation (1992) 72-73.
- Kim G.G., Kang J.A., Kim J.H., Kim S.J., Lee N.H., Kim S.J. (2006) Metallization of polymer through a novel surface modification applying a photocatalytic reaction. *Surface and Coating Technology* 201:3761-3766.
- Moulder J.F., Stickle W.F., Sobol P.E., Bomben K.D. (1992) Handbook of X-ray photoelectron spectroscopy, Physical Electronics.
- Murakami N., Chiyoya T., Tsubota T., Ohno T. (2008) Switching redox site of photocatalytic reaction on titanium(IV) oxide particles modified with transition-metal ion controlled by irradiation wavelength. *Applied Catalysis A: General* 348: 148-152.
- Musić, S., Krehula, S., Popović, S., Skoko, Z. (2003) Some factors influencing forced hydrolysis of FeCl₃ solutions. *Materials Letters* 57: 1096-1102.
- Sommer B., Mariño A., Solarte Y., Salas M. L., Dierolf C., Valiente C., Mora D., Rechsteiner R., Setter P., Wirojanagud W., Ajarmeh H., Al-Hassan A., Wegelin M., (1997) SODIS - An emerging water treatment process, *Journal of Water Supply: Research and Technology-AQUA*. 46:127-137.
- Spuhler D., Rengifo-Herrera J.A., Pulgarin C. (2010) The effect of Fe²⁺, Fe³⁺, H₂O₂ and the photo-Fenton reagent at near neutral pH on the Solar Disinfection (SODIS) at low temperatures of Water containing E. coli K12. *Applied catalysis B: Environmental* doi: 10.1016/j.apcatb.2010.02.010.
- Torres R.A., Nieto J.I., Combet E., Pétrier C., Pulgarin C. (2008) Influence of TiO₂ concentration on the synergistic effect between photocatalysis and high-frequency ultrasound for organic pollutant mineralization in water. *Applied Catalysis B: Environmental* 80: 168-175.
- Zhang W., Chen Y., Yu S., Chen S., Yin Y. (2008a) Preparation and antibacterial behavior of Fe³⁺-doped nanostructured TiO₂ thin films *Thin Solid Films* 516: 4690-4694.
- Zhang X., Lei L., (2008b) Preparation of photocatalytic Fe₂O₃-TiO₂ coatings in one step by metal organic chemical vapor deposition. *Applied Surface Science* 254: 2406-2412.

Zhou W., Fu H., Pan K., Tian C., Qu Y., Lu P., Sun C.-C. (2008) Mesoporous TiO₂/ α -Fe₂O₃: bifunctional composites for effective elimination of arsenite contamination through simultaneous photocatalytic oxidation and adsorption. *Journal of Physical Chemistry C* 112: 19584-19589.

Zou L., Zhu B. (2008) The synergistic effect of ozonation and photocatalysis on color removal from reused water. *Journal of Photochemistry and Photobiology A: Chemistry* 196: 24-32.

5- TiO₂ AND IRON OXIDE COATED POLYMER FILMS: INFLUENCE OF REACTION PARAMETERS ON PHOTOCATALYTIC ACTIVITY, LONG-TERM STABILITY

5.1 Introduction

The aimed characteristics for supported TiO₂-Fe oxide as heterogeneous photocatalysts are: (i) low leaching out of photoactive species from support surface during operation; (ii) adequate degradation rates at neutral pH and under solar illumination; (iii) resistance of support to oxidation by radicals in solution; (iv) catalyst showing long-term stability and (v) catalyst manufacture should be sustainable from the environmental and economical point of view.

Some recent studies described TiO₂-Fe oxide photocatalysts (Zhang, 2008; Akhavan, 2009). However, the effect of pH, temperature on rates has not been reported. In the case of supported heterogeneous photo-Fenton systems (Yuranova, 2004; Gumy, 2005; Song, 2006; Bandara, 2007; Moncayo, 2008), degradation rates are generally strongly pH-dependant with highest performance at pH 3 and lower as we move to neutral initial pH. In these systems, the degradation rates increase as the temperature increases (Ramirez, 2007). The effect of NaCl content on rates is also an important issue because of the utilization of sea water in some industrial processes.

The dissolution of iron ions is a common phenomenon during heterogeneous photo-Fenton oxidation. In the presence of ligands (aliphatic acids, humic acids...) and light, particularly under acidic conditions, iron is released by photo-reductive dissolution increasing the contribution of homogeneous photo-Fenton reaction (Sulzberger, 1995; Voelker, 1997).

In this chapter, hydroquinone (HQ) has been selected as a model substance whereas nalidixic acid (NA) was used because it is an antibiotic present in a real saline pharmaceutical wastewater. The objectives are: (i) to examine the performance of PVF^f-TiO₂-Fe oxide in the degradation of HQ and NA under different reaction conditions (pH, temperature, NaCl content), (ii) correlate the photo-activity enhancement to the surfaces modifications (iii) to test the long term stability of the catalyst.

5.2 Experimental

5.2.1 Chemicals

Hydroquinone (C₆H₆O₂), nalidixic acid (C₁₂H₁₂N₂O₃), NaOH, NaCl, HNO₃, FeSO₄·7H₂O, ferrozine, hydroxylamine hydrochloride, acetate buffer (pH = 4.65) were Fluka p.a. reagents (Buchs, Switzerland) and used as received. Hydrogen peroxide (35% by weight) was supplied by Merck AG (Darmstadt, Germany) and TiO₂ P25 (anatase to rutile weight ratio between 70:30 and 80:20) by Degussa.

5.2.2 Photocatalyst preparation

The photocatalyst used in this chapter is the optimized PVF^f-TiO₂-Fe oxide. Briefly, a TiO₂ PSFD treatment of 2 hours was applied to PVF film using aqueous TiO₂ suspensions (1 g/L) at natural initial pH (≈ 5) and under simulated sunlight irradiation leading to PVF^f-TiO₂; The films were afterward immersed in an aqueous solution of FeCl₃ (5 g/L) and heated at 80 °C under stirring for one hour. Then the resulting materials were dried in an oven at 100 °C during one hour.

5.2.3 Photo-reactor and irradiation procedure

The photo-reactor and irradiation procedure used for organic compounds degradation is described in detail points 2.2.2 and 3.2.3.

5.2.4 Analysis of the irradiated solutions

The quantitative determination of nalidixic acid was carried out by HPLC chromatography using a LC system HPLC-UV: Shimatzu LC-2010A equipped with a UV detector. Samples were injected via an auto-sampler. Samples of the treated NA solution were eluted at a flow rate of 1 mL/min through a column (nucleosil C8 HPLC) and using as mobile phase HPLC grade acetonitrile–formic acid solution (25 mM) in a 50%-50%.

The pH values were measured with a pH electrode SenTixH WPW connected to a pH 330i WTW device. The methods used for TOC, HQ, H₂O₂, dissolved iron quantification were described in detail point 3.2.4.

The analyses were performed as fast as possible after sampling in order to minimize the effect of dark Fenton reaction.

5.2.5 Photocatalyst characterization

The Characteristics of XPS and SEM apparatus are specified in point 4.2.6.

5.3 Results and discussions

5.3.1 Photocatalytic activity toward hydroquinone and nalidixic acid degradation

Figure 5.1 present the evolution of HQ and TOC concentrations within 240 min under different conditions. Trace a shows that HQ mineralization induced by the homogeneous photo-Fenton oxidation (Fe²⁺(0.3 mg/L)/H₂O₂/light) reached around 60%. For the system PVF-Fe oxide/H₂O₂/light (trace b), the TOC concentration increased during the first 30 minutes, due to PVF degradation by generated radicals, and thereafter rapidly decreased to reach 80% of mineralization after 240 min. For the system PVF^f-TiO₂-Fe oxide/H₂O₂/light (trace c), the TOC removal was faster, reaching a mineralization of 95% and the half-life time was about 20 minutes (trace d) for HQ under these conditions. A comparison between trace b and trace c in Figure 5.1 shows the beneficial effect induced by the TiO₂ PSFD treatment. These results shows that the presence of a TiO₂ layer between functionalized polymer surface and iron oxide layer prevents from the degradation and dissolution

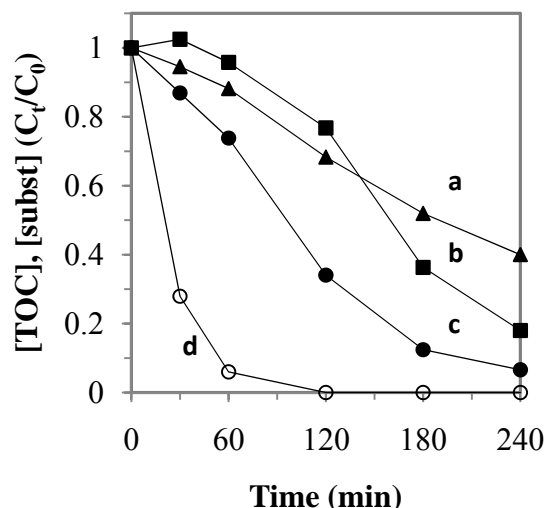


Figure 5.1 Degradation of 0.18 mM of HQ, initial pH 5.7, 30 °C, 1.6 mM H₂O₂, 75 cm² of heterogeneous photocatalyst under solar simulation (a) TOC removal by 0.3 mg/L Fe²⁺/H₂O₂/light; (b) TOC removal by PVF-Fe oxide/H₂O₂/light; (c) TOC removal by PVF^f-TiO₂-Fe oxide/H₂O₂/light; (d) HQ degradation by PVF^f-TiO₂-Fe oxide/H₂O₂/light. The traces represent an average over 3 runs.

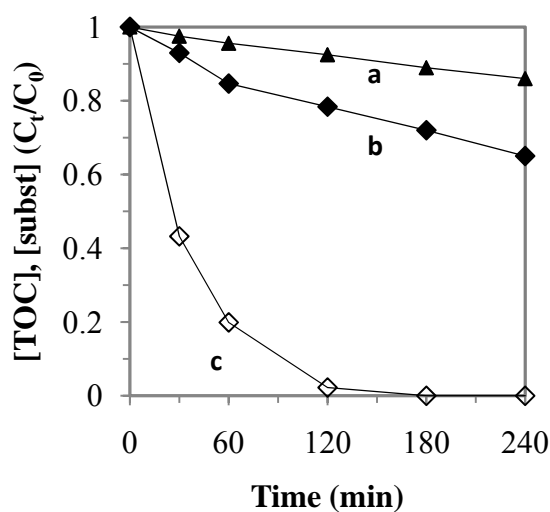


Figure 5.2 Degradation of 0.18 mM of NA, initial pH 6.5, 30 °C, 3.2 mM H₂O₂, 75 cm² of PVF^f-TiO₂-Fe oxide under solar simulation (a) TOC removal by 0.3 mg/L Fe²⁺/H₂O₂/light; (b) TOC removal by PVF^f-TiO₂-Fe oxide/H₂O₂/light; (c) NA degradation by PVF^f-TiO₂-Fe oxide/H₂O₂/light. The traces represent average over 3 runs.

of PVF (induced by photo-Fenton reactions in the case of PVF-Fe oxide) and accelerates degradation process. Figure 5.2 presents the evolution of normalized NA and TOC concentrations within 240 min under different conditions. During homogeneous photo-Fenton (Fe^{2+} (0.3 mg/L)/ H_2O_2 /light) oxidation (trace a), mineralization of NA was very slow (15%). For the system $\text{PVF}^{\text{f}}\text{-TiO}_2\text{-Fe oxide}/\text{H}_2\text{O}_2/\text{light}$ (trace b) the mineralization was higher (35%) and NA degradation (trace c) was fast with a half-time around 25 min.

5.3.2 Iron leaching and homogeneous photocatalytic contribution

Figure 5.3 shows the evolution of dissolved iron concentration ($[\text{Fe}]_{\text{d}}$) during the photocatalytic processes measured by the ferrozine method.

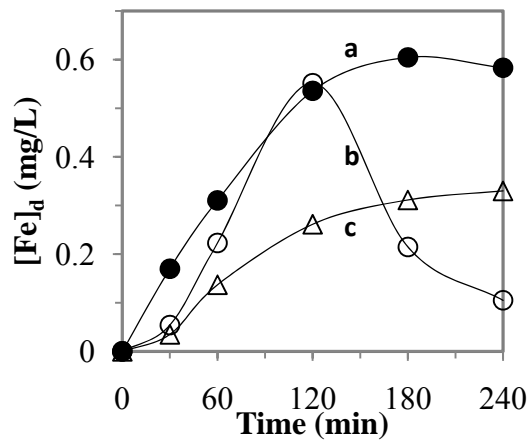


Figure 5.3. Evolution of dissolved iron concentration during degradation of 0.18 mM of pollutant, Initial pH 5.7, 30 °C, 75 cm² of heterogeneous photocatalyst under solar simulation (a) HQ, PVF-Fe oxide/ H_2O_2 (1.6 mM)/light; (b) HQ, $\text{PVF}^{\text{f}}\text{-TiO}_2\text{-Fe oxide}/\text{H}_2\text{O}_2$ (1.6 mM)/light; (c) NA, $\text{PVF}^{\text{f}}\text{-TiO}_2\text{-Fe oxide}/\text{H}_2\text{O}_2$ (3.2 mM)/light. The traces represent average dissolved iron over 3 runs.

For HQ degradation by the system PVF-Fe oxide/ H_2O_2 /light, (trace a), $[\text{Fe}]_{\text{d}}$ increased during the first 120 min of treatment up to 0.6 mg/L and stabilized during the following 120 min. For HQ degradation by the system $\text{PVF}^{\text{f}}\text{-TiO}_2\text{-Fe oxide}/\text{H}_2\text{O}_2/\text{light}$ (trace b), $[\text{Fe}]_{\text{d}}$ reached a maximum at 120 min with about 0.6 mg/L and decreased to 0.1 mg/L during the following 120 min. This phenomenon was also observed by other authors with different

heterogeneous photocatalysts containing iron (Bozzi, 2002; Feng, 2004). In the case of NA photocatalytic degradation by the system PVF^f-TiO₂-Fe oxide/H₂O₂/light, [Fe]_d increased during the first 120 min of treatment up to 0.3 mg/L (trace c).

When evaluating a catalyst based on iron oxide in presence of H₂O₂, it is essential to know the amount of leached soluble iron species into the aqueous solution during photocatalytic operation and to estimate the relative contribution of homogeneous photo-Fenton reaction to the overall degradation process.

For this purpose, average dissolved iron concentration ([Fe]_d^{av}, Eq. 5.1), TOC removal ($\Delta[\text{TOC}]_t = [\text{TOC}]_0 - [\text{TOC}]_t$), ratio *r* (Eq. 5.2) and homogeneous percentage *h_t* (Eq. 5.3) were calculated for different photocatalytic processes and times.

$$[\text{Fe}]_d^{\text{av}} = \int_0^t [\text{Fe}]_d dt/t \quad (5.1)$$

$$r = \Delta[\text{TOC}]_t / [\text{Fe}]_d^{\text{av}} \quad (5.2)$$

$$h_t = 100 * r_{\text{homo}} / r_{\text{hetero}} \quad (5.3)$$

Table 5.1 Homogeneous percentage relative to different processes and times (Values calculated from Figures 5.1-5.3).

Photo-Fenton processes	<i>h</i> ₆₀	<i>h</i> ₁₂₀	<i>h</i> ₂₄₀
PVF-Fe oxide HQ	100	100	100
PVF ^f -TiO ₂ -Fe oxide HQ	20	39	53
PVF ^f -TiO ₂ -Fe oxide NA	5	16	29

Table 5.1 shows that for the system PVF-Fe-oxide/H₂O₂/light, *h*₆₀, *h*₁₂₀ and *h*₂₄₀ are 100 %. Thus HQ mineralization by this system seems only due to homogeneous photo-Fenton oxidation. For HQ mineralization by the system PVF^f-TiO₂-Fe oxide/H₂O₂/light, *h*₆₀, *h*₁₂₀ and *h*₂₄₀ were about 20, 39, and 53 % respectively whereas for NA, *h*₆₀, *h*₁₂₀ and *h*₂₄₀ were about 8, 16, and 29 % respectively. This result suggests that the homogeneous contribution is significant particularly for HQ when the whole time is taken into account. However,

heterogeneous process is responsible for a major part of the mineralization process at the beginning of the treatment and for NA.

5.3.3 Initial activation of PVF^f-TiO₂-Fe oxide photocatalyst

Figure 5.4(i) shows the TOC removal during HQ degradation by the system PVF^f-TiO₂-Fe oxide/H₂O₂/light during the first two catalytic operations. During the first run (trace a), the TOC increased (until 30 min) due to degradation of the PVF inducing dissolution of

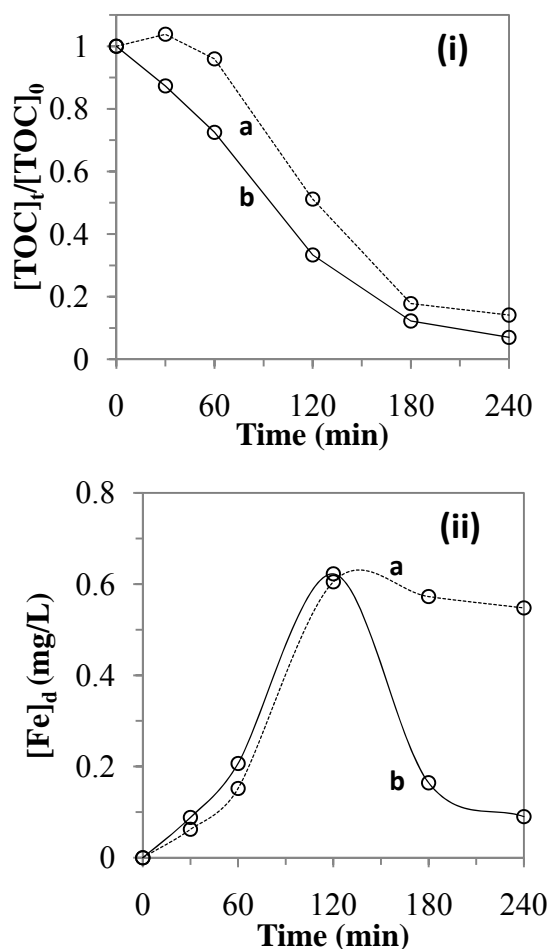


Figure 5.4 Evolution of (i) normalized TOC concentration and (ii) Dissolved iron concentration during the two first photocatalytic mineralization of HQ: (a) first; (b) second run (experimental conditions: 0.18 mM HQ, initial pH 5.7, 30 °C, 1.6 mM H₂O₂, 75 cm² of heterogeneous photocatalyst under solar simulation).

organic compounds and finishing polymer surface functionalization. After 240 min of treatment, the TOC removal reached 85%. In the second run (trace b), the TOC decreased from the beginning of the treatment reaching a removal of 95% after 240 min.

Figure 5.4(ii) shows the evolution of dissolved iron characteristic for the two first HQ degradations as a function of time. For the first run, $[\text{Fe}]_d$ reaches a maximum of 0.6 mg/L after 120 min of treatment and then stabilizes around 0.5 mg/L whereas for the second run, $[\text{Fe}]_d$ reaches a maximum of 0.6 mg/L after 120 min of treatment and then decreases rapidly until a value of 0.1 mg/L after 240 min. These differences in the extent iron leaching can be attributed to the washing of loosely bounded iron during the first run. Additionally the functionalization of polymer surface (oxygen groups formation) leads to the formation of vacant sites where iron species are likely to form complexes at the end of the second run. Figure 5.4(ii) (trace b) shows a singular pulse shape illustrating the re-adsorption of dissolved iron is much faster compare to other heterogeneous catalysts containing iron species (Bozzi, 2002; Feng, 2004).

5.3.4 Correlations between surface modifications and activation processes

5.3.4.1 X-ray photoelectron spectroscopy (XPS) analysis of $\text{PVF}^f\text{-TiO}_2\text{-Fe oxide}$

In all the spectra there was an energy shift to lower binding energies (BE) of about 3 eV, which occurred due to the low conductivity of the samples. In the present study, the corrected BEs are given.

Table 5.2 Composition of $\text{PVF}^f\text{-TiO}_2\text{-Fe oxide}$ surface (atomic percent) as prepared and after three runs.

Samples	C	O	F	Cl	Ti	Fe	Fe/C	Fe/Ti	Fe/Cl
$\text{PVF}^f\text{-TiO}_2\text{-Fe oxide}$	22.7	46.0	2.0	6.4	0	23.8	1.05	-	3.72
$\text{PVF}^f\text{-TiO}_2\text{-Fe oxide after use}$	35.1	45.1	1.5	1.7	0.3	16.8	0.47	56	9.88

The differences in the chemical composition of $\text{PVF}^f\text{-TiO}_2\text{-Fe oxide}$ surface before and after three photocatalytic runs were investigated by XPS. Fe (2p) photoelectron spectrum

was not significantly changed due to use (results not shown). Table 5.2 shows the variation of surface atomic composition induced by PVF^f-TiO₂-Fe oxide utilization. Before use, a relatively high amount of iron (23.8%) was found. The presence of important surface atomic concentration of chloride (6.4 %) suggests that the nature of oxide was probably akaganeite (β -FeOOH.Cl_n). XPS results shows as well that oxygen, fluorine, chlorine and iron relative surface concentrations decrease after the degradation runs but the concentration of carbon increases. The drastic Fe/C ratio fall from 1.05 to 0.47 on PVF^f-TiO₂-Fe oxide composite after utilization can be allocated to erosion of the surface induced by the washing or photo-leaching of iron species and to physical or chemical adsorption of organic compounds. The depletion of fluorine concentration can be explained by the degradation of the polymer surface during irradiation whereas the depletion of chlorine concentration can be allocated to anion exchange properties of akaganeite. Akaganeite is tunnel structured containing interstitial Cl⁻ that can be substituted by other small anions like F⁻, OH⁻ (Cai, 2001).

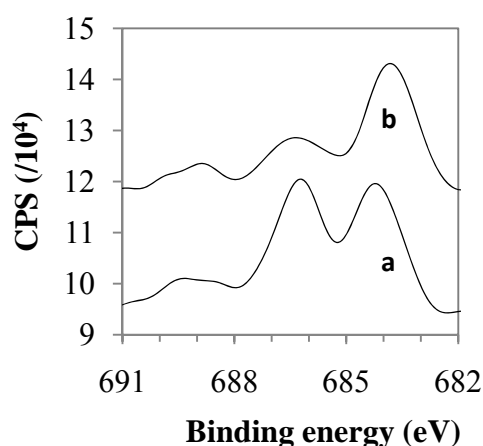


Figure 5.5 F(1s) photoelectron spectra of (a) PVF^f-TiO₂-Fe oxide as prepared (b) PVF^f-TiO₂-Fe oxide after three runs.

In Figure 5.5, the photoelectron spectrum of F (1s) core level of PVF^f-TiO₂-Fe oxide is represented. Before utilization (trace a), the F (1s) peak is triple with two predominant components at BEs of 684.2 and 686.3 eV, corresponding to fluorine incorporated into iron oxide (FeOF) due to the anion exchange properties of akaganeite, and to polymeric C-F bond, respectively. The small third F (1s) peak centered at a BE = 689 eV corresponds to F⁻

absorbed at iron oxide surface. After third run (trace b), the main difference is that the central peak corresponding to polymeric fluorine (C-F bond) decreased, pointing out that during HQ degradations mediated by $\text{PVF}^{\text{f}}\text{-TiO}_2\text{-Fe-oxide}$, the polymer surface continues to undergo modifications. Figure 5 suggests as well that fluorides from the polymer are incorporated into the tunnel sites and surface sites of akaganeite, and exchanges of Cl^- by OH^- may occur as well. Moreover the leaching of iron during utilization uncovers a part of the TiO_2 that was previously totally covered by iron oxide. Table 5.2 shows that after three runs, 0.3% of atomic surface composition is constituted by titanium. The presence of TiO_2 at the material surface plays a central role in the observed activation and synergistic processes.

5.3.4.2 Secondary electron microscopy (SEM)

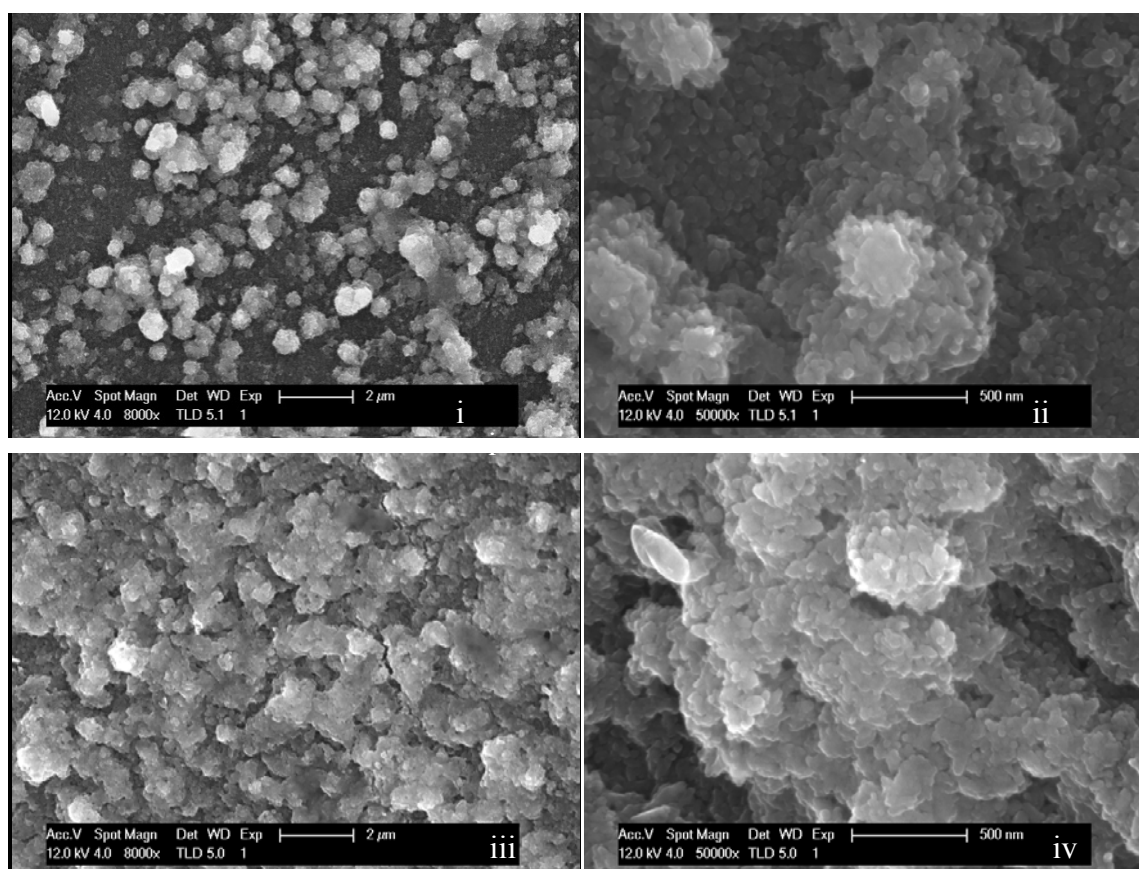


Figure 5.6 Scanning electron microscopic images of $\text{PVF}^{\text{f}}\text{-TiO}_2\text{-Fe oxide}$ (i)-(ii) before and (iii)-(iv) after three runs.

Figure 5.6 shows the catalyst surface morphology before and after utilization. In Figure 5.6(i) the PVF^f-TiO₂-Fe oxide surface with iron oxide aggregates of about 1 μm are shown. These aggregates are composed of nanoparticles of approximately 50 nm, which seem to cover the polymer surface (Figure 5.6(ii)). After the third run (Figure 5.6(iii)-(iv)) the surface seems more layer-structured and contains less relief than the as prepared catalyst pointing out the erosion of the surface during utilization.

5.3.4.3 Discussion about initial activation of PVF^f-TiO₂-Fe oxide and increase of synergistic effects

The enhancement of PVF^f-TiO₂-Fe oxide photo-activity after use, presented in Figure 5.4, can be assigned to different phenomena occurring on material surface: (i) continuation of the functionalization of the polymer surface and decreasing of Fe/C ratio during first run may favor substance adsorption, iron re-adsorption and polymer substrate stabilization which increase the photocatalyst performances; (ii) leaving of chlorine from PVF^f-TiO₂-Fe-oxide surface (Table 5.2) cause porous tunnel-like structure into the photocatalytic material and induce exchange with others anions (like OH⁻, F⁻) which might affect positively the catalyst activity; (iii) TiO₂ particles are exposed to the light after the first runs due to irreversible iron oxide dissolution. Thus TiO₂ is likely to contribute to the photocatalytic degradation processes. Besides photo-Fenton oxidation, radical generation and pollutant degradation are induced by photocatalysis occurring both at iron oxide and TiO₂ surfaces as well as by synergistic effects of TiO₂ and iron oxide. More details about these mechanisms were discussed in point 4.3.3.

5.3.5 Effect of reaction conditions on photocatalytic activity

5.3.5.1 Effect of pH

Even though the system PVF^f-TiO₂-Fe oxide/H₂O₂/light exhibited high photocatalytic activity for the degradation and mineralization of 0.18 mM HQ at natural initial pH, it is relevant to explore its activity at other initial pHs. The experiments were performed at initial pH 7.1, 5.7, 3.4 and they were not controlled during the experiment. The influence of

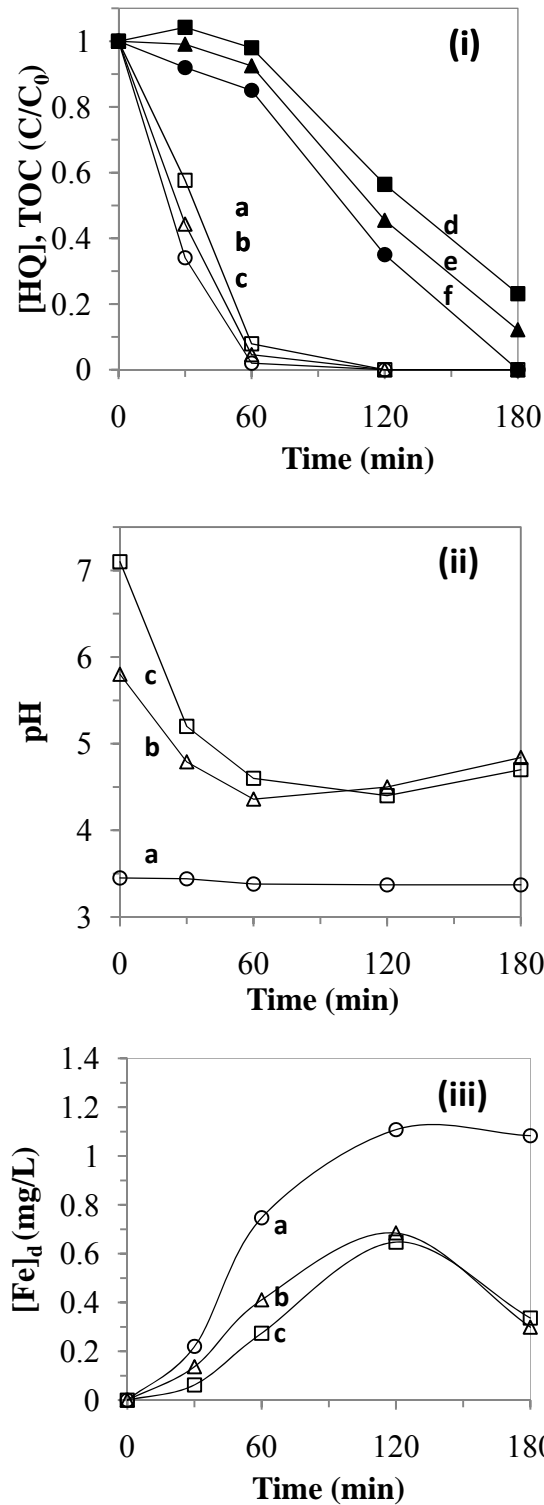


Figure 5.7 Variation of (i) HQ and TOC normalized concentrations (ii) pH and (iii) [Fe]_d during degradation of 0.18 mM of HQ, 1.6 mM H₂O₂, 30 °C, 75 cm² of PVF^f-TiO₂ Fe oxide under solar simulation and at different initial pHs.(a) 3.4, (b) 5.8, (c) 7.1.

initial pH on HQ degradation and mineralization by PVF^f-TiO₂-Fe-oxide/H₂O₂/light is shown in Figure 5.7(i). Total HQ abatement was rapidly observed in the studied initial pH range (trace a, b, c). Figure 5.7(i) shows that the initial (first 30 min) pH value did not affect substantially the degradation rates. The initial degradation (30 min) and mineralization (120 min) rates were increased only 1.5-fold varying initial pH from 7.1 to 3.4.

Figure 5.7(ii) illustrates the pH evolution during the process. While at initial pH of 3.4, this value remained nearly constant (trace a), for initial pH 5.7 and 7.1, the pH decreased during the process to reach a minimum value around 4.5 at 120 min (trace b, c). Then after, pH slightly increased probably due to the mineralization of aliphatic acid intermediates generated during the first step of HQ photocatalytic degradation.

The [Fe]_d measured during the processes (Figure 5.7(iii)) increased as the pH becomes more acidic. A final [Fe]_d of 1.1, 0.3 and 0.3 mg/L for initial pHs of 3.4, 5.8, 7.1 respectively was measured (Figure 8) corresponding to an augmentation of 3.5-fold as the pH decreases.

The results shown in Figure 5.7 (traces c) suggest that it may exist a pH interval where iron dissolution is minimal and photo-activity is high since 40% of HQ was degraded at pH between 5 and 7 with less than 0.1 mg/L of dissolved iron. Further experiments using pH regulation are required in order to confirm this hypothesis.

The relative independence of degradation rates from the initial pH can be assigned to several phenomena: (i) for PVF^f-TiO₂-Fe oxide/H₂O₂/light system, semiconductor photocatalysis and synergistic action of TiO₂ and iron oxide participate in observed HQ abatement; (ii) the reaction pH decreased to a value beside 5 after 30 min.

5.3.5.2 Effect of temperature

The results obtained for HQ degradation by the system PVF^f-TiO₂-Fe oxide/H₂O₂/light at three different temperatures (30, 40, 55 °C) are presented in Figure 5.8(i). The reaction rates increase when temperature increases due to the exponential dependency of the kinetic constant with the reaction temperature (Arrhenius). The activation energy was calculated using pseudo first order rates (k_1) and plotting $\ln(k_1)$ versus of $1/T$. The slope multiplied by

the gas constant gives $E_a = 57$ kJ/mol. Thus the oxidation of HQ needs low activation energy when PVF^f-TiO₂-Fe-oxide was used as catalyst. These values suggest ion-molecule and radical-molecule reaction requiring activation energy besides the radical-radical reactions that need no E_a .

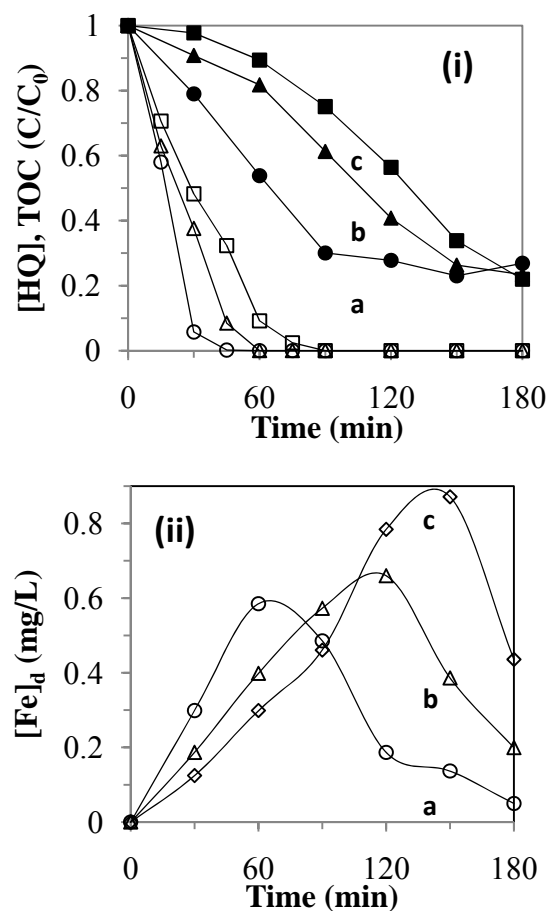


Figure 5.8 Variation of (i) HQ and TOC normalized concentrations and (ii) dissolved iron concentration during degradation of 0.18 mM of HQ, 1.6 mM H₂O₂, initial pH 5.7, 75 cm² of PVF^f-TiO₂-Fe-oxide under solar simulation and at different temperatures: (a) 55 °C, (b) 40 °C, (c) 30 °C.3

Figure 5.8(i) shows that the TOC removal is a function of the reaction temperatures. After 90 min treatment, 70% TOC is removed at 55 °C (trace a) whereas 40 and 25% TOC were removed at 40 (trace b) and 30 °C (trace c) respectively. When the temperature increases (up to 55 °C), the H₂O₂ consumption accelerates and mineralization processes stop sooner

than at a lower temperature. Thus for the trace a in Figure 5.8(i), the TOC abatement is slowed and stopped by a total H₂O₂ consumption after 90 min of treatment.

The degradation and initial mineralization (first 60 min in Figure 5.8(i)) rates increased 6 and 5-fold respectively when temperature increased from 30 to 55 °C. This is valuable as solar light can be used to activate this process since it is usually accompanied by a significant increase in the temperature of the bulk reactor. Although one could expect that an increase of temperature might increase extent of leaching, it was not the case with the PVF^f-TiO₂-Fe oxide composite as shown in Figure 5.8(ii). Iron leaching initial (first 30 min) rates were accelerated by the temperature of the treatment but the maximal concentration of dissolved iron was inversely proportional to temperature with a [Fe]_d around 0.6, 0.7 and 0.9 mg/L for 55 (trace a), 40 (trace b) and 30 °C (trace c) respectively.

5.3.6.3 Effect of NaCl.

The effect induced by the addition of NaCl (5 g/L) on NA degradation and mineralization mediated by the systems PVF^f-TiO₂-Fe oxide/H₂O₂/light (i) and Fe²⁺(2 mg/L)/H₂O₂/light (ii) is illustrated in Figure 5.9. The salt adjunction was detrimental for the mineralization process of both homogeneous and heterogeneous systems. The initial mineralization rate (first 60 min) was around 2 times lower in presence (trace a) than in absence (trace b) of salt. For NA degradation in absence of salt, the rate relative to homogeneous system (trace d Figure 5.9(ii)) was 3 times higher than those of heterogeneous system (trace d Figure 9(i)). However, in presence of salt (traces c), the rates observed were similar for homogeneous and heterogeneous systems.

This comparison suggests that the heterogeneous system is advantageous for the treatment of saline wastewater since the degradation process is slightly faster in presence of salt. It is known that the inhibitory effect of Cl⁻ on Fenton reaction is due to the scavenging of •OH by this ion (Pignatello, 2006). Thus for PVF^f-TiO₂-Fe oxide/H₂O₂/light system: (i) mineralization process seems largely controlled by photo-Fenton reaction initially induced by •OH attacks and then by charge transfers occurring on iron oxide surface or dissolved complexes with intermediates; (ii) degradation process is heterogeneous and involves charge transfers from catalyst surface to pollutant rather than the participation of •OH.

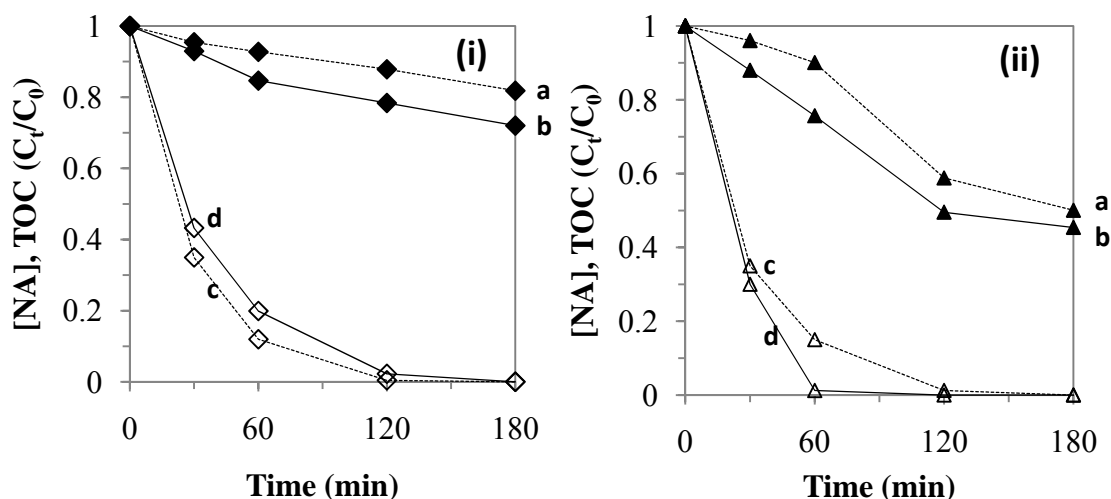


Figure 5.9 Variation of HQ and TOC normalized concentrations during degradation of 0.18 mM NA by (i) 75 cm² of PVF^f-TiO₂-Fe oxide, (ii) 2 mg/L Fe²⁺: TOC removal (a) in presence and (b) without NaCl; NA degradation (c) in presence and (d) without NaCl. (experimental conditions at initial pH 6.5, 30 °C, 3.2 mM H₂O₂, 0.86 M NaCl under solar simulation).

5.3.6 Long term Stability of PVF^f-TiO₂-Fe oxide

The long term stability of PVF^f-TiO₂-Fe oxide was studied by evaluating catalytic performances during repetitive nalidixic acid degradations. Figure 5.10 represents the results of this stability showing NA evolution as a function of time. These results show that the PVF^f-TiO₂-Fe oxide is extremely stable during 47 consecutive runs corresponding to about 150 hours of operation. The degradation rate relative to the first run, an average of runs 2-6, 10-30 and 45-47 were calculated. Surprisingly, instead of a slow decrease of the degradation rates, a slow increase was observed. The rate undergoes a 1.5-fold increase between runs 2-6 and runs 45-47. These results suggest that the presence of TiO₂ particles deposited on PVF substrate not only increased iron oxide formation and deposition on polymer surface (Chapter 3) but also other beneficial effects: (i) as long as the PVF^f-TiO₂-Fe oxide is used, the TiO₂ uncovering and exposition to light, induced by iron photo-dissolution, increases the Ti/Fe surface concentration (Table 5.2) which increases the synergistic effects and the degradation rates and (ii) The catalyst was protected from self-degradation since TiO₂ diminished the contact between radicals and polymer surface and

can trap charges which otherwise would degrade the polymeric substrate (see point 3.3.2).

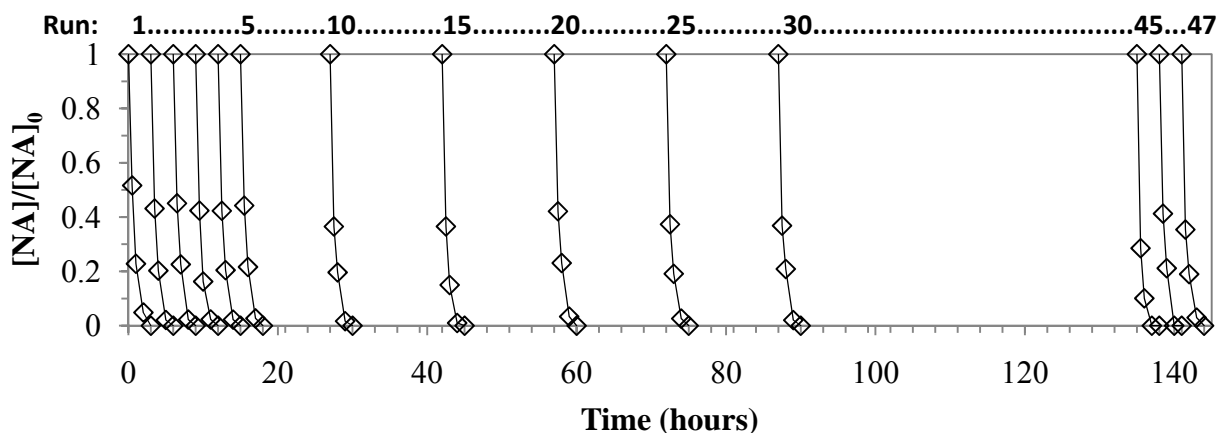


Figure 5.10. Repetitive NA degradation (experimental conditions: 0.18 mM NA, 30 °C, solar simulation, initial pH = 6.5, PVF^f-TiO₂-Fe oxide 75 cm², H₂O₂ 3.2 mM).

5.3.7 Reversible iron dissolution

During this work, leaching of iron species from oxide surface to the solution was probably caused by the simultaneous presence of light, dissolved organic substances (or polymer substrate) and H₂O₂. The mechanisms involved like photo-reductive dissolution were discussed in the introduction (point 1.2.4.3).

The pH of the reaction media influenced considerably the iron photo-dissolution process since the more the initial pH is acidic the more iron dissolved was found in solution (see section 3.4.1, in Figure 5.7(iii)).

The decrease of dissolved iron concentration (observed in Figures 5.3-5.4, 5.7-5.8) could be due to iron ions re-deposition (Eq. 5.11) which might take place as follows. First the dissolved Fe(II) species undergo oxidation processes as Fenton-like reaction producing Fe(III) species. These species are not stable in aqueous phase under the experimental conditions (pH = 4.5; absence of dissolved organic ligands) at the end of the treatment. Thus Fe(III) species re-deposit on vacant site (=) located at iron oxide, TiO₂, polymer and reactor surfaces.



The observed phenomena of dissolved iron concentration depletion could have important theoretical and practical implications and may allow new alternatives for dissolved iron removal in homogeneous photo-Fenton processes.

5.4 Conclusions

The aimed characteristics for supported TiO_2 -Fe oxide as heterogeneous photocatalysts have been reached when using PVF^f- TiO_2 -Fe oxide/ H_2O_2 /light system:

- The photo-dissolution of iron ions and their relative homogeneous contribution to HQ and NA initial mineralization was low. Besides, the re-deposition of dissolved species on the photocatalyst was observed.
- HQ and NA photo-assisted degradation rates were high and mostly independent of initial pH and NaCl presence but increased with temperature.
- The film substrate was resistant to self-degradation by generated radicals.
- The photocatalytic activity was highly stable toward repetitive pollutant degradation and it was even slightly increasing after 150 hours operation.
- The preparation method proposed is sustainable as it used solar light, water as solvent and low temperatures.

The presence of TiO_2 particles on photocatalyst surface was found to engender three principal beneficial effects: (1) the iron oxide deposition was higher on TiO_2 coated PVF surfaces than in commercial PVF; (2) the initial and long term activations were assigned to the uncovering of TiO_2 due to irreversible iron dissolution which increased its exposition to light and consequently its synergistic contribution to the overall photocatalytic degradation process; (3) the resistance to self-degradation was assigned to TiO_2 which may acts as a charge trap and diminish the contact between active iron species and polymer surface.

5.6 References

- Akhavan O., Azimirad R. (2009) Photocatalytic property of Fe₂O₃ nanograin chains coated by TiO₂ nanolayer in visible light irradiation. *Applied Catalysis A: General* 369:77-82.
- Bandara J., Klehm U., Kiwi J. (2007) Raschig rings-Fe₂O₃ composite photocatalyst activate in the degradation of 4-chlorophenol and Orange II under daylight irradiation. *Applied Catalysis B: Environmental* 76: 73-81.
- Bozzi A., Yuranova T., Mielczarski J., Lopez A., Kiwi J. (2002) Abatement of oxalates catalyzed by Fe-silica structured surfaces via cyclic carboxylate intermediates in photo-Fenton reactions. *Chemical Communications* 19: 2202-2203.
- Cai J., Liu J., Gao Z., Navrotsky A., Suib S.L. (2001) Synthesis and anion exchange of tunnel structure akaganeite. *Chemistry of Materials* 13: 4595-4602.
- Feng J., Hu X., Po L.Y. (2004) Discoloration and mineralization of Orange II using different heterogeneous catalysts containing Fe: A comparative study. *Environmental Science and Technology* 38: 5773-5778.
- Gumy D., Fernández-Ibáñez P., Malato S., Pulgarin C., Enea O., Kiwi J. (2005) Supported Fe/C and Fe/Nafion/C catalysts for the photo-Fenton degradation of Orange II under solar irradiation. *Catalysis Today* 101: 375-382.
- Moncayo-Lasso A., Torres-Palma R.A., Kiwi J., Benítez N., Pulgarin C. (2008) Bacterial inactivation and organic oxidation via immobilized photo-Fenton reagent on structured silica surfaces. *Applied Catalysis B: Environmental* 84: 577-583.
- Pignatello J.J., Oliveros E., MacKay A. (2006) Advanced oxidation processes for organic contaminant destruction based on the fenton reaction and related chemistry. *Critical Reviews in Environmental Science and Technology* 36:1-84.
- Ramirez J.H., Costa C.A., Madeira L.M., Mata G., Vicente M.A., Rojas-Cervantes M.L., López-Peinado A.J., Martín-Aranda R.M. (2007) Fenton-like oxidation of Orange II solutions using heterogeneous catalysts based on saponite clay. *Applied Catalysis B: Environmental* 71: 44-56.
- Song W., Cheng M., Ma J., Ma W., Chen C., Zhao J. (2006) Decomposition of hydrogen peroxide driven by photochemical cycling of iron species in clay *Environmental Science and Technology* 40: 4782-4787.
- Sulzberger B., Laubscher H. (1995) Photoredox reactions at the surface of iron(III)(hydr-)oxides. *Marine chemistry* 50: 103-115.
- Voelker B.M., Morel F.M.M., Sulzberger B. (1997) Iron redox cycling in surface waters: Effects of humic substances and light. *Environmental Science and Technology* 31: 1004-1011.
- Yuranova T., Enea O., Mielczarski E., Mielczarski J., Albers P., Kiwi J. (2004) Fenton immobilized photo-assisted catalysis through a Fe/C structured fabric. *Applied Catalysis B: Environmental* 49: 39-50.
- Zhang X., Lei L., (2008) Preparation of photocatalytic Fe₂O₃-TiO₂ coatings in one step by metal organic chemical vapor deposition. *Applied Surface Science* 254: 2406-2412.

6- SCALE UP: FIELD SOLAR DEGRADATION OF PESTICIDES AND EMERGING WATER CONTAMINANTS

6.1 Introduction

The natural and free energy that provides the sun is a source of many interesting and emerging applications that could improve the sustainability of human activities. The applications are versatile namely in the field of energy production (thermal, photovoltaic...), chemical synthesis and water treatment (detoxification, disinfection, desalinization). This chapter focuses on the use of the PVF^f-TiO₂-Fe oxide at pilot scale for the detoxification of water contaminated with real pollutants such as pesticides or emerging contaminants.

6.1.1 Solar resource

The earth receives about 1.7×10^{14} kW of solar radiation, meaning 1.5×10^{18} kWh per year. Extraterrestrial radiation has an intensity of 1367 W/m^2 (Ikbal, 1983) and a wavelength between $0.2 \text{ }\mu\text{m}$ and $50 \text{ }\mu\text{m}$, which is reduced to between $0.28 \text{ }\mu\text{m}$ and $4.0 \text{ }\mu\text{m}$ when reaching the planet's surface due to the absorption of the rest by different atmospheric components (mainly ozone, oxygen, carbon dioxide, aerosols, steam, clouds). The solar radiation that reaches the ground without being absorbed or scattered is called direct beam radiation; radiation that reaches the ground but has been dispersed before is called diffuse radiation, and the sum of both is called global radiation.

The standard solar radiation spectrum at ground level on a clear day is presented in Figure 6.1 (Hulstrom et al. 1985). The dotted line corresponds to the extraterrestrial radiation in the same wavelength interval.

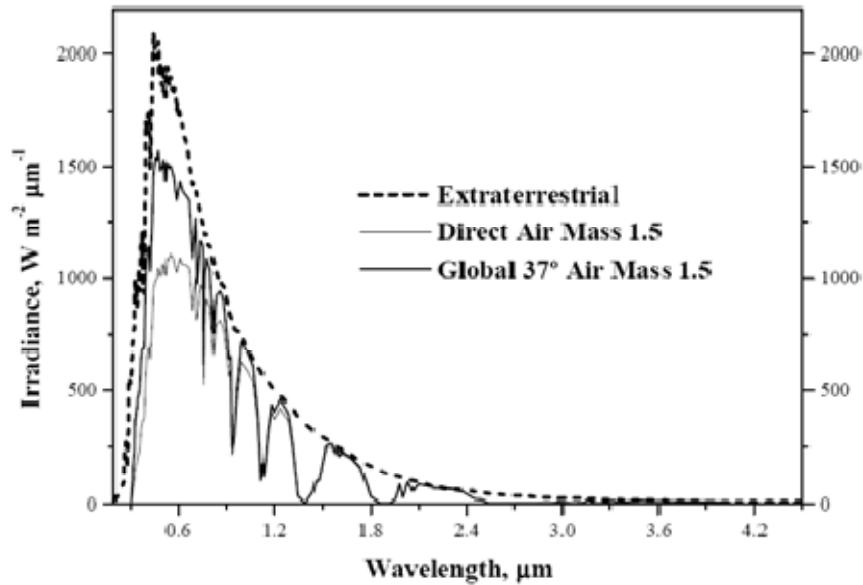


Figure 6.1 solar radiation spectra from 0.2 to 4.5 μm .

The spectral irradiance data are given at a solar zenith angle of 48.19° . This zenith angle corresponds to an AirMass (AM) of 1.5 (Figure 6.2), which is the ratio of the direct-beam solar irradiance path length through the atmosphere at a solar zenith angle of 48.19° to the path length when the sun is in a vertical position. Air mass is equal to 1 when the sun is directly overhead (zenith). As air mass increases, the direct beam traverses longer path lengths in the atmosphere, which results in higher scattering and absorption of the direct beam and a lower percentage of direct total radiation (for the same atmospheric conditions). Solar ultraviolet radiation is only a very small part, between 3.5% and 8%, of the total solar spectrum as demonstrated by measurement, although this percentage may vary for a given location and depending on the weather conditions. The percentage of global UV radiation (direct + diffuse) generally increases with respect to the total global radiation when atmospheric transmissivity decreases, mainly because of clouds, aerosols and dust. In fact, the UV average percentage with respect to total radiation on cloudy days is up to two percent points higher than values on clear days. The UV radiation values vary from one location to another, and obviously, at different hours of the day and in different seasons, making necessary to know these data for any particular location in real time.

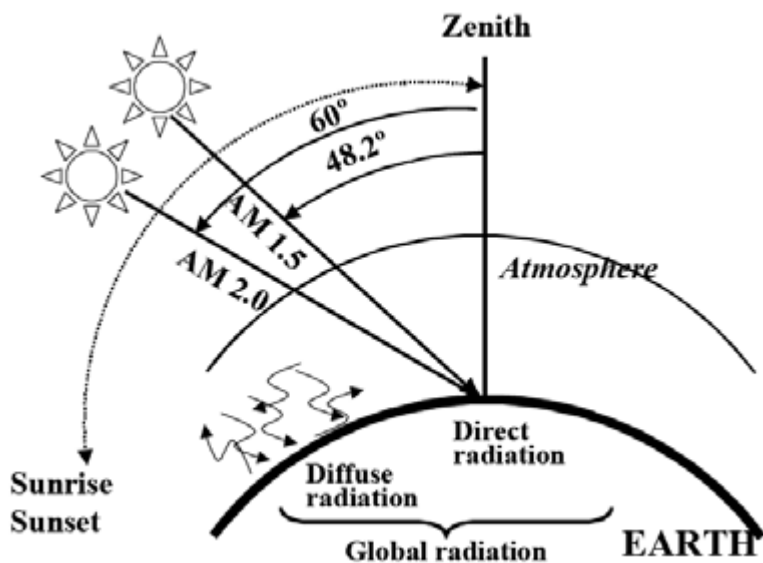


Figure 6.2 Air mass and solar components.

6.1.2 Solar collector technology

6.1.2.1 Concentrating collectors

The first solar photo-reactor designed for photochemical applications were based on line focus parabolic-trough concentrators (PTC). In this type of concentrators an absorber tube is placed in the focus of a parabolic reflector. The reflector redirects radiation parallel to the axis of the parable towards the absorber tube in the focus. Consequently, this type of concentrator has to track the sun and can use only parallel direct beam radiation. One-axis and two-axis tracking systems can be used for this purpose. Advantages of concentrating solar collectors:

- They can be easily set-up and scaled-up due to the simple engineering concepts involved (tubular plug-flow photo-reactor with turbulent flow conditions).
- Turbulent flow ensures good mass-transfer and maintains TiO_2 particles in suspension in case of TiO_2 slurry photocatalysis.
- The photo-reactors are closed systems. Therefore, no vaporization of volatile compounds takes place.

Disadvantages of concentrating solar collectors:

- Due to their geometry they can use only direct beam radiation, which makes them practically useless, when the sky is clouded.
- They also are rather expensive systems due to the necessary sun tracking system (investment and maintenance costs because of moving parts).

6.1.2.2 Non concentrating collectors

The elevated prices of PTCs have encouraged the search for cheaper reactor concepts with non-concentrating geometry. Different types of non-concentrating solar reactors such as Free-falling film, (Wyness, 1994) or Pressurized flat plate (Well, 1997) were proposed.

A major advantage is that they do not only harvest direct beam but also diffuse radiation. Consequently, they can as well be operated under cloudy sky conditions. One problem common to non-concentrating collectors is mass transfer problems caused by laminar flow in non-concentrating systems. So, although non-concentrating collectors potentially present several important advantages, their scale-up can be difficult due to reasons such as high pressure drop, inhomogeneous flow conditions etc.

6.1.2.3 Compound parabolic collectors (CPC)

CPC are an interesting cross between PTCs and non-concentrating collectors without their respective disadvantages. CPC are static collectors with a reflective surface formed by two connected parabolic mirrors with an absorber tube in the focus and have been found to provide the most efficient light-harvesting optics for low concentrating systems (Muschaweck, 2000). They have no tracking system and the design permits the solar rays to be reflected onto the absorber tube attaining a low concentration factor.

The concentration factor is defined as the ratio of the collector aperture to the absorber tube perimeter and is usually between 1 and 1.5 depending on the type of application. Thanks to the reflector design, almost all the radiation (not only direct, but also diffuse) incident at the CPC aperture area can be collected and is available for the process in the reactor. The light

reflected by the CPC is distributed around the back of the tubular photo-reactor (see Figure 6.3).

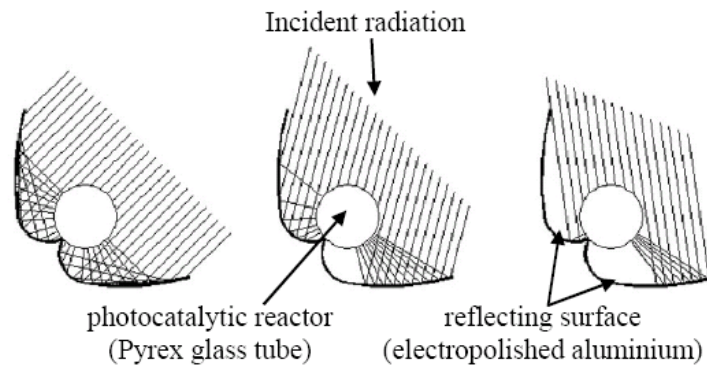


Figure 6.3. CPC: Collector design and radiation geometry profiles.

Advantages of CPC:

- Wastewater can be circulated under turbulent flow conditions. They can be easily up scaled due to the simple engineering concepts involved.
- Excellent performance of CPC collectors in solar photochemical and photocatalytic applications.

The photochemical reactor must contain the working fluid, including the catalyst or the sensitizer, and must transmit solar UV-light efficiently with minimal pressure drop across the system. It must also provide a good mass transfer from the fluid stream to an illuminated photocatalyst. Adequate flow distribution inside the reactor must be ensured. Reactor material must be inert to chemicals and resistant to high or low pH. The choice of materials that are both transparent to UV light and resistant to its destructive effects is limited to quartz glass, fluoropolymers and borosilicate glass. Low-iron-content borosilicate glass has good transmissive properties in the solar range to about 285 nm, is cheaper than the others and therefore, seems to be the most adequate (Ajona, 2000). The ideal reflective surface for solar photochemical applications must be highly UV-reflective, weather-resistant to guarantee long lifetime and reasonably priced. The currently available materials that best fit these requirements are electropolished anodised aluminium and organic plastic films with an aluminium coating (Ajona, 2000).

In this chapter, the photocatalytic performances of PVF^f-TiO₂-Fe oxide are evaluated at pilot-scale in CPC reactors, for different wastewaters. The photocatalytic degradation of phenol, nalidixic acid, a mixture of pesticide another of emerging contaminants were mediated by PVF^f-TiO₂-Fe oxide in water allowing the assessment of the new photocatalyst efficiency for real pollutants, under more realistic conditions.

6.2. Experimental

6.2.1 Chemicals

P.A. reagent phenol ($C_0 = 0.7$ mM) and nalidixic acid ($C_0 = 0.13$ mM) were supplied by Panreac and Fluka, respectively. Pesticide mixtures were prepared from commercial formulations of Vydate (10%, w/v oxamyl), Metomur, (20%, w/v methomyl), Couraze (20%, w/v imidacloprid), Ditimur-40 (40%, w/v dimethoate) and Scala (40%, w/v pyrimethanil). The mixture contained 20% of each commercial formulation and had an original TOC of 50 mg L⁻¹. The amounts of active ingredients in the mixture were 21 mg L⁻¹ of oxamyl, 5.1 mg L⁻¹ of methomyl, 5 mg L⁻¹ of imidacloprid, 8 mg L⁻¹ of dimethoate, and 13.5 mg L⁻¹ of pyrimethanil. Analytical standards (>98%) for chromatographic analysis were purchased from Sigma-Aldrich. The emerging contaminants were atenolol, metoprolol, sulfamethoxazole, flumequine, ketorolac and diclofenac, acetaminophen and progesterone p.a. reagents from Sigma-Aldrich. Antipyrine, caffeine, hydroxybiphenyl and triclosan were Fluka p.a. reagents; atrazine and isoproturon were p.a. reagents from Riedel-De-Haën. The mixture contained a 100 µg L⁻¹ concentration of each emerging contaminants. The structures of all the organic compounds used were shown in Figure 1.7-1.9 NaOH, HNO₃, FeCl₃.6H₂O were Fluka p.a. reagents (Buchs, Switzerland) and used as received. TiO₂ P25 (anastase to rutile ratio between 70:30 and 80:20) was supplied by Degussa. The polyvinyl fluoride (PVF) films were 72µm thick and were supplied by Goodfellow (Cambridge Ltd. United Kingdom). Distilled water used in the pilot plant was supplied by the plataforma solar de Almería (PSA) distillation plant (conductivity<10 microScm⁻¹, Cl⁻ = 0.2-0.3 mg/L, NO₃⁻<0.2 mg/L, organic carbon <0.5 mg/L). The experiments were performed using reagent-grade hydrogen peroxide (30% w/v).

6.2.2 Photocatalyst preparation

The detailed preparation procedure has been described in chapter 4. In this study, optimized material was prepared: a 3-hour TiO₂ PSFD treatment was applied to PVF film using aqueous TiO₂ P25 suspensions (1 g/L) at natural pH (≈ 5) and under simulated sunlight irradiation. For the deposition of an iron oxide coat, PVF^f-TiO₂ was immersed in an aqueous solution of FeCl₃ (5 g/L) and heated at 80°C while stirring for one hour. The resulting materials were dried in an oven at 120 °C for one hour.

6.2.3 Photo-reactor and irradiation procedure

The solar degradation experiments were performed under natural sunlight in a pilot plant installed at the Plataforma Solar de Almeria in Spain, consisting of compound parabolic collectors (CPC), a reservoir tank, a recirculation pump and connecting tubing. The configuration of this pilot plant was adapted for these experiments to insert the PVF^f-TiO₂-Fe oxide photocatalyst in the CPC glass tubes. Solar ultraviolet radiation (UV) was measured by a global UV radiometer (KIPP&ZONEN, model CUV 3) mounted on a platform 37°-tilted (the same as the CPC). With Eq. (6.1), combination of the data from several days' experiments and their comparison with other photocatalytic experiments is possible (Malato, 2003).

$$t_{30w,n} = t_{30w,n-1} + \Delta t_n \frac{UV}{30} \frac{V_i}{V_T}; \Delta t_n = t_n - t_{n-1} \quad (6.1)$$

where t_n is the experimental time for each sample, UV is the average solar ultraviolet radiation measured during Δt_n , and t_{30w} is a “normalized illumination time”. In this case, time refers to a constant solar UV power of 30 W m⁻² (typical solar UV power on a perfectly sunny day around noon). V_T is the total volume of the water loaded in the pilot plant (8.5 L), V_i is the total irradiated volume (1.8 L). The flow rate was 4.5 L/min. The operation temperature of the pilot plant was around 35 (+/- 5) °C.

Several PVF^f-TiO₂-Fe oxide films (26 x 12 cm) were inserted concentrically inside two CPC tubes (1.8 L) in the pilot plant and were used for all the following experiments (Figure 6.4). Before experiments started, the CPC reactor was covered to prevent any

photochemical reaction, and filled with distilled water. The chemicals were added directly into the pilot-plant and homogenized by recirculation for 15 min. Then hydrogen peroxide was added and homogenized for 15 min, the collectors were uncovered and the photocatalytic reaction began. Samples were taken every 15 minutes for the first hour after uncovering the reactor, then every 30 minutes for the rest of the experiment.



Figure 6.4 Picture of PVF^f-TiO₂-Fe oxide films in the CPC photo-reactor

6.2.4 Analysis of the irradiated solutions

High-performance liquid chromatography HPLC (Agilent Technologies, series 1100) was used to monitor the compounds using a reverse-phase C-18 analytical column (LUNA 5 mm, 3 mm x 150 mm from Phenomenex) with a UV-DAD detector. The UV signal was recorded at a different wavelength for each compound depending on its maximum light absorption wavelength. The mobile phases H₂O/methanol (60/40), methanol/formic acid 0.25 mM (50:50), acetonitrile/H₂O (15/85), acetonitrile/formic acid 0.25 mM (1:10) to 100% acetonitrile (in 40 min), were used for phenol, nalidixic acid, pesticide mixture, and, emerging contaminant mixture, respectively. Mineralization was followed by measuring the dissolved organic carbon (DOC) by direct injection of filtered samples (PTFE 0.22 μm, Millipore Millex1 GN) into a Shimadzu 5050A TOC analyzer with an NDIR detector and calibrated with standard solutions of potassium phthalate. Spectrophotometry for the determination of iron and hydrogen peroxide was performed with a UNICAM 2 spectrophotometer. Total iron was determined with 1,10-phenanthroline, at 510 nm,

following ISO 6332, hydrogen peroxide was analyzed using ammonium metavanadate, at 450 nm. The peroxide concentrations are calculated from absorption measurements by a ratio found by Nogueira et al. (Nogueira, 2005).

6.2.5. Photocatalyst characterization

The characteristics of the XPS apparatus are specified in point 4.2.6.

6.3. Results and discussion

Experiments were performed on consecutive days separated by a dark period of 17 hours. The illumination time (t_{30W}) included in the discussion was calculated by Eq. 6.1, which takes this into consideration. The same PVF^f-TiO₂-Fe oxide photocatalyst films were used for all the consecutive experiments included in this chapter.

6.3.1 Photocatalytic degradation of single compounds

Figure 6.5(i) shows phenol concentration, DOC and pH over t_{30W} [min] during the first degradation experiments mediated by PVF^f-TiO₂-Fe oxide/H₂O₂/light. Only one of two replications is shown, as there was no significant difference between the two consecutive runs. Figure 6.5(i) shows that the phenol concentration remained almost constant during the first 30 min of treatment and then decreased rapidly until the end of the treatment (60 min). During phenol degradation, pH fell from 6.5-5 from 0 to 25 min to 5-4 after 25 min due to the formation of carboxylic acids. Iron leaching from the catalyst to the solution took place likely by iron oxide photo-reductive dissolution (Borer, 2009). Dissolved iron concentration was always below 0.2 mg/L, suggesting that phenol degradation is mainly induced by a heterogeneous reaction at the catalyst surface although a significant participation of dissolved iron ions in a homogeneous photo-Fenton reaction cannot be totally excluded (dissolved iron concentration is not reported in any of the following experiments, because the quantities of iron ions detected were always below the method detection limit (< 0.2 mg/L)).

The observed enhancement of phenol degradation rate after 25 min treatment can be attributed to (i) the formation of degradation intermediates such as hydroquinone which exhibit significant catalytic action in photo-Fenton reaction (Eq. 1.38-1.42, Chen, 2002) and (ii) the pH value drops below 5 which may simultaneously increase iron oxide reductive dissolution (Huang, 2009) and the catalytic action of iron ions (adsorbed at the interface solid-liquid or dissolved in solution) in photo-Fenton reaction.

Phenol degradation was repeated after 7 runs using PVF^f-TiO₂-Fe oxide (called “old” photocatalyst, see also Section 6.3.3) to test long-term stability of the catalyst. The results are shown in Figure 6.4 (ii). Mineralization was almost complete (>90%) after 135 min of irradiation and during the 17-hour night phase a significant amount of DOC (20%) was removed by dark Fenton reaction. With the old photocatalyst, degradation was slow at the beginning (35%) until $t_{30w} = 60$ min, then the rate increased and total abatement was observed after 120 min. This sharp enhancement of degradation rates occurred when pH fell below 5. A significant difference in initial phenol degradation rate between new (0.10 mg/(L min)) and old (0.27 mg/(L min)) PVF^f-TiO₂-Fe oxide was observed when pHs > 5. This difference can be attributed to changes occurring on the PVF^f-TiO₂-Fe oxide surface during use, that is, TiO₂ was uncovered, allowing the photocatalyst to be efficient even at high pH. In contrast, in the freshly prepared photocatalyst, only iron oxide is present on the surface (Table 6.2) explaining the low degradation rates observed close to pH 7. When the operating pH is below 5, smaller differences in degradation rate between new (1.0 mg/(L min)) and old (1.5 mg/(L min)) PVF^f-TiO₂-Fe oxide were observed suggesting that under acidic conditions, photo-Fenton oxidation plays a stronger role in degradation.

The degradation of nalidixic acid mediated by PVF^f-TiO₂-Fe oxide/H₂O₂/light is shown in Figure 6.5(ii). The pH was kept above 7 by appropriate addition of NaOH because the degradation was efficient in neutral solutions. Nalidixic acid, completely degraded rapidly, had a half-life of only 3 minutes under these conditions. This result demonstrates that PVF^f-TiO₂-Fe oxide is highly active for nalidixic acid, even at neutral operating pH. Mineralization was about 35% after 100 min which suggests that a biological coupling could be performed (Sarria, 2001).

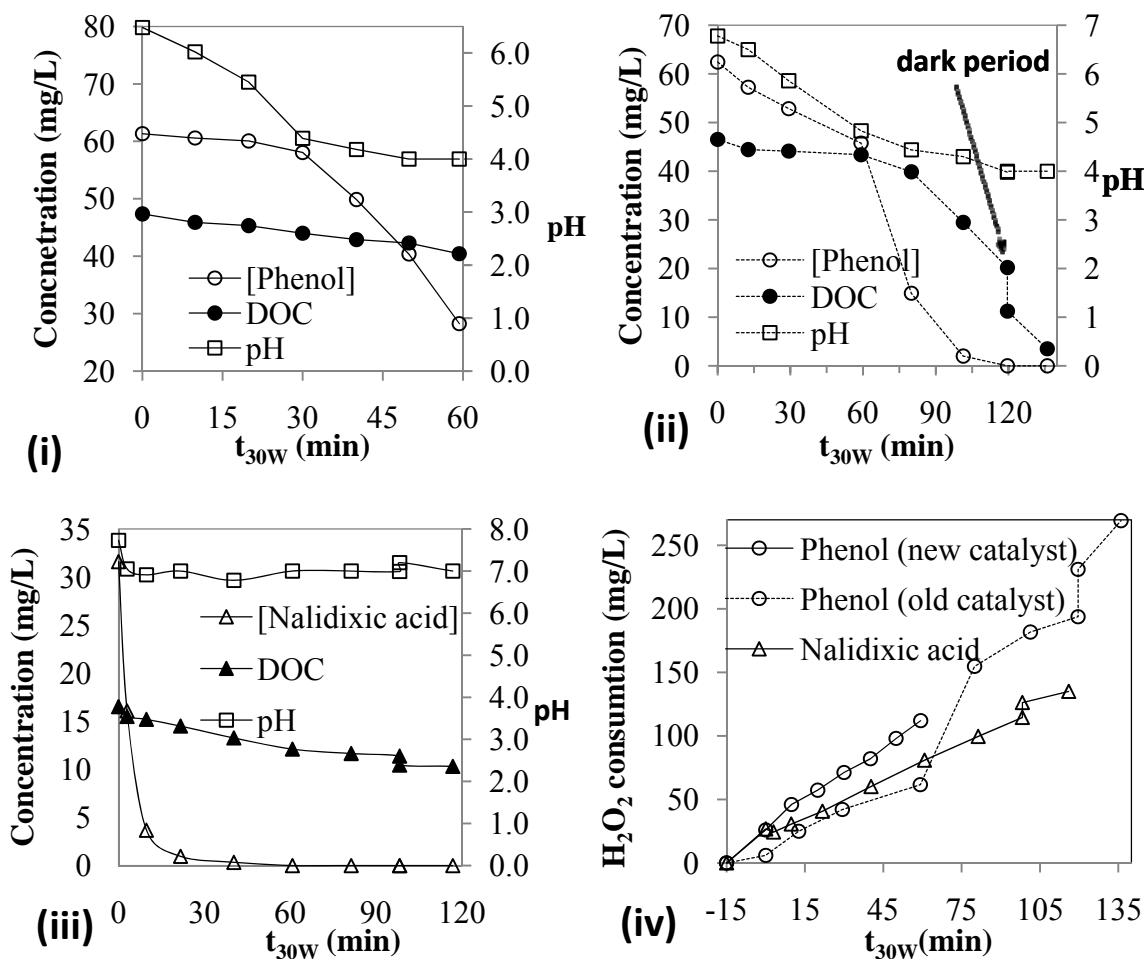


Figure 6.5 DOC and pH during phenol degradation (0.7 mM phenol, 6.2 mM H₂O₂) (i) first and (ii) second set of experiments, (iii) DOC and pH during nalidixic acid degradation (0.13 mM nalidixic acid 3.1 mM H₂O₂), and (iv) evolution of H₂O₂ consumption. The degradations were mediated by PVF^f-TiO₂-Fe oxide under solar light.

The differences of reactivity between nalidixic acid and phenol can be assigned to the fact that these two molecules have different abilities to bind with photocatalyst. Nalidixic acid (see Figure 1.7) has a chelating ability and a carboxylate group susceptible to bind with TiO₂, iron oxide surface or iron ions. In contrast phenol has only an alcohol function and is not charged. A recent article (Xue, 2009) claims that organic compound degradation mediated by Fenton heterogeneous oxidation is significantly improved by using chelating agents at neutral pH.

Figure 6.5(iv) shows the evolution of hydrogen peroxide consumption during single compounds degradation. For phenol degradation the initial hydrogen peroxide concentration used was 6.2 mM. Initial H₂O₂ consumption rates (first 30 min) were higher for the new catalyst than for the old one although the degradation rates were higher for the old catalyst. This result suggests that, initially, in contrast with new catalyst, phenol degradation mediated by the old catalyst, involves mechanisms efficient without H₂O₂, such as TiO₂ photocatalysis and synergistic effects. Between 60 and 80 min of treatment, the H₂O₂ consumption rate relative to old catalyst increased significantly but then decreased due to the shortage of H₂O₂. Thus at the end of the first day, H₂O₂ was added until a concentration of 2 mM and during the night phase a significant amount of H₂O₂ was consumed (40 mg) by Fenton process. For nalidixic acid degradation, the initial H₂O₂ concentration used was 3.1 mM and hydrogen peroxide was added when the concentration was too low (60% of consumption).

6.3.2 Photocatalytic degradation of compound mixtures

6.3.2.1 Pesticide mixture

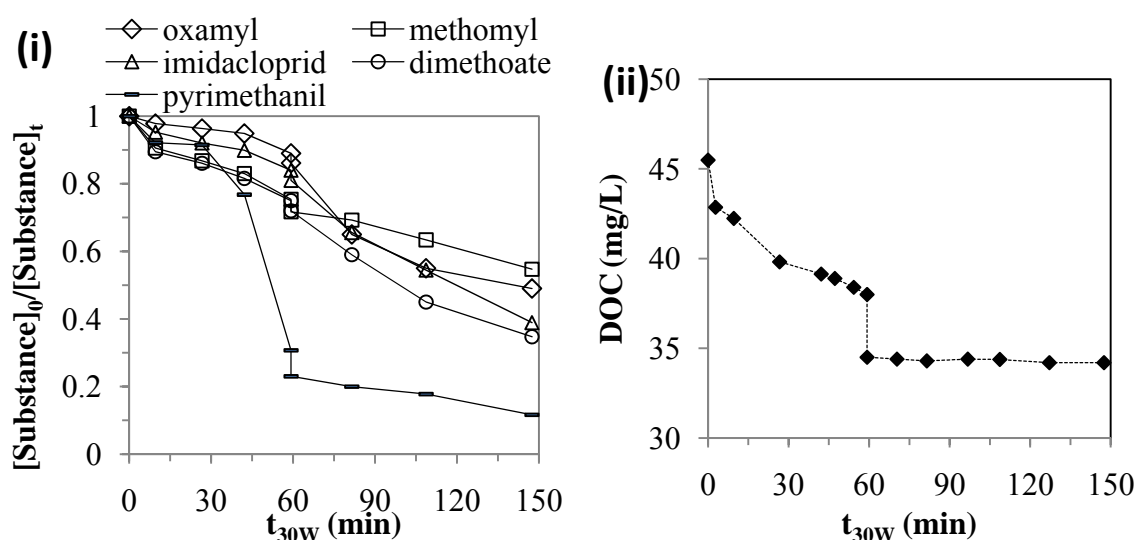


Figure 6.6 Normalized pesticide concentrations (i), DOC (ii) during degradation mediated by PVF^f-TiO₂-Fe oxide in presence of 3.1 mM H₂O₂ (constant) under sunlight (DOC₀ = 50 mg/L).

Figure 6.6(i) shows oxamyl, methomyl, imidacloprid, dimethoate and pyrimethanyl concentrations over t_{30w} during the degradation experiment mediated by PVF^f-TiO₂-Fe oxide/H₂O₂/light.

For all compounds (except pyrimethanyl), initial degradation rates were low and at the end of the treatment (150 min), only about 50% of the substances were degraded. Degradation of compounds during the 17-hour dark phase was negligible. This slow degradation of the pesticides could be due to the use of commercial pesticide formulations, in which some coadjuvants might compete with the pesticides in the degradation processes. Pyrimethanyl appeared to be rapidly degraded between 30 and 60 min treatment. However, this fast depletion could be due to an adsorption of the substance to the discovered PVF surface until saturation after 60 min. Pyrimethanyl is the less water soluble of the tested pesticides (0.1 g/L, 25 °C) and could have high affinity with PVF film.

Figure 6.6(ii) shows that 30% of the total DOC was removed during the treatment. Most of the DOC decayed the first day under illumination (20%) and during the dark phase (10%). Afterwards, mineralization stopped, possibly because of the formation of resistant intermediates complexing Fe with carboxylic acids produced during degradation and adsorption of part of the organics on the PVF^f-TiO₂-Fe oxide, or because the coadjuvants easily mineralized had been completely removed.

Table 6.1 Initial degradation rates with PVF^f-TiO₂-Fe oxide /H₂O₂/light and zero order rate with Fe³⁺/H₂O₂/light (in µg/(L.min)) for each compound in the pesticide mixture.

Compound	R ₀ ^a	k (Fe ³⁺ 5 mg/L) ^b	k/R ₀
Oxamyl	27	290	11
Methomyl	21	100	5
Imidacloprid	15	100	7
Dimethoate	28	240	9
Pyrimethanyl	73	390	5

^a Calculated from Figure 4 (i) (first 60 min).

^b Reproduced from Zapata et al. (Zapata, 2009).

Table 6.1 shows the initial degradation rates (R_0) relative to each pesticide for the process mediated by PVF^f-TiO₂-Fe oxide/H₂O₂/light and the constants for homogeneous photo-Fenton oxidation (5 mg/L Fe³⁺/H₂O₂/light) reported by Zapata et al. (Zapata, 2009). This comparison shows that homogeneous rates were between 5 to 10 times higher than heterogeneous rates. However, in the homogeneous process, pH was close to 3.

6.3.2.2 Emerging contaminants mixture

The 14-compound mixture used in this study is a reconstruction of pollution typical of a municipal wastewater treatment plant effluent. In such wastewater, there is a large number of low-concentration (<0.1 mg/L) pollutants (Martínez Bueno et al 2007). Concentration of each substance in the two consecutive experiments is shown over t_{30W} in Figure 6.7. Eight of the fourteen compounds (atenolol, acetaminophen, metropolol, flumequine, hydroxybiphenyl, diclofenac, progesterone and triclosan) were efficiently degraded by PVF^f-TiO₂-Fe oxide/H₂O₂/light after 150 min and after 100 min of treatment in two consecutive experiments (Figure 6.7 a₁ b₁ and a₂ b₂, respectively). The other six compounds, caffeine, antipyrine, sulfamethoxazole, ketorolac, atrazine and isoproturon were more resistant, with around 40-70% (Figure 6.7 c₁) and 50-80% (Figure 6.7 c₂) degradation after 180 min for the first and second consecutive runs, respectively. Caffeine and antipyrine were degraded the least (50%) under illumination and only caffeine and isoproturon showed significant degradation ($\approx 10\%$ decay) during dark Fenton.

In the two successive experiments, substances showed a rather similar trend, although degradation rates were 1 to 5 times higher in the second experiment. In Figure 6.7, degradation rates are dependent on the nature of the substance, from 0.2 to 2 $\mu\text{g}/(\text{L min})$ for antipyrine (minimum) and for flumequine (maximum), respectively. Thus PVF^f-TiO₂-Fe oxide/H₂O₂/light degraded pollutants selectively, which was not the case for homogeneous photo-Fenton degradation of the emerging contaminant mixture (Klamerth, 2009). The differences observed in degradation rates between the emergent compounds can be assigned to several possible mechanisms: (i) the electrostatic attraction or repulsion between photocatalyst surface and substance (ii) the intrinsic reactivity of the substance

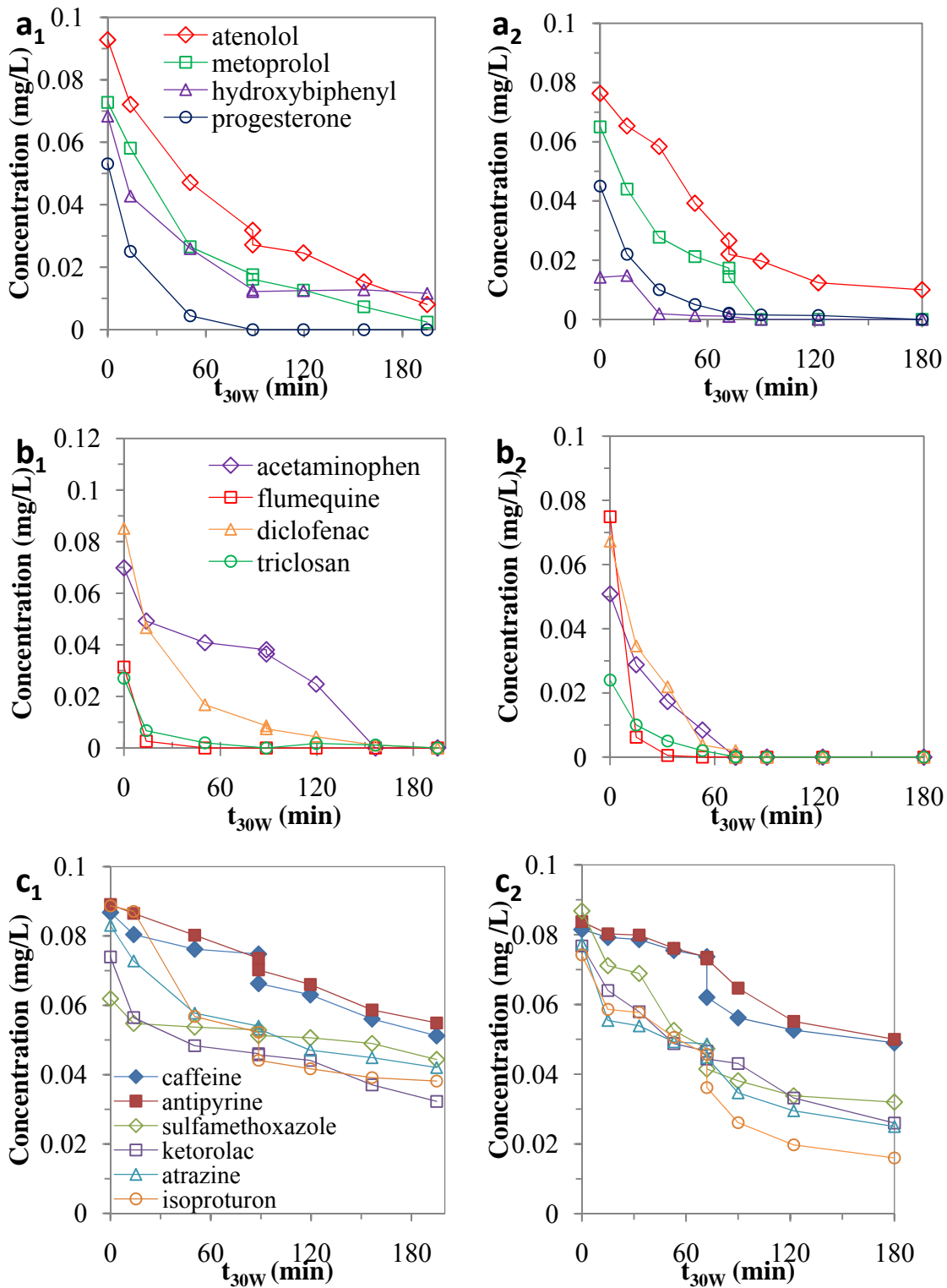


Figure 6.7 Emerging contaminant concentrations during first (a_1 - c_1) and second (a_2 - c_2) consecutive degradation tests mediated by PVF^f-TiO₂-Fe oxide under solar light and in presence of 3.1 mM (constant) H₂O₂.

(presence of weak bonds or electron donor groups, possibility to form complex with iron surface species). Figure 1.9 shows the chemical structure of the different compounds: some of the more recalcitrant compounds, namely, caffeine (pKa 10), ketorolac (pKa 10.3), contain tertiary amine which are protonated and thus positively charged under the pH of experiments (<7). The presence of this positive charge and/or the absence of negative or complexing group (such as carboxylic acid or chelating agent), possibly induced repulsion or weak attraction between the substance and the catalyst surface leading to a slow degradation. In contrast, atenolol, metoprolol (although positively charged under experimental condition, pKa 9.6, 9.7, respectively) and triclosan contain a chelating group, flumequin and diclofenac contain a carboxylic acid function and are halogenated (weak bonds). Thus the results suggest that reactivity is controlled by the presence of Fe(III) complexant moieties (carboxylic acid, chelate) rather by the electrostatic attraction/repulsion mechanism. In contrast, in the case of homogeneous photo-Fenton structure reactivity relationships (Chapter 2), the substances able to form complexes with iron were not removed faster which highlights the intrinsic differences between homogeneous and heterogeneous systems. However, a systematic study under more controlled conditions is required to draw a definitive conclusion on the structure reactivity relationship for heterogeneous photo-Fenton systems.

6.3.3 Long-term stability and photocatalyst activation

PVF^f-TiO₂-Fe oxide films were active in the photo-assisted degradation of pollutants in solution for 20 days under exposure to sunlight without any observable loss of efficiency. As described in section 6.3.1 for phenol degradation, the rates were even higher after having used PVF^f-TiO₂-Fe oxide for 7 runs. A similar trend was observed in compound mixtures with higher rates in the second consecutive run (Figure 6.7 a₂ b₂ c₂) than in the first (Figure 6.7 a₁ b₁ c₁) which confirm the finding of chapter 5 where a similar trend during repetitive nalidixic acid degradation runs was observed. Although a slight increase in photocatalyst activity was observed, the appearance of the PVF-TiO₂-Fe oxide film changed considerably

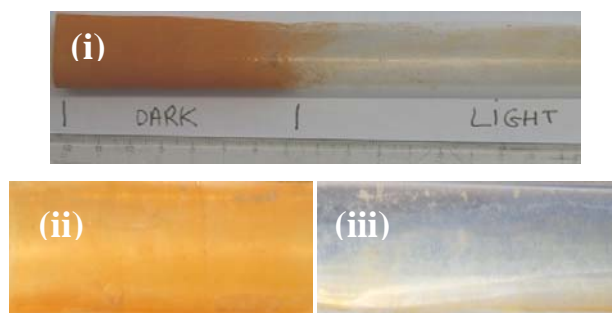


Figure 6.8 Appearance of PVF^f-TiO₂-Fe oxide after 20 days of experiments: (i) effect of light on changes in appearance; (ii) almost undamaged piece; (iii) severely damaged piece.

As shown in Figure 6.8(i), light played a key role in these changes which suggests that the leaching is not due to the detachment of labile iron oxide particles by fluid frictions. Credibly, iron oxide photo-reductive dissolution (Borer, 2009) is one of the main reasons for iron leaching. Figure 6.8(ii)-(iii) show the considerable differences in what two films prepared following the same procedure look like after 20 days of experiments.

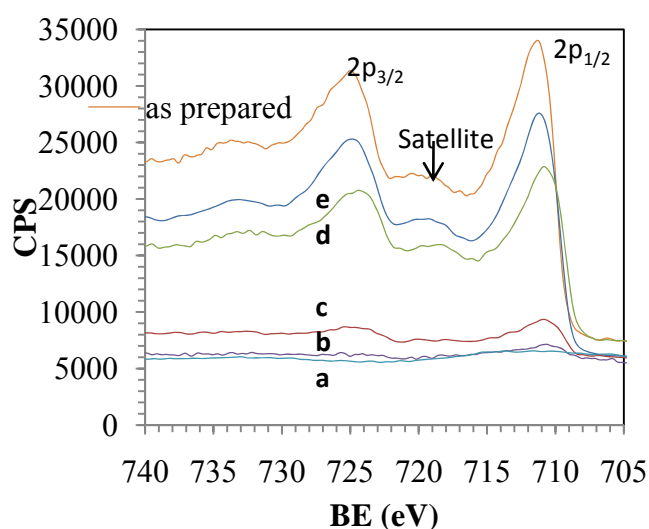


Figure 6.9 Fe (2p) core level photoelectron spectrum of as-prepared catalyst (PVF^f-TiO₂-Fe oxide), and pieces of catalysts (a-e) after 20 days of experiments.

These changes were characterized by XPS for the as prepared PVF^f-TiO₂-Fe oxide and a set of samples (a)-(e) (which performed the same degradation experiments for 20 days) as given in Figure 6.9 and Table 6.2. Figure 6.9 shows the Fe (2p) core level photoelectron

spectrum: for the samples (a)-(b), the signals shows a low intensity due to the important leaching of iron. The Fe (2p) spectra of as prepared material, of samples (e) and (d) are pretty similar and unambiguously characteristic of Fe³⁺ in an oxide (Fe 2p_{1/2}, Fe 2p_{3/2} and satellite peaks are at a binding energy of 725, 711 and 719 eV, respectively; the satellite peak is a distinct peak, Yamashita, 2008) which suggests that no significant change in the iron oxidation state occurred after 20 days of experiments.

Table 6.2 Composition of original polymer surface (PVF), as-prepared catalyst (PVF^f-TiO₂-Fe oxide), and pieces of catalysts (a-e) after 20 days of experiments.

Sample	C	F	O	Fe	Ti	Fe/Ti
PVF	66.0	30.3	3.7	0	0	-
a	67.5	27.6	4.0	0.9	0	-
b	63.9	27.2	7.3	1.3	0.4	3.3
c	63.9	15.1	17.3	2.7	1.0	2.7
d	34.2	13.2	35.5	15.1	2.2	6.9
e	17.1	1.4	54.6	26.7	0.3	89
PVF ^f -TiO ₂ -Fe oxide	22.7	1.5	46	23.8	0	-

Table 6.2 shows the surface composition of each piece of PVF^f-TiO₂-Fe oxide was modified to a different extent from absence of photoactive species (a) to almost unmodified material (e). The results in Table 6.2 show that the atomic percentage of the Ti surface increased from 0 for the as prepared material to a maximum of 2.2% for sample d. Moreover, the Fe/Ti surface ratio of 3 to 7 for pieces b-d suggests that TiO₂ makes a significant contribution to the process.

As shown in chapter 5 and Figures 6.5 and 6.7, PVF^f-TiO₂-Fe oxide/H₂O₂/light degradation rates are slightly enhanced by use, as the TiO₂ particles are uncovered (see Figure 6.10). Pure TiO₂ thin film (PVF^f-TiO₂) was about one order of magnitude less photoactive for organics degradation than PVF^f-TiO₂-Fe oxide in presence of H₂O₂ (Table 4.2). Besides, as iron oxide oxidation state remains constant, the observed enhancement seems to be due to

the uncovering of TiO₂, increasing the synergy between iron and titanium oxide (Figure 4.10). In this study it appeared, in average over all the photocatalyst pieces, that the loss of activity due to the leaching of photoactive species was compensated by the beneficial effects induced by increased synergy due to surface chemical composition changes.

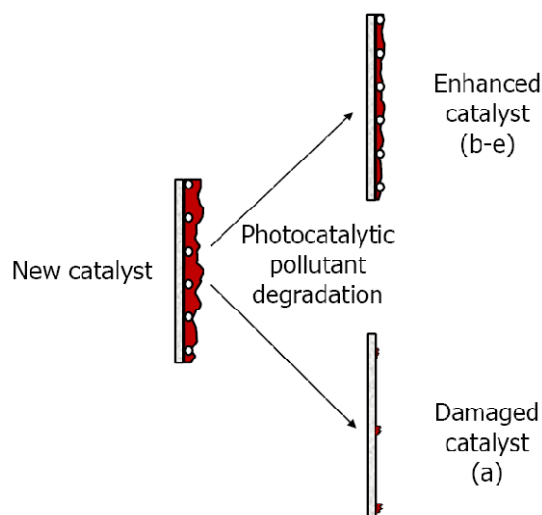


Figure 6.10 Schematic changes occurring on PVF^f-TiO₂ Fe oxide surface after use (not to scale).

6.4. Conclusions

This work demonstrated that PVF^f-TiO₂-Fe oxide can be adapted to a pilot-scale solar photo-reactor resulting in high performance even with controlled neutral pH for nalidixic acid. However, pesticides were more resistant, with 50% degradation in 1.5 hours. In contrast with homogeneous photo-Fenton, emerging pollutant degradation mediated by PVF^f-TiO₂-Fe oxide/H₂O₂/light was found to be selective. Degradation rates were higher for the compounds containing moieties (carboxylic acid, chelating group) able to form complexes with Fe(III). Although significant changes in the appearance and surface composition of PVF^f-TiO₂-Fe oxide took place during degradation experiments, the photocatalyst activity was conserved toward repetitive pollutant degradations and even slightly increased during the 20 days of operation. This enhancement confirms that the uncovering of TiO₂ increased its exposure to light and consequently its synergistic contribution to the overall photocatalytic degradation process.

6.5 References

- Ajona J.I. and Vidal A. (2000) The use of CPC collectors for detoxification of contaminated water: design, construction and preliminary results. *Solar Energy* 68: 109-120.
- Borer P., Sulzberger B., Hug S.J., Kraemer S.M., Kretzschmar R. (2009) Photoreductive dissolution of iron(III) (Hydr)oxides in the absence and presence of organic ligands: Experimental studies and kinetic modeling. *Environmental Science and Technology* 43: 1864-1870.
- Chen F., He J., Zhao J., Yu J.C. (2002) Photo-Fenton degradation of malachite green catalyzed by aromatic compounds under visible light irradiation. *New Journal of Chemistry* 26: 336-341.
- Dalrymple O.K., Yeh D.H., Trotz M.A. (2007) Removing pharmaceuticals and endocrine-disrupting compounds from wastewater by photocatalysis. *Journal of Chemical Technology and Biotechnology* 82: 121-134.
- Feng J., Hu X., Yue P. L., Qiao S. (2009) Photo Fenton degradation of high concentration Orange II (2mM) using catalysis containing Fe: A comparative study. *Separation and Purification Technology* 67: 213–217.
- Gumy D., Fernandez-Ibanez P., Malato S., Pulgarin C., Enea O., Kiwi J. (2005) Supported Fe/C and Fe/Nafion/C catalysts for the photo-Fenton degradation of Orange II under solar irradiation. *Catalysis Today*, 101: 375-382.
- Hosseini S.N., Borghei S.M., Vossoughi M., Taghavinia N. (2007) Immobilization of TiO₂ on perlite granules for photocatalytic degradation of phenol. *Applied Catalysis B: Environmental* 74: 53–62.
- Huang, C.-P., Chen, C.-R., Huang, Y.-F., Lu, Y.-W., Huang, Y.-H. (2009) Reductive dissolution and oxidative catalysis of an immobilized iron oxide in the presence of catechol and phenol. *Journal of Molecular Catalysis A: Chemical* 304: 121-127.
- Iqbal M. (1983). An Introduction to Solar Radiation. Academic Press, Oxford.
- Klamerth N., Miranda N., Malato S., Agüera A., Fernández-Alba A. R., Maldonado M.I and Coronado J. M. (2009) Degradation of emerging contaminants at low concentration in MWTPs effluents with mild solar photo-Fenton and TiO₂. *Catalysis Today* 144: 124–130.
- Klavarioti M., Mantzavinos D., Kassinos D. (2009) Removal of residual pharmaceuticals from aqueous systems by advanced oxidation processes. *Environment International* 35: 402-417.
- Malato S., Blanco J., Vidal A., Alarcón D., Maldonado M. I., Cáceres J., Gernjak W. (2003) Applied studies in solar photocatalytic detoxification: an overview. *Solar Energy* 75:329.
- Malato S. (2008) Removal of emerging contaminants in waste-water treatment: Removal by photo-catalytic processes. *Handbook of Environmental Chemistry, Volume 5: Water Pollution* 5 S2: 177-197.
- Martínez Bueno M. J., Agüera A., Gómez M. J., Hernando M. D., García-Reyes J. F., Fernández-Alba A.R. (2007) Application of liquid chromatography/quadrupole-linear ion trap mass spectrometry and time-of-flight mass spectrometry to the determination of pharmaceuticals and related contaminants in wastewater. *Analytical Chemistry* 79: 9372-9384.

- Méndez-Arriaga F., Maldonado M. I., Gimenez J., Esplugas S., Malato S. (2009) Abatement of ibuprofen by solar photocatalysis process: Enhancement and scale up. *Catalysis Today* 144: 112–116.
- Murakami N., Chiyoya T., Tsubota T., Ohno T. (2008) Switching redox site of photocatalytic reaction on titanium(IV) oxide particles modified with transition-metal ion controlled by irradiation wavelength. *Applied Catalysis A, Chemical* 348: 148–152.
- Muschaweck J., Spirkl W., Timinger A., Benz N., Dörfler M., Gut M. and Kose E. (2000) Optimized reflectors for non-tracking solar collectors with tubular absorbers. *Solar Energy* 68: 151-159.
- Muthuvel I., Swaminathan M. (2008) Highly solar active Fe(III) immobilized alumina for the degradation of Acid Violet 7. *Solar Energy Materials and Solar Cells* 92 (8), 857–863.
- Nogueira R. F. P., Oliviera M. C., Paterlini W. C. (2005) Simple and fast spectrophotometric determination of H₂O₂ in photo-Fenton reactions using metavanadate. *Talanta* 66: 86.
- Parra S., Stanca S. E., Guasaquillo I., Thampi K. R. (2004) Photocatalytic degradation of atrazine suspended and supported TiO₂. *Applied Catalysis B, Environmental* 51: 107–116.
- Pulgarin C., Peringer P., Albers P., Kiwi J. (1995) Effect of Fe ZSM-5 zeolite on the photochemical and biochemical degradation of 4-chlorophenol. *Journal of Molecular Catalysis A, Chemical* 95: 61-74.
- Sarria, V., Parra, S., Invernizzi, M., Péringer, P., Pulgarin, C. (2001) Photochemical-biological treatment of a real industrial biorecalcitrant wastewater containing 5-amino-6-methyl-2-benzimidazolone. *Water Science and Technology* 44: 93-101.
- Schwarzenbach R. P., Escher B. I., Fenner K., Hofstetter T. B., Johnson C. A., Von Gunten U., Wehrli B. (2006) The challenge of micropollutants in aquatic systems. *Science* 313 (5790), 1072-1077.
- Tryba B. (2008) Immobilization of TiO₂ and Fe-C-TiO₂ photocatalysis on the cotton material for application in a flow photocatalytic reactor for decomposition of phenol in water. *Journal of Hazardous Material* 151 (2-3), 623–627.
- Well M., Dillert R.H.G., Bahnemann D.W., Benz V.W. and Mueller, M.A. (1997) A novel nonconcentrating reactor for solar water detoxification. *Journal of Solar Energy Engineering, Transactions of ASME* 119: 114-119.
- Wyness P., Klausner J.F. and Goswami D.Y. (1994). Performance of Nonconcentrating Solar Photocatalytic Oxidation Reactors, Part I: Flat-Plate Configuration. *Journal of Solar Energy Engineering, Transactions of ASME* 116: 2-7.
- Xue X., Hanna K., Despas C., Wu F., Deng N. (2009) Effect of chelating agent on the oxidation rate of PCP in the magnetite/H₂O₂ system at neutral pH. *Journal of Molecular Catalysis A, Chemical* 311: 29–35.
- Yamashita T., Hayes P. (2008) Analysis of XPS spectra of Fe²⁺ and Fe³⁺ ions in oxide materials. *Applied Surface Science* 254: 2441–2449
- Zapata A., Velegraki T., Sanchez-Perez J. A., Mantzavinos D., Maldonado M. I., Malato S., (2009) Solar photo-Fenton treatment of pesticides in water: Effect of iron concentration on degradation and assessment of ecotoxicity and biodegradability. *Applied Catalysis B, Environmental* 88: 448-454

7 GENERAL CONCLUSIONS AND PERSPECTIVES

The strategy consisting in the deposition of iron oxide on modified polymer films surface to prepare supported photo-Fenton catalyst, for solar water decontamination, was presented as a good alternative to minimise iron dissolution (and consequent sludge formation) and to extend the operational pH range of the photo-Fenton process. However, the efficiency of the new process depends on the particular type of wastewater and experimental conditions. Hence the eventual benefit induced by the proposed supported catalyst, if compared with homogeneous photo-Fenton or other processes, has to be determined for each particular case. The development of this new photocatalyst involved an optimisation of preparation procedure by the evaluation of the materials photocatalytic activity using model contaminants; the surface characterization of most efficient materials (by XPS, SEM etc.), the study of the influence of reaction conditions (pH, salt content etc.) on degradation rates and the field scale application of the most efficient materials (for real contaminants degradation) under direct sunlight using parabolic collectors. More fundamental aspects such as the study of the influence of organic contaminants structure on reactivity for homogeneous (and supported) photo-Fenton reaction and the proposition of mechanisms that could be involved in material preparation and contaminants degradation were also investigated.

The relationship between various physico-chemical parameters and photo-reactivity in homogeneous photo-Fenton system was investigated. *Para*-substituted phenol reactivity was found to be a function of the electronic effects induced by the substituents. The homogenous Fenton and photo-Fenton degradation was faster when the electronic density of the aromatic ring is high, favoring electrophilic radical attack on the ring. The degradation rates were higher when half wave potential (relative to Eq. 2.2) is low. These results suggest different reactions occurring at different positions on the molecule on the

aromatic ring, alcohol function, or on the substituent. Generally, the electronic descriptors fitted well with the kinetic parameters, particularly with the Fenton rates but also with the photo-Fenton degradation rates. However, the photo-Fenton rates can be non-linearly correlated with electronic descriptors especially when the reaction occurs rapidly at the substituents (e.g. for 4-chlorophenol) which is possibly due to the presence of a weak bond. Homogeneous photo-Fenton process exhibits generally low selectivity in the degradation and mineralization of most of organic compounds and the experimental conditions were adapted to observe the slight differences between *para*-substituted phenols. In contrast, in the case of contaminant degradation mediated by supported photo-Fenton reaction (chapter 6), the reactivity was found to be significantly dependant of substance structure with higher rates for the compounds containing functional groups (such as carboxylic acids or chelate groups) allowing the formation of iron complexes and/or adsorption on catalyst surface.

A new way to prepare supported photo-Fenton catalyst on commercial PVF films by a sequential procedure consisting in functionalizing polymer films (by plasma, vacuum-UV or photocatalytic treatments) and performing a subsequent iron oxide coating by forced hydrolysis of FeCl_3 was proposed. It was found that iron oxide-coated functionalized polymer films are suitable materials to degrade and mineralize hydroquinone under simulated solar irradiation in presence of hydrogen peroxide. The UV visible absorption measurements have shown that implementing an initial functionalization of the polymer surface can be an efficient strategy to improve the attraction between iron oxide and polymer film supports. As a result, a higher amount of iron oxide was immobilized on catalyst surface leading to more efficient photocatalysts. Besides TiO_2 photocatalysis, when performed as polymer surface functionalization technique, was found to lead to the deposition of additional active specie (TiO_2 particles). Among the functionalization methods evaluated, only radio frequency plasma and more markedly TiO_2 photocatalytic treatments were useful to improve material photocatalytic activity and long-term stability. Furthermore the latter functionalization method is sustainable as it uses solar light, water as solvent, low temperatures and ambient pressure.

The effect of TiO_2 photocatalytic surface functionalization and deposition treatment (PSFD) on PVF surface chemical composition and morphology was studied in more detail. XPS measurements have shown that this innovative modification method induced the

formation of oxygen functional groups (C-OH, COOH etc.) and the elimination of fluorine on the PVF surface. Besides, XPS and SEM analysis have shown that the TiO₂ PSFD lead to the deposition of aggregated TiO₂ particles on PVF increasing its surface roughness. It was possible to control the extent of TiO₂ deposition by varying the pH, which suggested that the TiO₂ particles were bound to functionalized PVF by an electrostatic interaction. The nature of the iron oxide coat was also investigated by XPS and is probably constituted by akaganeite (β -FeOOH).

The photocatalytic activity study using hydroquinone as model contaminants has shown that significant synergistic effects occurred between TiO₂ and iron oxide for the system PVF^f-TiO₂-Fe oxide/H₂O₂/light. These synergistic effects were assigned to different mechanisms leading to =Fe(II) regeneration which is the rate-limiting step in Fenton processes. PVF, PE or PET supports led to catalysts showing similar photoactivity ruling out the possibility that the polymer nature influence significantly the catalyst efficiency. PET bottle employed as reactors and catalysts support (PET_b-TiO₂-Fe oxide) was an efficient heterogeneous photocatalyst to inactivate bacteria and no dissolved iron ions were detected in the filtered solution opening perspectives for SODIS applications.

The reactivity of PVF^f-TiO₂-Fe oxide/H₂O₂/light system was investigated, the contribution of dissolved iron and the influence of reaction parameters were assessed as well as long term stability. It was found that the photo-dissolution of iron ions and their relative homogeneous photo-Fenton contribution to HQ and NA initial mineralization was low but significant. Besides, most of dissolved iron ions were re-deposited on the photocatalyst at the end of the treatment. The rates of organic compounds photo-assisted degradation were high and mostly independent of initial pH and NaCl presence but increased with temperature. The photocatalytic activity was highly stable toward repetitive nalidixic acid degradations as no decrease in the degradation rates were observed during 45 consecutive runs of three hours.

The presence of TiO₂ particles on the photocatalyst surface, induced by the TiO₂ PSFD treatment, was found to engender three principal beneficial effects: (1) the iron oxide deposition was higher on TiO₂ coated PVF surfaces than in commercial PVF as TiO₂ particles acted as iron oxide nucleation initiator; (2) the initial and long term photo-activity

increase were assigned to the uncovering of TiO₂ due to irreversible iron dissolution which increased its exposition to light and consequently its synergistic contribution to the overall photocatalytic degradation process; (3) the resistance to self-degradation was assigned to TiO₂ which may act as a charge trap and diminish the contact between active iron species and polymer surface.

Finally PVF^f-TiO₂-Fe oxide was successfully adapted to a pilot-scale parabolic solar photo-reactor showing good performances in aromatic organic compounds degradation, even at controlled neutral pH in the case of nalidixic acid. However, other compounds such as pesticides were more resistant. In contrast with homogeneous photo-Fenton, emerging pollutant degradation mediated by PVF^f-TiO₂-Fe oxide/H₂O₂/light was found to be selective. Degradation rates were higher for the compounds containing moieties (carboxylic acid, chelating group) that can be adsorbed to catalyst surface and/or form complexes with Fe(III). Although significant changes in the appearance and surface composition of PVF^f-TiO₂-Fe oxide took place during degradation experiments, the photocatalyst activity was conserved toward repetitive pollutant degradations and even slightly increasing during the 20 days of operation. This enhancement confirmed that the uncovering of TiO₂ increased its exposure to light and consequently its synergistic contribution to the overall photocatalytic degradation process.

Perspectives

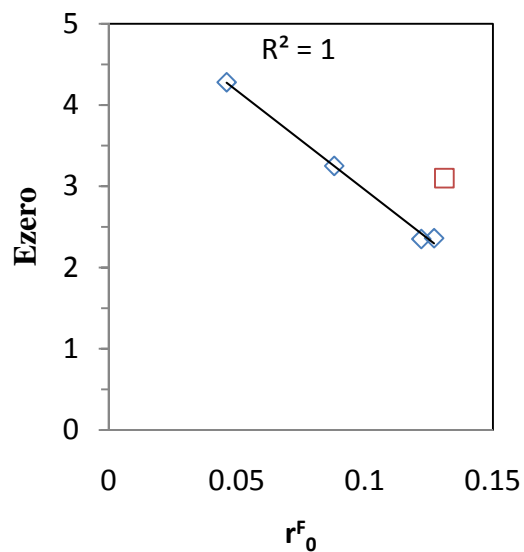
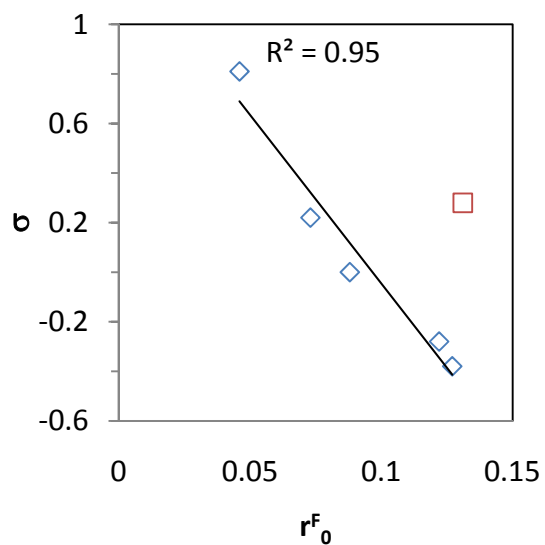
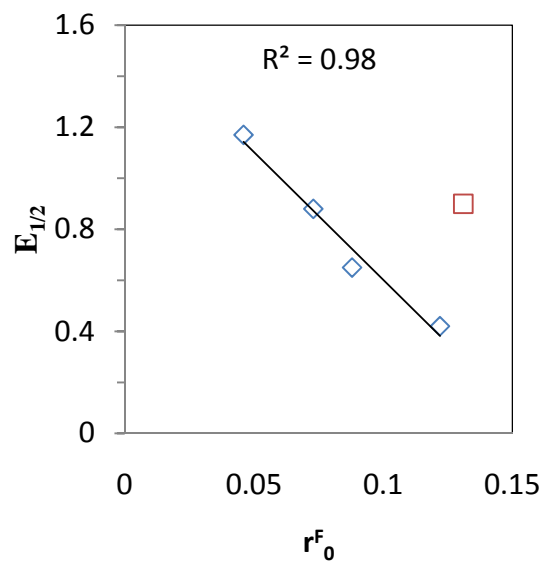
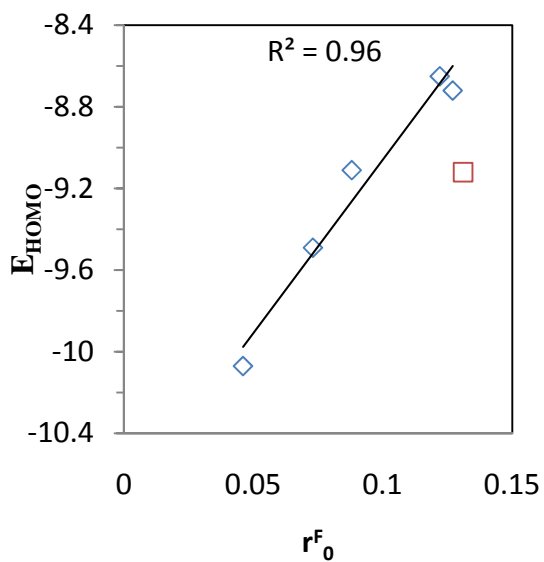
The perspectives opened by this work are wide and it would be difficult to enumerate all of them. However, some of the issues that would need further investigations are:

- Additional studies with TiO₂ and iron oxide coated polymer films could be carried out to determine the optimal Fe/Ti surface ratio. In this work this surface ratio was between 3 and 90 but a value inferior to 1 could be optimal. In this sense the development of iron oxide coated-TiO₂ supports is an interesting alternative to be developed.
- The mechanisms involved in the synergistic effects could be studied in more details by quantum calculations or by advanced spectroscopic techniques (time resolved spectroscopy, paramagnetic electronic resonance etc.)

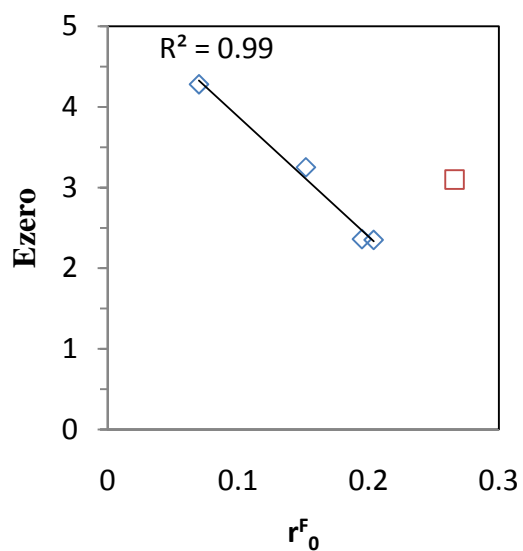
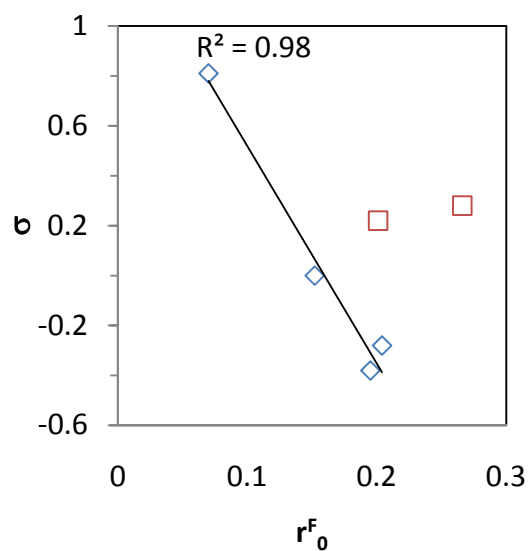
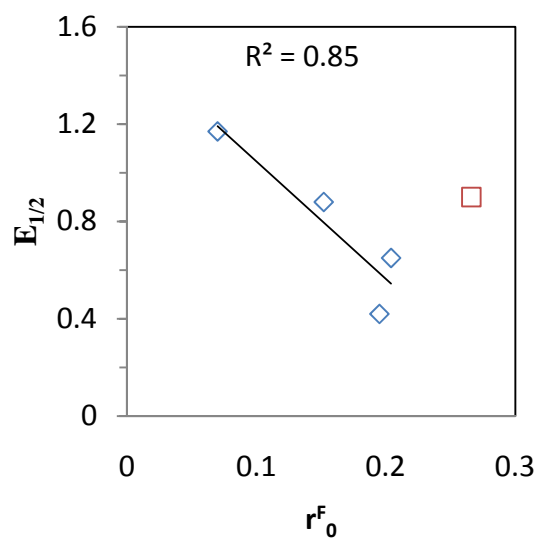
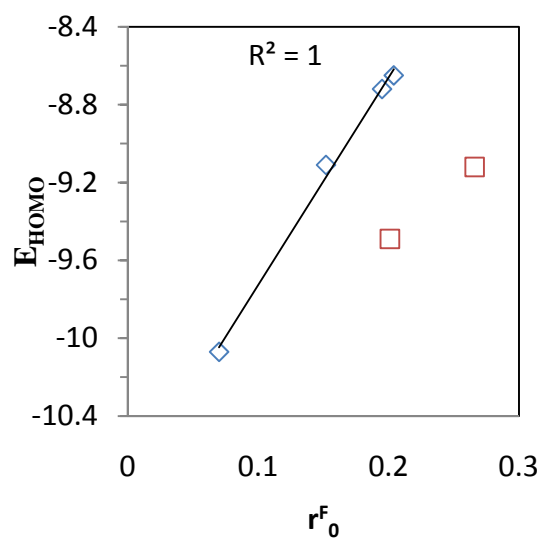
- The use of a different iron oxide coat (magnetite, green rust, goethite, ferrihydrite etc.) may drive to a higher photocatalytic activity or could decrease iron dissolution.
- An additional thin TiO_2 coat could be deposited on the surface of P- TiO_2 -Fe oxide (leading to an iron oxide sandwiched between two TiO_2 coats) aiming to suppress iron photo-dissolution.
- Other semiconductors than TiO_2 (like Fe_2O_3 , ZnO , etc.) could modify polymer surfaces (and eventually be deposited) under adequate irradiation conditions.
- The preparation procedure proposed could be applied to other supports based on carbon such as organic membranes, activated carbon, carbon fibers or nanotubes, cellulose etc.
- The activity of TiO_2 and iron oxide coated PET bottles in presence of H_2O_2 for the solar disinfection of water could be investigated in more details using different biological indicators (virus, more resistant bacteria etc.) and real contaminated waters.
- The TiO_2 PSFD could be performed to different polymers to increase their biocompatibility, their adhesive properties, or could be a way to prepare self-cleaning surfaces. On the other hand, TiO_2 photocatalysis could be used to mineralize polymer waste.

APPENDICES

I- Electronic descriptors (E_{HOMO} , $E_{1/2}$, σ , E_{ZERO}) as a function of initial rates of degradation (r^{F_0}) for the Fenton reaction and linear fittings (p-Cl excluded)



II- Electronic descriptors (E_{HOMO} , $E_{1/2}$, σ , E_{ZERO}) as a function of initial rates of degradation (r_{pf0}) for the photo-Fenton reaction and linear fittings (p-Cl and p-CHO excluded)



CURICULUM VITAE

Félicien MAZILLE
Chemin de Charmettes, 7
1003 Lausanne
Telephone: 021 311 60 69
Mobile: 078 739 41 98
E-mail: felicien.mazille@epfl.ch

Education:

2006 Swiss Institute of Technology Lausanne Switzerland
M. Sc. in Molecular and Biological Chemistry

2000 Lycée Charles Baudelaire Cran Gevrier France
Baccalaureat Scientific

Employment:

2004-2006 Swiss Institute of Technology Lausanne Switzerland
Assistant: general chemistry exercises.

2004-2005 Swiss Institute of Technology Lausanne Switzerland
Laboratory of Photonics and Interfaces (EPFL-LPI)
Research work: Stability and performance of new ionic liquids based dye sensitized solar cells.

2005-2006 Swiss institute of technology Lausanne Switzerland
Laboratory Environmental Biotechnology (EPFL-LBE)
Master work: Effect of a helio-photocatalytic treatment on pollutants of industrial interest

2006 Valle State University (Univalle) Cali Colombia
Group of Advanced Oxidation Processes (GAOX)
Research work: Photocatalysis for removing the herbicide Ametryn in water, and photocatalysis as an alternative to chlorination for drinking water production.

2007-2010 Swiss Institute of Technology Lausanne Switzerland
Laboratory of electrochemical engineering (EPFL-GGEC)
Assistant in Chemical Engineering
PhD thesis about heterogeneous photo-Fenton catalysis
Participant of European project (INNOWATECH).

Skills:

Languages:

French: mother tongue
English: good knowledge
Spanish: good knowledge

Knowledge and experience in:

- Material science: nanomaterials innovative preparation, polymer surface modification, surface characterization (XPS, SEM...).
- Industrial wastewater treatment : photocatalytic methods
- Analysis of water: chromatography (HLPC, GC-MS...), spectrophotometry, biodegradability (BOD₅), dissolved carbon (TOC, DOC) etc.
- Energy production: dye sensitized solar cells.
- Teaching, writing scientific papers, oral presentations, fund finding, research projects.

Personal Details:

Date of birth: 7th august 1982
Nationality: Swiss, French
Gender: Male

Publications:

1. F. Mazille, Z. Fei, D. Kuang, D. Zhao, S.M. Zakeeruddin, M. Gratzel, P.J. Dyson. Influence of ionic liquids bearing functional groups in dye-sensitized solar cells. *Inorganic Chemistry* 45 (2006) 1585-90.
2. F. Mazille, T. Schoettl, C. Pulgarin, Synergistic effect of TiO₂ and iron oxide supported on fluorocarbon films. Part 1: Effect of preparation parameters on photocatalytic degradation of organic pollutant at neutral pH.

Applied Catalysis B: Environmental 89 (2009) 635–644.

3. F. Mazille, A. Lopez, C. Pulgarin,
Synergistic effect of TiO₂ and iron oxide supported on fluorocarbon films. Part 2: Long term stability and influence of reaction parameters on photoactivated degradation of pollutants.
Applied Catalysis B: Environmental 90 (2009) 321-329.
4. F. Mazille, T. Schoettl, A. Lopez, C. Pulgarin
Physico-chemical properties and photo-reactivity relationship for para-substituted phenols in photo-assisted Fenton system.
Journal of Photochemistry and Photobiology A: Chemistry 210 (2010) 193-199
5. F. Mazille, T. Schoettl, N.Klamerth, S. Malato, C. Pulgarin.
Field solar degradation of pesticides and emerging water contaminants mediated by polymer films containing titanium and iron oxide with synergistic heterogeneous photocatalytic activity at neutral pH.
Water Research 44 (2010) 3029-3038.
6. F. Mazille, A. Moncayo-Lasso, D. Spuhler, A. Serra, J. Peral, N.L Benítez, C. Pulgarin.
Comparative evaluation of polymer surface functionalization techniques before iron oxide deposition. Activity of the iron oxide-coated polymer films in the photo-assisted degradation of organic pollutants and inactivation of bacteria.
Chemical Engineering Journal 160 (2010) 176-184.

International conferences:

1. Participation in the conference SILAPAO (simposio latinoamericano de procesos avanzados de oxidacion) Cali (Colombia) November 2006
2. F. Mazille, T. Schoettl, C. Pulgarin, “Innovative and highly synergistic action of titanium and iron oxides coated on polymer previously modified by TiO₂ photocatalysis” Poster communication in “SPEA 5 (5th European conference Solar chemistry and Photocatalysis: Environmental Applications)” Palermo (Italy) PP3.39, 4-8 October 2008 .
3. F. Mazille, T. Schoettl, C. Pulgarin, “Innovative and highly synergistic action of titanium and iron oxides coated on functionalized polymer films” Oral communication. SILAPAO (simposio latinoamericano de procesos avanzados de oxidacion) Medellin (Colombia) p.120-136, 24-26 November 2008.
4. Participation and presentation in the european project INNOWATECH group meeting in Almeria, Zürich, Aachen, Bari and Gent. Between 2007 and 2010.